On Detection and Ranking Methods for a Distributed Radio-Frequency Sensor Network: Theory and Algorithmic Implementation

James Paul Browning

Supervisors:
Professor H.D. Griffiths
Professor C.J. Baker
Professor M.C. Wicks

A dissertation submitted in partial fulfillment
of the requirements for the degree of
Doctor of Philosophy
of
University College London

Department of Electronic and Electrical Engineering
University College London

5 December, 2017

To my loving, supportive and eternally patient wife, Hilary, who opened my eyes to the world beyond my own, and endowed me with the self-confidence and ability to realize my only limitation in life are those that I impose upon myself.

To my brilliant daughter, Fizzy, who is constantly reintroducing me to the wonderous and colorful world in which we live, may her innocence, curiosity and happiness never fade.

And to my parents, Jim and Kathy, who provided me the best support and educational experiences possible that allowed me to pursue my PhD programme at such an internationally prestigious university as UCL.

I, James Paul Browning, confirm that the work presented in this thesis is my own, unless otherwise indicated, and has not been submitted in any form for another degree or diploma at any university or other institute of tertiary education. Information derived from other sources has been indicated in the thesis.

Abstract

A theoretical foundation for pre-detection fusion of sensors is needed if the United States Air Force is to ever field a system of distributed and layered sensors that can detect and perform parameter estimation of complex, extended targets in difficult interference environments, without human intervention, in near real-time. This research is relevant to the United States Air Force within its layered sensing and cognitive radar/sensor initiatives. The asymmetric threat of the twenty-first century introduces stressing sensing conditions that may exceed the ability of traditional monostatic sensing systems to perform their required intelligence, surveillance and reconnaissance missions. In particular, there is growing interest within the United States Air Force to move beyond single sensor sensing systems, and instead begin fielding and leveraging distributed sensing systems to overcome the inherent challenges imposed by the modern threat space.

This thesis seeks to analyze the impact of integrating target echoes in the *angular domain*, to determine if better detection and ranking performance is achieved through the use of a distributed sensor network. Bespoke algorithms are introduced for detection and ranking ISR missions leveraging a distributed network of radio-frequency sensors: the first set of bespoke algorithms area based upon a depth-based nonparametric detection algorithm, which is to shown to enhance the recovery of targets under lower signal-to-noise ratios than an equivalent monostatic radar system; the second set of bespoke algorithms are based upon random matrix theoretic and concentration of measure mathematics, and demonstrated to outperform the depth-based nonparametric approach. This latter approach shall be shown to be effective across a broad range of signal-to-noise ratios, both positive and negative.

Acknowledgements

I would like to first thank former AFOSR Chief Scientist Dr. Thomas Hussey for his strong support of my AFOSR proposal entitled:" Heterogeneous Sensor Heterogeneous Data Fusion." Dr. Hussey's strong advocacy of this particular research area provided the initial ideas and concepts, a subset of which, comprise this thesis document. I would also like to thank my former AFOSR Programme Manager, Dr. Tristan Nguyen, for supporting this effort under Air Force contract FA8650-11-RY- 09COR.

Like so many other great journeys, there are many individuals along the way that assisted me with the completion this UCL PhD programme, and I would like take time to highlight their respective contributions:

- Special thanks to Dr. Michael Wicks, former Air Force Research Laboratory ST, for his endearing mentorship, constant support, and persistent encouragement to pursue my PhD and realize my full intellectual potential. As it was so eloquently explained through a mutual colleague, Dr. Michael Wicks is very much a father figure to me; an intellectual father who is simultaneously able to unleash my creative talents and channel them into productive outlets (no small feat, I assure you!).
- To Barbara Masquelier, Chief of the Air Force Research Laboratories Radio-Frequency Spectrum Warfare Branch, for her very strong support, and for affording me the time and flexibility to complete this PhD programme; given the audaciousness of this undertaking whilst gainfully-employed full-time.
- To Professor Pinyuen Chen, of the Syracuse University Department of Mathematics, who's patience and keen mathematical insights introduced me the exciting nonparametric maths world of data-depth that resulted in Chapter 4.
- To Professor Robert Qiu, of Tennessee Technological University Department of Electrical and Computer Engineering, for countless hours exploring, explaining and connecting the many mathematical theories that resulted in Chapter 5 and 6 of this thesis.
- Many thanks to my Thesis Advisor, Professor Hugh Griffiths of University College London Department of Electronic and Electrical Engineering, and Thesis Co-Advisors, Professor Christopher Baker of The Ohio State University Department of Electrical and Computer Engineering and Dr. Michael Wicks a

Distinguished Scientist of the University of Dayton Research Institute; without their strong guidance, patient mentorship and unwavering support, this PhD would have been an impossibility.

- Special thanks go to my mentor Glenn Cicero for his many helpful comments and suggestions on how to take this from a TRL 1 draft document to a TRL 7 polished thesis. Or as Glenn would say: [COMMENTS REDACTED].

Table of Contents

List of Abbreviations

AMBF	Ambiguity Function
ATR	Automatic Target Recognition
BAMBF	Bistatic Ambiguity Function
B2SGLRT	Bayesian Two-Step Generalized Likelihood Ratio Test
CFAR	Constant False Alarm Rate
CNR	Clutter-to-Noise Ration
CRLB	Cramer-Rao Lower Bound
DOA	Direction-of-Arrival
FIFO	First-In First-Out
GIP	Generalized Inner Product
GLRT	Generalized Likelihood Ratio Test
IID	Independent Identically Distributed
ISR	Intelligence, Surveillance, Reconnaissance
KA	Knowledge-Aided
KB	Knowledge-Based
LEC	Low-Energy Coherence
LFM	Linear Frequency Modulation
MF	Multi-Frequency
MP	Multi-Perspective
NHD	Non-Homogeneity Detector
OAS	Oracle Approximation Estimation
PCT	Partially Coherent Target
PD	Positive Definite
PDF	Probability Density Function
PEC	Perfect Electrical Conductor
PhD	Doctor of Philosophy
RCS	Radar Cross-Section
RF	Radio-Frequency
ROC	Receiver Operating Characteristics
SCNR	Signal-to-Clutter-Plus-Noise-Ratio
SDP	Semi-Definite Positive
SIRV	Spherically Invariant Random Vector
SNR	Signal-to-Noise Ratio

STAP	Space-Time Adaptive Processing
UAS	Unmanned Aerial System
UCL	University College London
US	United States
USAF	United States Air Force

List of Symbols for Chapter 2

H_0	Null Hypothesis
H_1	Alternative Hypothesis
γ	Detection threshold statistic
$\mathrm{s}(t)$	Signal Vector
$n(t)$	Noise Vector

List of Symbols for Chapter 3

H_0	Null Hypothesis
H_1	Alternative Hypothesis
$n(t)$	noise vector
$s(t)$	signal vector
α	False alarm rate
β	Missed detection rate
Δ	Decision space
$\delta(\boldsymbol{s}-0)$	Function describing signal process
$\ell(\cdot)$	Likelihood ratio
Γ	Observation Space
γ	Threshold parameter, threshold statistic
λ_{NP}	Lagrange multiplier for Neyman-Pearson criterion
$\mathbf{d}$	Set of decision rules
$\mathbf{n}$	Vector of noise realizations
$\mathbf{p}$	*a priori* Probabilities for an observed signal absent
$\mathbf{q}$	*a priori* Probabilities for an observed signal present
$\mathbf{s}$	Vector of signal realizations
$\mathbf{v}$	Joint probability distribution of signal and noise echoes during an observational period
Ω	Signal Space
Ω_0	Region spanned by null hypothesis decision region
Ω_1	Region spanned by alternative hypothesis decision region
$\delta(\mathbf{s})$	Signal probability distribution fucntion
$C_{1-\alpha}$	Cost function to decide a correct decision with respect to false alarm rate
$C_{1-\beta}$	Cost function to decide a correct decision with respect to the missed detection rate
$\mathrm{L}(\cdot)$	Loss function
$\mathrm{L}_c(\cdot)$	Conditional loss function
$\mathbf{p}(\mathbf{n})$	Noise space
$\mathbf{w}(\mathbf{s})$	Function describing the noise process
$r(t)$	received signal vector

$\boldsymbol{C}(r)$	covariance function
n	number of samples
x_i	i[th] observation of a *k*-dimensional random variable
$\bar{x}$	sample mean of *k*-dimensional random variable
$\boldsymbol{U}$	$k \times k$ unitary matrix
$\boldsymbol{\Sigma}$	$k \times k$ diagonal matrix with non-negative real numbers
$\boldsymbol{V}$	$k \times k$ unitary matrix
$*$	complex transpose
λ_i	i[th] eigenvalue of a *k*-dimensional matrix of singular values
$\frac{N_0}{2}$	Spectral Height of Zero-Mean Gaussian Noise Process
P_F	Probability of false-alarm
P_M	Probability of missed detection
$erfc_*$	Complimentary error function
$K_s(t,u)$	Target covariance function
$\phi_i(t)$	Complex envelope of received signal
$\phi_i(u)$	Matched filter
$u(s)$	Threshold function for low-energy coherence case
d^2	Signal to noise ratio
$l_R^{(1)}$	Signal energy
$E(\cdots)$	Expectation
$f(t-\lambda)$	Time-shifted complex envelop of received signal
$f(u-\lambda)$	Matched filter
$\tilde{S}_R(\lambda)$	Target scattering function
$\tilde{b}_R(\lambda)$	Spatial sample random variable
$\tilde{h}(t,u)$	Range-spread covariance
E	Signal energy
$\mathrm{Re}(\cdots)$	Real-value function
$e^{j\omega_c t}$	Carrier frequency
T_d	Pulse duration
$\tilde{a}$	Complex gain
τ	Time delay
ω_d	Doppler shift
$\phi(t)$	Complex envelope of received signal
$\phi^*(T_d-t)$	Matched filter

N	Number of radio-frequency sensors
$b(\tau)$	Target impulse response
L	Target range delay
μ_i	Coefficients for scaling time domain signal
$S(\omega)$	Power spectral density
$R_c(t,u)$	Covariance of received signal in absence of target
$R'(t,u)$	Pre-whitened covariance
$h_\omega(t,\omega)$	Multi-dimensional pre-whitened filter
$S_\omega(\omega)$	Power spectral density of the multi-dimensional pre-whitening filter
$v_j(\boldsymbol{x})$	Localized variation in speed of light caused by a dielectric reflector
$\boldsymbol{x_j}$	Cartesian coordinate location of reflector *j*
η_j	Dielectric contrast
Ω_j	Compactly supported spatial domain with volume l_j
$\boldsymbol{l}_{\Omega_j}$	Characteristic function of Ω_j
c	local speed of light
c_0	speed of light
$\boldsymbol{z}$	Cartesian coordinates for a localized point-source radiator
ω	frequency
$\boldsymbol{x}$	Null Hypothesis
M	Array of transmitter sources
N	Array of receiver elements
$\boldsymbol{z}_M$	Cartesian coordinates of transmitter source locations
$\boldsymbol{y}_N$	Cartesian coordinates of receiver element locations
A_{nm}	Time-reversal operator
$\hat{\mu}(\boldsymbol{y}_N, \boldsymbol{z}_M)$	Field received by the n^{th} element when the wave is transmitted by the m^{th} transmit element
$\hat{G}(\omega, \boldsymbol{y}_N, \boldsymbol{z}_M)$	Homogeneous Green's function
$H_0^{(1)}$	Hankel function of the first kind, zero order
ρ_j	Reflection coefficient for the j^{th} target body
σ_j	Singular value for the j^{th} target body
$\boldsymbol{\mu}(\boldsymbol{x})$	Normalized vector of Green's functions for the receiver array to the target body located at point $\boldsymbol{x}$
$\boldsymbol{v}(\boldsymbol{x})$	Normalized vector of Green's functions for the transmitter array from the target body located at point $\boldsymbol{x}$

$\mathbf{A}$	General form of the time-reversal operator
$\mathbf{W}$	General form of the measurement additive noise matrix
$\mathbf{W}_{i,j}$	Complex entries of the measurement additive noise matrix
$\mathbf{B}$	General form of the measured time-reversal operator
ψ	Clutter reflectivity
$\mathcal{P}$	General form of the clutter noise process
$\boldsymbol{P}_{i,j}$	Complex entries of the clutter corruptive noise process
Ψ_j	Singular value of the observed clutter reflectivity
$\mathbf{P}$	General form of the clutter additive noise matrix

List of Symbols for Chapter 4

π_i	Multivariate population
$\mathbb{R}^{\boldsymbol{d}}$	Real
P_i	Continuous distribution
X_i	Random variables
$D(x;P)$	Tukey's half-space depth
H	A closed half-space
P	Continuous distribution
Θ	Center of P, or deepest point for P
$D^{\alpha}(P)$	Volume of an α-trimmed depth-region
V^{p}	Scale curve for $p\ \epsilon\ (0,1)$
B	Borel set
$I_B(x)$	Indicator function of B
H_0	Null Hypothesis
H_1	Alternative Hypothesis
$n(t)$	Noise vector
$s(t)$	Signal vector
$\delta_{\mathrm{Threshold}}$	depth-based threshold value
$\mathbf{A}$	General form of the time-reversal operator
$\mathbf{W}$	General form of the measurement additive noise matrix
$\mathbf{B}$	General form of the measured time-reversal operator
$\hat{V}_{[i]}$	Differential dispersion value for population of measured time-reversal operator
$\hat{V}_{[\mathrm{Threshold}]}$	Differential dispersion of noise matrix with arbitrary distribution
δ	Depth-based detection statistic derived from a ratio of differential dispersion values
$\hat{V}^{\beta}_{\mathrm{Threshold}}$	Differential dispersion volume defined by contour β
$\hat{V}^{p}_{\mathrm{Threshold}}$	Differential dispersion volume defined by contour p
β	Contour boundary defined by $\beta \simeq 1$, or all populations values
p	Contour boundary defined by $p \in (0,1)$, or a subset of contour boundary defined by β
$\hat{V}_i$	Differential volume for a given population of the measured time-reversal operator formed from the product of $\hat{V}_i^{\beta} - \hat{V}_i^{p}$

$\hat{V}_i^{\beta}$	Differential dispersion volume for a given population of the measured time-reversal operator defined by contour $\beta \simeq 1$
$\hat{\nabla}_i^{p}$	Differential dispersion volume for a given population of the measured time-reversal operator defined by contour $p \in (0,1)$
D^{β}	Depth contour bounded by β
D^{p}	Depth contour bounded by $p \in (0,1)$
μ	Statistical mean
σ	Statistical standard deviation
P_D	Probability of detection
P_{FA}	Probability of false alarm
$\mathcal{N}(0,\sigma^2)$	Normal Gaussian distribution
H_0^j	Null hypothesis for the j^{th} rank value
H_1^j	Alternative hypothesis for the j^{th} rank value
$s^j(t)$	Signal vector for the j^{th} rank value
$\delta_{\text{Threshold}}^{j}$	Threshold statistic for the j^{th} rank value
D^{β^j}	Depth contour bounded by β for the j^{th} rank value
$\hat{V}^{\beta^j}$	Volume of depth contour bounded by β for the j^{th} rank value
$\hat{V}^{p}$	Volume of depth contour bounded by $p \in (0,1)$
$\hat{V}_{[i]}^{p}$	Volume of depth contour bounded by $p \in (0,1)$ calculated from training data of length $[i]$
$\hat{V}_{[i]}^{\beta^j}$	Volume of depth contour bounded by β for the j^{th} rank value calculated from training data of length $[i]$
$\hat{V}_{\text{Threshold}}^{j}$	Annular volume of the depth contour for the j^{th} rank value defined by $\hat{V}_{\text{Threshold}}^{\beta^j} - \hat{V}_{\text{Threshold}}^{p}$, where $\beta \simeq 1$ and $p \in (0,1)$
$\hat{V}_{\text{Threshold}}^{\beta^j}$	Volume of the depth contour bounded defined by $\beta \simeq 1$ for the j^{th} rank value

List of Symbols for Chapter 5

P_x	Probability distribution
x	Random variables, or observations
$\langle f(x) \rangle$	First moment, or mean,
$E(x)$	Expectation, or first moment, or mean
$\boldsymbol{x}$	Random vector
$\boldsymbol{\chi}$	A measurable space
$f : \boldsymbol{\chi} \to \mathbb{R}$	A measurable map
$\mathbb{P}(\cdots)$	Mathematical bound operation on quantity $(\cdots)$
$X_1, \ldots, X_n$	Sequence of independent random variables
S_n	Quantity defined by the summation of $X_1, \ldots, X_n$
G	Gaussian distribution
$\mathbb{R}^n$	A collection of random variables, X_i, on a common probability space
σ	Statistical standard deviation
$\|\|\boldsymbol{x}\|\|^2$	Euclidian norm of $\boldsymbol{x}$
$F : \mathbb{R}^n \longmapsto \mathbb{R}$	Function defining the mapping of $\mathbb{R}^n$ into a convex function $\mathbb{R}$
K	Positive Lipschitz function
t	Any positive number
Tr$(\cdots)$	Trace functional
$\mathbf{A}$	General form of the signal time-reversal operator
$\lambda_i(\cdots)$	Eigenvalue of matrix $(\cdots)$
$\boldsymbol{U}$	Unitary matrix
$\boldsymbol{D}$	Diagonal matrix
$\|f\|_\ell$	Lipschitz constant
C	Constant
$\boldsymbol{H}$	Wigner matrix
$h_{i,j}$	Entries of the Wigner matrix
$f : \mathbb{R} \longmapsto \mathbb{C}$	Function defining the mapping of $\mathbb{R}$ into complex number line $\mathbb{C}$
$g : \mathbb{R}^m \longmapsto \mathbb{R}$	Function defining the mapping of $\mathbb{R}^m$ into a Lipschitz function $\mathbb{R}$ with constant $\|G\|_\ell$
x_{ij}	Off-diagonal real entries of a squared random variables matrix
y_{ij}	Off-diagonal imaginary entries of a squared random variables matrix

x_{ii}	Diagonal entries of a squared random variables matrix
$\mathbf{X}$	Matrix comprised of elements of a squared random variables probability space
$G(\mathbf{X})$	Matrix function on $\mathbf{X}$
σ^2	General form of mathematical eigenvalue, or general form of engineering singular value
$\mathrm{In}(\cdots)$	Inertia of matrix $(\cdots)$
$\pi(\cdots)$	Positive eigenvalues of matrix $(\cdots)$
$\zeta(\cdots)$	Zero eigenvalues of matrix $(\cdots)$
$\nu(\cdots)$	Negative eigenvalues of matrix $(\cdots)$
c_n	Noise scaling coefficient
$\mathbf{W}$	General form of the measurement additive noise matrix
$\mathbf{B}$	General form of the measured time-reversal operator
$\mathcal{N}(0,\sigma^2)$	Normal Gaussian distribution
H_0	

List of Symbols for Chapter 6

H_0	Null Hypothesis
H_1	Alternative Hypothesis
S	Signal
N	Noise
$\mathbf{W}$	General form of the measurement additive noise matrix
$\mathbf{B}$	General form of the measured time-reversal operator
$\mathbf{A}$	General form of the signal time-reversal operator
ρ	General form of an operator
$\boldsymbol{x_j}$	Cartesian coordinate location of reflector j
r	Number of reflectors
$\boldsymbol{u}(\boldsymbol{x}_j)$	Normalized vector of Green's functions for the receiver array to the target body located at point $\boldsymbol{x_j}$
$\boldsymbol{v}(\boldsymbol{x}_j)$	Normalized vector of Green's functions for the receiver array to the target body located at point $\boldsymbol{x_j}$
$\otimes$	Kronecker product
$\odot$	Dot product
σ_{j}	Singular value for the j^{th} target body
M	Array of transmitter sources
$\prec$	Mathematical symbol for majorized
$\mathrm{E}\{\cdots\}$	Expectation
$\widehat{\mathbf{\Sigma}}$	OAS estimator matrix
$\widehat{\mathbf{F}}$	Shrinkage target matrix
$\mathbf{R}_x$	Sample covariance matrix
$\widehat{\mathbf{R}}_x$	Estimated sample covariance matrix
$\mathbf{I}$	L-dimensional unitary matrix
$\hat{\rho}$	Shrinkage coefficient
$\mathbf{I}$	L-dimensional unitary matrix
$\hat{\rho}$	Shrinkage coefficient
$\widehat{\mathbf{\Sigma}}_0$	Initial guess for $\widehat{\mathbf{\Sigma}}$
$\hat{\rho}$	Shrinkage coefficient
$\hat{\rho}_{\mathrm{OAS}}$	OAS convergence
$\widehat{\mathbf{\Sigma}}_{\mathrm{OAS}}$	Estimated OAS covariance matrix

$\sigma(\cdots)^{\downarrow}$	Ordered in *descending* order
$\prec_w$	Mathematical symbol for weakly majorized
$\mathbf{B}_{\text{OAS}}$	General form of the estimated oracle of the measured time-reversal operator
$\mathbf{W}_{\text{OAS}}$	General form of the estimated oracle measurement additive noise matrix
$\mathbf{A}_{\text{OAS}}$	General form of the estimated oracle signal time-reversal operator
$\widehat{\mathbf{B}}$	General form of the estimated measured time-reversal operator
$\widehat{\mathbf{W}}$	General form of the estimated measurement additive noise matrix
$\widehat{\mathbf{A}}$	General form of the estimated signal time-reversal operator
$C\mathbb{M}_{\boldsymbol{M}}$	$M \times M$ matrix comprised of complex-valued entries
$\mathbb{R}^{+}$	Positive random variables
$\gamma_{\text{Threshold}}$	detection threshold variable
$d_i(\cdots)$	Diagonal elements of matrix $(\cdots)$
$\lambda_i(\cdots)$	Eigenvalues of matrix $(\cdots)$
$\hat{\gamma}_{\text{Threshold}}$	Estimated threshold statistic
$\bar{\mu}_{\gamma}$	Estimated mean of the estimated threshold statistic
$\bar{\sigma}_{\gamma}$	Estimated standard deviation of the estimated threshold statistic
k_{FA}	Desired false alarm rate
P_D	Probability of detection
P_{FA}	Probability of false alarm
$\gamma_{\text{Threshold}_{i:M}}$	Detection threshold statistic for the i^{th} singular value
$\hat{\gamma}_{\text{Threshold}_{i:M}}$	Estimated detection threshold statistic for the i^{th} singular value
$\bar{\mu}_{\gamma;i:M}$	Estimated mean of the estimated threshold statistic for the i^{th} singular value
$\bar{\sigma}_{\gamma;i:M}$	Estimated standard deviation of the estimated threshold statistic for the i^{th} singular value
μ_r	Dielectric relative permittivity
ϵ_r	Dielectric relative permeability
g	rank of $\boldsymbol{B}$ matrix

List of Tables

List of Figures

1 Introduction

1.1 Thesis Introduction

The impetus for this thesis came forth from a discussion between the author and his co-advisor, Dr. Michael Wicks. The subject of the discussion was heterogeneous sensor heterogeneous data fusion; wherein non-similar sensors attempt to fuse inherently dissimilar data. In attempting to scale the problems associated with fusing heterogeneous data, six major research areas were discussed, investigated, and eventually became the subjects of Chapters 4 and 6. One item that was agreed upon, was the topic of distributed sensing, and its paramount importance to the future of United States Air Force intelligence, sensing, and reconnaissance (ISR) missions. Indeed, numerous efforts to realize *Distributed and Layered* Sensing were well underway within the United State Air Force, and of great interest as far back as the early 1990's. In keeping focused on *distributed sensing*, we settled on shelving the topic of heterogeneous sensor fusion for a more simplified investigation into the realm of *non-parametric* algorithms for the detection of targets. Our logic was, and still is, that target detection is the ultimate goal of ISR sensors, and a *non-parametric* framework for target detection is central to the understanding, and ultimately the development of, a methodology for fusing heterogeneous data sources; since the underlying nature of the fused data is not as critical under a non-parametric framework-ie data is data, regardless of sensor origin. This initial investigation became the subject of Chapter 4.

Following our initial discussions on *non-parametric detection algorithms*, we realized we were missing a key benefit of having numerous sensors focusing their resources on a common target set, and that was the fact we were exploiting diversity in the *angular domain* to achieve target detection, versus traditional monostatic sensors that rely on *time domain* integration of multiple target echoes to bring the signal-to-noise ratio above the noise floor to achieve detection with thresholding. This inspired us to build upon the concept of a non-parametric detection algorithm, and push the bounds of the possible by exploring the concept of *integration of target echoes in the angular domain* as opposed to the *time domain*, to investigate whether distributed sensing increases the ability to recover targets from a background noise environment. In reality, the goal of this

investigation was to determine if the recovery of so-called *weak* targets in a background environment comprised of noise, clutter, or clutter and noise, could be improved upon in comparison to a traditional monostatic sensor. Whilst the contribution of Chapter 4 is the introduction of a method of *non-parametric* algorithm for target detection with a distributed network of sensors, the contribution of Chapter 6 is the realization of a framework for the exploitation of *angular domain diversity* for target detection.

In summary, this thesis focuses on six challenges introduced through the use of a distributed network of radio-frequency (RF) sensors for target detection and ranking:

1. Development of a pre-detection fusion algorithm that coalesces the received signals from each RF sensor in the network into a unified time-reversal operator, thereby simplify subsequent processing algorithms [Chapter 3].
2. Detection of range-extended target without requirements for knowing the target covariance function *a priori* [Chapters 4 and 6].
3. Ranking of a range-extended target to determine effective number of scattering centers comprising the target body, without knowing the nature of the extended target *a priori* [Chapters 4 and 6].
4. Development of detection threshold criterion that is non-parametric and does not require *a priori* knowledge of the background interference environment; to include noise and/or clutter [Chapters 4].
5. Detection and ranking in signal-to-noise ratio regimes that are weaker than typically required for monostatic radar system detection algorithms [Chapters 4 and 6].
6. Detection and ranking that is independent of sensor network density, and is able to operate under both sparse and dense sensor density regimes [Chapters 6].

A common thread that found in all three major thesis chapter themes is if you have a number of sensors distributed around a target of interest, do you gain any increase in detection performance versus a standard monostatic sensor? More importantly, how does the use of multiple sensors-regardless of configuration- lead to anything other than a variation of standard detection methodologies? This progression of thought led to the concept of a distributed network of radio-frequency sensors surrounding a target in the *angular domain*, and the necessity of breaking from the paradigm of *post-detection fusion* or *time-domain pulse*

integration, and exploring the realm of the possible in *pre-detection fusion* or *angular-domain integration*. Pre-detection fusion would be necessary, as the distributed sensor network is exploiting *angular diversity*, and post-detection fusion would be nothing more than a variation on standard monostatic time-domain detection methodologies.

Further expanding angular diversity concept, the third research topic focused on the detection of targets that were non-isotropic in the angular domain. Non-uniform target reflectivity exists in the angular domain, complicating the previously developed pre-detection fusion algorithm. One possible implication of this third research focus, is that if a target has a salient scattering feature that is only observable from certain angular ambits, a distributed sensor network should perform better at detecting the *angularly selective* target than a traditional monostatic sensor. This ability to exploit *angular diversity* is a unique contribution and consequence of the pre-detection fusion algorithms introduced in Chapter 3.

Upon discussing the nature of real-world targets, and scattering phenomenology, it was decided that for all three research topics, the target under consideration should be *range-extended* (multiple adjacent scattering centers), and be comprised of isotropic dielectric scattering spheres with real-valued permittivity, and unity permeability. This later point has major implications for the nature of the detection algorithms, and is discussed more in Chapter 3. Also, using a more realistic target body provides yet another unique contribution of this these for detecting real-world target objects, in that most detection algorithms focus on detecting a single point-type target and not a target comprised of multiple scattering features.

One additional benefit of using a *range-extended* target for the development of the various detection algorithms in Chapters 4 and 6, is that having more than one target allows for the inclusion of *statistical ranking* via a *recursive process*. *Statistical ranking* is a method of determining the number of statistically significant values in a set, and serves the purpose of permitting the recovery of all salient scattering features of the range-extended target body present within the observational area of the distributed sensing network. For the pre-detection fusion algorithm, statistical ranking allows for the inclusion of a rudimentary cognitive intelligence, wherein the algorithm determines if, and how many, targets are present in the background interference environment. This is of great interest to those investigating sensor network fusion, as it reduces the necessity of human-

in-the-loop interactions, and allows the analysis of post-detected and ranked data to be presented to an analyst, reducing the overall workload on a (hypothetical) distributed sensor network operator.

As with any detection algorithm, the choice of threshold detection statistic is paramount to the development of the statistical binary hypothesis test, and to that end, the associated Neyman-Pearson criterion are developed and demonstrated for each of the detection algorithms introduced in Chapters 4 and 6. In particular, Neyman-Pearson criterion are derived non-parametrically in Chapter 4 using a differential dispersion determination, as well as a Chebyshev inequality statistic to determine the presence of statistical outlier which is considered significant, and therefore indicative of a target present. A statistical ranking algorithm is then introduced to recover the number of target scattering features from the observed background environment using am extension of the same Neyman-Pearson criteria introduced earlier.

In Chapter 6, we depart from a strict emphasis on the requirement for deriving detection and ranking algorithms via non-parametric statistical maths, and instead investigate the leading edge of mathematical developments in free-probability and concentration of measures. This investigation is undertaken with the aim of increasing the ability of our detection and ranking algorithms to operate in domains wherein the target of interest may not be particularly distinguishable from the background environment. These so named *weak signal-to-noise ratio domains* are stressing for traditional detection algorithms and demonstrate the ability of a distributed sensing network to outperform current monostatic sensing modalities through the clever application of bespoke detection algorithms. Neyman-Pearson criteria is derived from an innovations process based upon the concept of the *trace functional*. System performance is demonstrated to exceed the non-parametric algorithms of Chapter 4.

For cases in which the background environment is benign, or permits the application of non-parametric detection and ranking methodologies, the bespoke algorithms introduced in Chapter 4 are germane. However, under more stressing ISR conditions, or for those target bodies that exhibit non-isotropic reflectivity profiles, the bespoke detection and ranking algorithms of Chapter 6 are more applicable. In all instances, the distributed sensing network is shown to increase detection performance over its equivalent monostatic counterpart.

1.2 Thesis Goals and Aims

A theoretical foundation for pre-detection fusion of heterogeneous sensors is needed if the US Air Force is to ever field a system of distributed and layered sensors that can detect and perform declaration of complex, extended targets in difficult interference environments, without human intervention, in near real-time. Numerous studies have fused homogeneous and heterogeneous sensors using post detection and track data. The fusion of independent sensor processing chains after detection will not lend itself to emulating sensor fusion comparable to that of a human.

The ambition of this thesis is the development of detection and ranking algorithms for the recovery of extended target structures under *weak signal*, low signal-to-noise ratio, regimes. This thesis proposes to formulate a mathematical paradigm that will utilize the fusion of signal returns of multiple sensors in the pre-target declaration stage. Algorithms will detect and estimate the rank of an extended target (number of targets present) without the necessity for human interaction. Legacy work in the area of low-energy coherence is used to build a foundation for the development of a mathematical paradigm that realizes distributed sensor fusion. Low-energy coherence relies on the existence of a known *target covariance function* in order to condition the associated receiver matched filter inner product space to emphasize the received target received energy, over that of the interfering environment. This requirement to know the target and associated *target covariance function* is a limiting factor in the real-world implementation of a low-energy coherence receiver.

Further, this work seeks to analyze the impact of integrating target echoes in the distributed domain (angular domain) when the *target covariance function* is not known *a priori*, to determine if better detection performance is achieved through the use of a distributed sensor network, under low-energy condition-i.e. *weak signal-to-noise ratio* detection regimes. Two bespoke algorithms are introduced for distributed sensor networks: the first is based upon a depth-based nonparametric detection algorithm, which is shown to enhance the recovery of targets under lower signal-to-noise ratios than an equivalent monostatic radar system; the second is based upon random matrix theoretic and concentration of measure maths, and demonstrated to outperform the depth-based nonparametric approach. This latter approach shall be shown to be effective across a broad range of signal-to-noise ratios, both positive and negative.

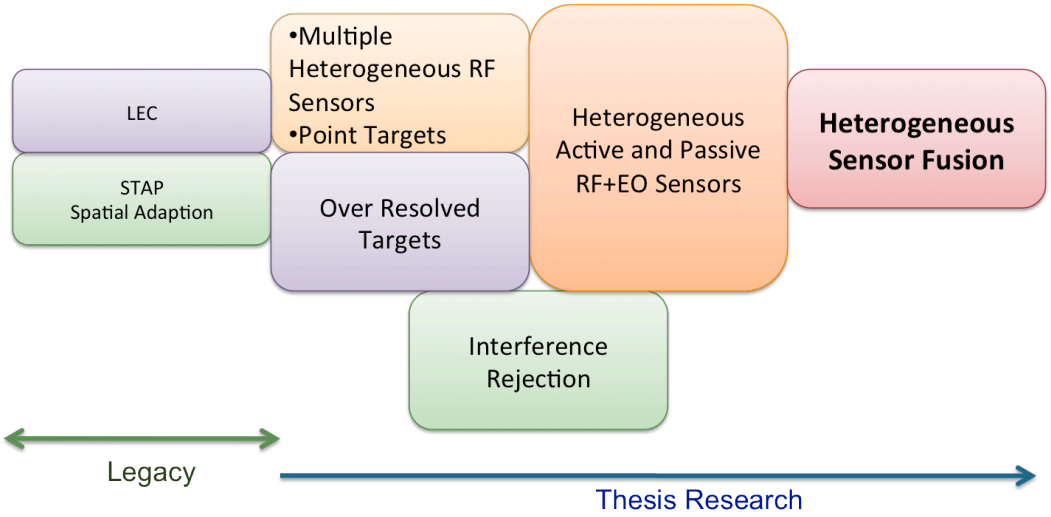

Figure 1: Roadmap to Heterogeneous Sensor Fusion

1.3 Contributions of this Thesis

Throughout this work, an effort has been made to increase the body of knowledge on mathematical paradigms for distributed radio-frequency (RF) sensor networks to enable both *pre-detection fusion of the sensor network*, and *detection under weak signal-i.e. low signal-to-noise ratio regimes*. Whilst each chapter goes into exacting detail regarding significant results, the following list attempts to capture the salient and bespoke contributions of this thesis for the reader interested in understanding the *bottom line up front*; and to that end, this thesis focuses on the development of mathematical paradigms for distributed radio-frequency (RF) sensor networks to enable:

1. Development of a pre-detection fusion algorithm that coalesces the received signals from each RF sensor in the network into a unified time-reversal operator, thereby simplify subsequent processing algorithms [Chapter 3].
2. Detection of range-extended target without requirements for knowing the target time-reversal operator *a priori* [Chapters 4 and 6].
3. Ranking of a range-extended target to determine effective number of scattering centers comprising the target body, without knowing the nature of the extended target *a priori* [Chapters 4 and 6].
4. Development of detection threshold criterion that is non-parametric and does not require *a priori* knowledge of the background interference environment; to include noise and/or clutter [Chapter 4].

5. Detection and ranking in signal-to-noise ratio regimes that are weaker than typically required for monostatic radar system detection algorithms. [Chapters 4 and 6].
6. Detection and ranking that is independent of sensor network density, and is able to operate under both sparse and dense sensor density regimes [Chapter 6].

Within the subsequent chapters, the author attempts to develop a mathematical framework for distributed sensor network pre-detection fusion, target detection and ranking for extended target structures. This framework will serve as the basis for analyzing distributed sensor network densities, establish detection thresholds and assess system performances.

1.4 Structure of Thesis

Chapter 2 focuses on a literature review of the current state of the art. Emphasis is placed on detection from the perspective of legacy radar system topologies. Detection via mono- and bi-static, and netted radar systems is reviewed, along with adaptive signal processing strategies for various bistatic and netted radar network topologies. Target models are discussed, as well as the concept of extended target bodies. A discussion on the distributed sensor network topology used for this work is introduced next, along with a roadmap of where this work fits into the overall future of USAF ISR sensing, see figure 1.

Chapter 3 introduces the reader to radar target detection and the basics of statistical decision theory. An overview of low energy coherence (LEC) receiver, as well as extensions of the original mathematical formulation to multiple sensors, is covered in some detail. As the basis for many of the concepts that are introduced in this work, and proposed for future work in Chapter 8, the LEC receiver paradigm is discussed in great detail; as are its associated shortcomings. Finally, the pre-detection fusion algorithm is introduced and derived from first principles. The pre-detection fusion process is a critical component of each of the bespoke detection and ranking algorithms introduced in Chapters 4 and 6, and as such, is the final theoretical concept covered in Chapter 3. A summary provides the motivation to move beyond the LEC, and into the realm of distributed sensing for targets whose covariance function is not known *a priori*.

In Chapter 4, a novel nonparametric depth-based method for the range-extended target detection, and scattering center ranking problem in noisy

environments under nominal signal-to-noise ratios, is considered. An algorithm is introduced for the determination of the presence of single or multiple isotropic scattering centers in a background medium defined by an additive corruptive noise process. The detection performance versus signal-to-noise ratio is developed for a given false alarm rate, incorporating the Neyman-Pearson Criterion, and detection performance compared to a typical single-pulse and envelope monostatic sensor detection approach. The statistical field of ranking is introduced, and the nonparametric detector is extended for the sensing of range-extended target structures. Of interest is that in [1], the actual signal-to-noise ratio that delineates the *weak* target from a *nominal* target is not defined, and left to the reader to interpret. Therefore, whilst the particular signal-to-noise ratios in Chapter 4 are more equivalent to a *nominal* value, they represent an improvement over the standard monostatic single-pulse and envelope detectors-therefore represent a relevant application of a *pre-detection fusion* algorithm that is *nonparametric* in formulation, and is therefore more conducive to the realization of our goal of a *heterogeneous sensor heterogeneous data* fusion algorithm. This latter goal is the overarching reason for exploring non-parametric pre-detection fusion algorithms in Chapter 4.

However, whilst the bespoke non-parametric detection algorithm for our pre-detection fusion process allows for a realization of a heterogeneous sensor heterogeneous data fusion process, the detection performance does not greatly exceed that of traditional monostatic radio-frequency sensor systems. In Chapter 6, a new bespoke random matrix theoretic detection algorithm is developed that greatly increases the sensitivity that our distributed radio-frequency sensor network is able to detect targets, both singular and over-resolved; simulation results show efficacy across a broad range of signal-to-noise ratios, spanning from positive to negative.

Chapter 6 takes a slightly different look at the detection problem for a target that is weak in every given observational sensor; the concept of *weakness* is attributed to the translation of the signal-to-noise ratio from the positive to the negative. The weak reflector detection problem is analyzed and impacts to the performance bounds of the distributed radio-frequency sensor network are investigated. Methods for ranking under weak reflectivity scenarios are considered for a target comprised of multiple scattering centers, which represents an improvement over the bespoke non-parametric detection algorithm introduced in

Chapter 4. Simulation results show efficacy across a broad range of signal-to-noise ratios, spanning from positive to negative.

Chapter 7 contains a summary of results from Chapters 4 and 6. Emphasis is placed on the contribution of each chapter, and on the contributions of this work as a whole.

Chapter 8 focuses on the large number of selected open problems that spawned from this thesis; which include research areas the author intends to investigate in the near term, along with those problems which are more suitable to PhD topics and ending with a future work section that is showcases the long-range vision for this research work.

1.5 Research Publications Resulting from this Thesis:

[1] Browning, J.P.; Griffiths, H.D.; Entner, J.; Chen, P., “Depth-Based Method for Target Detection in Noisy Environments,” *IEEE Radar Conference 2013*, May 2013.

[2] Schneible, J.; Browning, J.P.; Wicks, M.; Yuhong Zhang; , "Geometric diversity versus frequency diversity an imaging example," *2012 International Waveform Diversity and Design*, pp.262-269, 8-13 Aug. 2010.

[3] Wicks, M.C.; Yuhong Zhang; Schneible, R.; Browning, J.P., "A Hotelling T-Squared GIP Test for Detection of Over Resolved Targets," *2010 European Wireless Conference (EW)*, pp.766-773, 12-15 April 2010

[4] Lin, F; Qiu, R.C.; Browning, J.P., "Spectrum Sensing with Small-Sized Datasets in Cognitive Radio: Algorithms and Analysis," *IEEE Transactions on Vehicular Technology*, vol. 64, pp. 77-87, Jan. 2015.

[5] Bonior, J.; Z. Hu; T.N. Guo; R.C. Qiu; J.P. Browning; M.C. Wicks, "Software-Defined Radio Based Wireless Tomography: Experimental Demonstration and Validation," *IEEE Geoscience and Remote Sensing Letters*, vol. 12, pp. 175-179, Jan 2015.

[6] X. Li; Hu, Z.; Qiu, R.C.; Wu, Z.; Browning, J.P.; Wicks, M.C. “Demonstration of Cognitive Radar for Target Localization Under Interference,” *IEEE Transations on Aerospace and Electronic Systems*, vol. 50, no. 4, pp. 2440-2455, Oct. 2014.

[7] Qiu, R.; Z. Hu; C. Zhang; J.P. Browning; M.C. Wicks, "A Novel Single-Step Approach for Self-Coherent Tomography Using Semidefinite Relaxation,"

IEEE Geoscience and Remote Sensing Letters, vol. 11, pp. 114-118, Jan. 2014.

[8] Lin, F.; Qiu, R.C.; Browning, J.P.; Wicks, M.C., "Target Detection with Function of Covariance Matrices Under Clutter Environment," *IET International Conference on Radar Systems*, pp. 1-6, 22-25 October 2012.

[9] Lin, F.; Qiu, R.C.; Hu, Z.; Hou, S.; Browning, J.P.; Wicks, M.C., "Generalized FMD Detection for Spectrum Sensing under Low Signal-to-Noise Ratio," *IEEE Communications Letters*, vol. 16, no. 5, pp. 604-607, May 2012.

[10] Hou, S.; Qui, R.C.; Browning, J.P., Wicks, M.C., "Target Detection with Linear and Kernel Subspaces Matching in the Presence of Strong Clutter," *2012 IEEE Radar Conference*, pp. 372-376, 7-11 May 2012.

[11] Browning, J.P.; Griffiths, H.D.; Baker, C.J.; Wicks, M.C., “On the Detection of Weak Targets that Exhibit Partial-Coherence,” *IEEE International Symposium on Antennas and Propagation and USNC-URSE National Radar Science Meeting*, 8-14 July 2012.

[12] Browning, J.P.; Baker, C.H.; Griffiths, H.D., “Generalized Low-Energy Coherence for Partially-Coherent Targets,” *2012 International Waveform Diversity and Design Conference (WDD)*, 22-27 January 2012.

[13] Lin, F.; Qiu, R.C.; Hu, Z.; Hou, S.; Browning, J.P.; Wicks, M.C., Cognitive radio network as sensors: Low signal-to-noise ratio collaborative spectrum sensing," *2012 International Waveform Diversity and Design Conference (WDD)*, Kauai, HI, 22-27 January 2012.

[14] S. Hou; Qiu, R.; Browning, J.P.; Wicks M.C., "Spectrum sensing in cognitive radio with robust principal component analysis," 2012 International *Waveform Diversity & Design Conference (WDD),* Kauai, HI, 22-27 January 2012.

[15] Qiu, R.C.; Wicks, M.C.; Li, L.; Hu, Z.; Hou, S.J.; Chen, P.; Browning, J.P.; , "Wireless tomography, Part I: A novel approach to remote sensing," *2010 International Waveform Diversity and Design Conference (WDD)*, pp.244-256, 8-13 Aug. 2010

1.6 Patents Resulting from this Thesis

[1] “Method and Apparatus for Heterogeneous Sensor, Heterogeneous Data Fusion.” Submitted December 2017.

2 Background

2.1 Literature Review of Current State of the Art

The purpose of this chapter is to induce the reader to current state of the art in radar target detection, and then to relate this background primer to open problems that are being addressed within this work. In reviewing the current state of the art, we typically focus on the detection of targets that have a large dynamic range at the sensor receiver in order to be able to more readily separate the signal from competing clutter, noise, and/or interference-a ratio, called the signal-to-noise ratio (SNR). Additionally, typical radio frequency (RF) sensors in operation today rely on the coherent integration of multiple return pulses, plus the destructive behavior of the statistically independent background interference environment, and the constructive behavior of the signal of interest to effectively increase the signal-to-noise ratio. This may require the sensor to observe the target for an extended period of time in order to effectively capture a sufficient number of pulses to integrate the target returns above the background interference environment.

The penultimate goal for this work is the development of mathematical tools and algorithms to realize distributed sensor data fusion. Initially considered in this thesis are pre-detection fusion algorithms for a distributed radio-frequency network, as well as bespoke algorithms for the detection and ranking of over-resolved targets. Another secondary goal of this thesis is to deduce target phenomenology that is not readily captured by a single sensor in the traditional SNR sense. This may be due to the fact that the partial coherent track of a target is less than that required to integrate the signal above the noise floor (under sample support constrained scenario), or this may be due to the fact the signal is weak in the case of an extended target with respect to the surrounding environment-thereby inhibiting the sensor from detecting the presence of the extended target. This will result in the target phenomenology being hidden.

For the case of a weak extended target, the use of multiple distributed radio-frequency sensors, will result in more data being captured, with each of these particular distributed sensors looking at an extended target structure from multiple unique look and target pose angles, and fusing the resultant collected data in an intelligent adaptive manner. In the case of an extended target that is weak in any one observational sensor, the resultant eigendecompositon of the pre-detection

fusion process will reveal non-dominant eigenvalue behavior, thereby providing an indication that the actual signal is spread out amongst all the available imperfect basis functions [1] and [2]. The formation of appropriate detection and ranking algorithms for distributed sensing networks should permit the target to be recovered, even with the signal not being dominant compared to the environmental clutter plus noise [1]-the so called *weak target case*.

This thesis seeks to analyze the impact of integrating target echoes in the *angular domain*, to determine if better detection and ranking performance is achieved through the use of a distributed sensor network.

2.2 Detailed Literature Review Overview and Relevancy to the United States Air Force

The following detailed literature review focuses on several salient research areas within the more general field of remote sensing. An effort has been made by the author to provide as complete an overview as necessary for the reader to become familiar with previous research topics and subsequent results, as befitting the *new contributions* presented in this thesis. Whilst, by no means exhaustive, the proceeding sections provide an abbreviated account of the author's journey from an understanding of the current state-of-the-art, and to the identification of potential shortfalls within published results that are germane to the research addressed within this thesis.

Initially, we turn our focus towards the general problem of target detection using mono- and bi-static, and netted radar systems. The foundation of radar signal processing is the *detection* of a target and, deducing from time-delay, the distance to that detection target. As target detection for a network is the focus of this research, this background primer is considered required background material.

Next, attention is given to the concept of extended target objects. In addition to *detection* of a target, the detection of a target comprised of multiple scattering centers is another area of focus for this thesis. In fact, extended target objects give rise to the development of the various *recursive ranking* algorithms that are introduced within this thesis.

However, up to this point, all current state-of-the-art is still focused primary on problems encountered by *monostatic* radar systems-i.e. those sensors that detect single targets with the same transmit and receiver aperture, see figure 2 [81]. However, as our focus is on the detection of range-extended targets via a

distributed sensor network, a review of the foundations of *bistatic radar* (a single transmitter and single receiver that are no longer co-located in space-time),

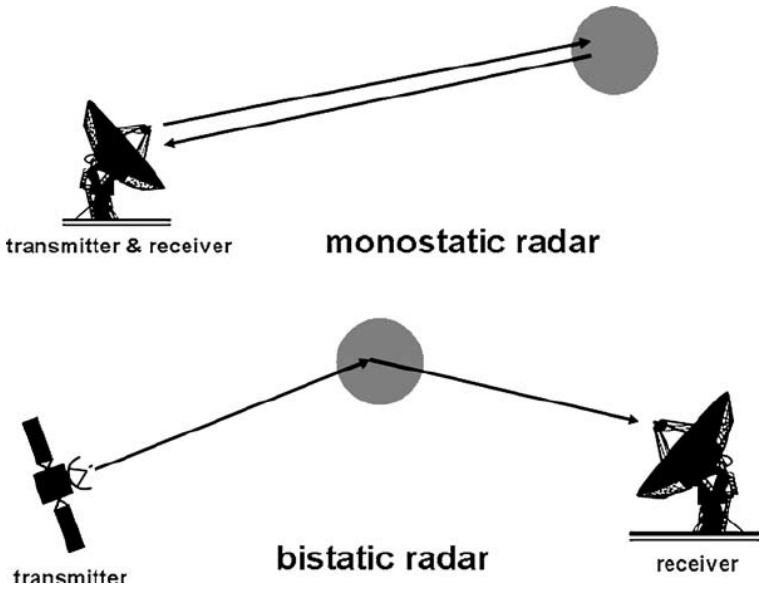

Figure 2: Monostatic vs Bistatic Radar

and *netted radar* (a method of multilateration leveraging more than one transmitter and more than one receiver, often non-collocated) is considered essential source material for the algorithms developed in Chapters 4 and 6, see figure 3 [82].

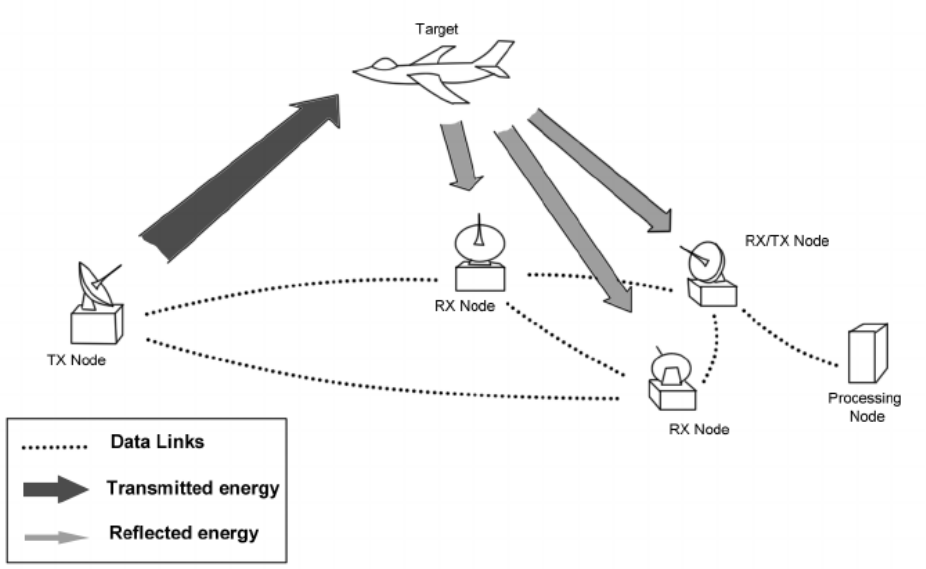

Figure 3: Netted Radar Example

The aim of this work is to provide a mathematical framework and initial roadmap into the future of the distributed and layered sensing paradigm. This roadmap is one developed by the author based upon observations and the ever-changing landscape of USAF ISR initiatives. More importantly, this roadmap serves as a outline of a research and development guide to allow the interested reader to discover and make their own contribution to the future of distributed and layered sensing, and potentially those priorities of the USAF. To that end, the following

figure also helps to guide our discussion as to where this work fits into the larger aim of current autonomy and cognitive sensing initiative, leading to the eventual goal of contextual sensing and dynamic/predictive sensing. Shifting the reader from traditional monostatic sensing to sensing involving a multitude of sensors eases the technical transition to the concepts of distributed sensor networks, which form the basis for the detection and ranking algorithms developed within this thesis.

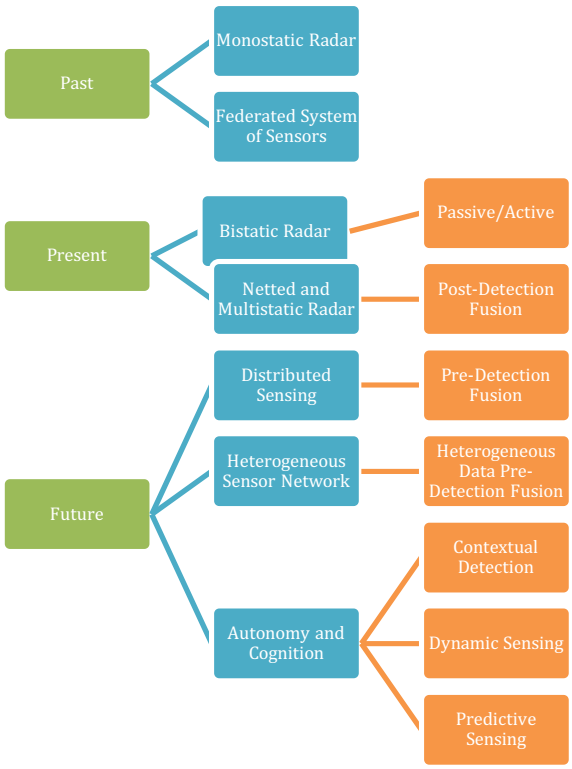

Figure 4: Roadmap to the Future of Autonomous and Cognitive Sensing

Following the discussion on past and present radar system topologies, a primer on adaptive signal processing serves to round out current state-of-the-art by introducing to the reader to methods researchers have developed to increase the detection performance of mono- and bi-static sensor, in terms of its detection performance. This review of adaptive signal processing methods also shows the extent to which previous generations of sensor and sensor systems have been enhanced to overcome their architectural limitations, and permits a fairer comparison of newly introduced algorithms of Chapters 4 and 6, with adaptive signal processing algorithms more familiar to the average reader of this work.

Having covered sensor topologies and adaptive processing schemes, there is a brief introduction to the concept of target and target modeling, as well as a more in-depth description of the target model used throughout this work to test the efficacy of the proposed detection and associated ranking algorithms. Attention is paid to common assumptions made to develop target models, and what

assumptions were chosen to develop the target model of this work. Finally, we cover the proposed distributed sensor network topology, as well as its associated communications topology, and the role of the fusion center as it pertains to the processing of data from the distributed sensing network. The need to move beyond the requirement for *a priori* knowledge of the target provides the necessary impetus for this work, and its relevancy to the current needs of the United States Air Force.

2.2.1 Single Target Detection

Current paradigms in receiver design and target detection are based upon the long-standing requirement for a single target signal to exceed the surrounding environment [see 3 and 4 and the references therein]. Emphasis is placed on the detection performance of radar systems, wherein the detection algorithms of targets are modeled as point-source targets. Particular bounds on the ambiguity of range-Doppler measurements for sensors systems with respect to point-source targets, are described in the vernacular by variations of Woodward's ambiguity function [5]. Suitable attention has been paid to the point target case, but not to the case in which the target is best described by a set of scattering sources; the so-called *extended target* case. This limitation on requirement for point-source targets causes information decimation on over-resolved targets by collapsing the detected phenomenology into a single singular value. An attempt has been made in this work to demonstrate the utility and benefit of detecting and ranking an over-resolved target, but showing the successful recovery of multiple scattering centers; whose recovery could be leveraged by subsequent algorithms for parameter estimation or target identification algorithms.

2.2.2 Detection of Extended or Over-Resolved Targets

Traditional signal processing methodologies seek to reconcile the apparent disparity in reflectivity profiles of scene clutter and target reverberations, thereby exploiting variations in the signal-to-clutter plus noise-ratio (SCNR) to determine target detections and parameter estimation. However, not all targets of interest are best described as a point-source target. For the case of a system possessing a high-resolution sensor, the illuminated target under observation may more aptly be described as an extended target structure. Extended target structures are going to occupy multiple adjacent range bins in a sensor receiver. For this case, the

extended target may possess spectral characteristics that are similar to the illuminated scene clutter, foiling the ability of current adaptive signal processing algorithms to detect or estimate target parameters. In [6] a method is proposed for the scattering center extraction of extended targets using a linear autoregressive-model, assuming the complex reflectivity profile of the extended target structure is known; leading to a unique method of formulating reduced-noise target models with application to automatic target recognition (ATR). In [7] a method is proposed to deduce a detection and subsequent angle estimation process for an extended target structure, including a derivation of the maximum likelihood estimate for the direction-of-arrival information of the over-resolved target structure presented. Both [6] and [7] assumed that some level of *a priori* information was available for the over-resolved target under observation. In [8] the adaptive detection problem for an extended target structure embedded in Gaussian noise is presented with the covariance matrix being unknown; although, secondary target-free training data was assumed, the resulting detector relies on a formulation of the generalized-likelihood ratio test (GLRT), with the constant false alarm rate (CFAR) property being preserved, with respect to the unknown quantities. Vespe, et. al. in [9] utilize a combination of multi-frequency (MF) and multi-perspective (MP) to determine the role of frequency and look-angle for target information content; in MF, a large bandwidth waveform is transmitted at a target over the range of 1-40GHz to analyze the variation in target information content versus frequency diversity, whilst the information content of a target is analyzed with the sensor illuminating the target under observation from various azimuthal directions. The conclusion drawn in reference [9] states the information content of a target under the MF scenario is more robust than that of the MP case, a result that is both intuitive and satisfactory (see [10]). Therefore, the use of a MF target classifier for automatic target recognition guarantees acceptable performance with a coherently reconstructed reflectivity profile since the center frequency of the transmitted high bandwidth waveform can be chosen randomly. However, the use of MP within a classifier requires *a priori* knowledge of target kinematics in order to be robust, and thus, is more generally useful for the purpose of providing independence of target information to a classifier algorithm.

In this work; however, we seek to formulate a pre-detection fusion process in combination with non-parametric and concentration of measure detection and ranking algorithms, that do not require *a priori* knowledge of the extended target.

Further, the detection and ranking algorithms based upon concentration of measure maths are shown to be robust to non-isotropic over-resolved target reflectivities, as well as weak targets with negative signal-to-noise ratios at the detector. In this regard, this work improves over state-of-the-art by allowing the distributed sensing network to achieve detection performance in challenging signal-to-noise ratio regimes in which no prior knowledge may be available on the targets, or the surrounding environment in which they operate.

2.2.3 Detection Using Bistatic and Netted Radar Systems

Starting with his seminal work in [11] and [12], Willis and Griffiths reintroduced to the radar community the concept of bistatic radar and applications (both past and present). In [12] bistatic radar is introduced as being a radar with two antennas, at geographically disparate locations, in which one is for transmission and the second antenna is for reception. In general, bistatic radar could be generalized to the case of multistatic radar, in which *N* transmitters are located in geographically separate locations from *M* receivers. Bistatic and multistatic radar systems can be used for target states estimation-target position, velocity, and acceleration, to name a few-utilizing multilateration, or the simultaneous use of range-Doppler data from the spatially overlapping areas of coverage for the multistatic radar system. Bistatic radar can be thought of as both active and passive; in active form the transmitter is dedicated and all parameters of the transmit waveform are controlled and known *a priori*, whereas in passive bistatic radar, the signal captured by the receiver can be any radiator of opportunity. Another consideration for passive bistatic radar is the imperfect *a priori* information regarding the transmitter of opportunity, which leads to a further complication during target detection and parameter estimation of the illuminated target structure. A few salient points of discussion regarding the efficacy in using bistatic radar configurations for target detection and parameter extraction [13] rely on fundamental advantages posed by the bistatic configuration: bistatic cross-section, receiver immunity from jamming threats, interferometric methods between the transmitter and receiver antennas results in high azimuthal discrimination. To highlight a few of those points presented in [13], the bistatic radar cross-section (RCS) of a target is generally larger, due to the inherent bistatic configuration illuminating a given target pose-angle and receiving from a different look-angle than the transmitter. Thus, bistatic radar has the potential to perform better in the presence of low-RCS targets, aiding target detection; however, this

assumption is valid as the monostatic RCS is assumed low, while a bistatic target RCS is assumed larger. Parameters that are commonly extracted from a given target skin return are those of range, velocity (Doppler), and direction of arrival (DOA); by using the receiving and transmitting as an interferometer, accurate azimuthal DOA of a target under illumination is possible. Also highlighted in [13] is the role of transmitter waveform selection in determining the role of bistatic radar system performance. To this end, a series of work funded by the Rome Research Laboratory are surveyed to determine the role of the ambiguity function in determining system bistatic radar performance. In [14], germane to the topic of target detection is the determination of the correct reference point in which the calculations for target range and velocity are based; in this respect, the bistatic ambiguity function is unique for each point of reference of the bistatic radar system. Further, the bistatic configuration has a drastic effect on both the resultant bistatic ambiguity function (BAMBF) and parameter extraction. Reference [15] presents a more detailed mathematical framework for the derivation of the BAMBF, with a new result indicating that for certain bistatic geometries, delay and Doppler parameters may fall within the ambiguity function's null regions. For [15], the waveform utilized had a Gaussian pulse envelope, indicating that even with a simple waveform class, the BAMBF is a challenge to derive and only unique for a given bistatic configuration and given reference point. Greco et. al. in [16] took the derivation of the BAMBF further, utilizing a linear-frequency modulated (LFM) waveform and formulated the Cramer-Rao lower bound (CRLB) for the target delay and velocity parameters; the results indicated that the CRLB for the bistatic radar scenario is nearly always higher than for the monostatic radar case. Typically, the clutter environments for a bistatic radar appear nonstationary, complicating the requirements on an adaptive radar receiver processor to detect and estimate parameters of a target under illumination. This issue is addressed in [17], where the issue of reducing the clutter-to-noise (CNR) ratio of a bistatic radar system is considered via space-time adaptive processing (STAP). Generally, the estimation of the clutter covariance matrix determines the effective system response in STAP, since the clutter is nonstationary for the bistatic radar system, a localized method of estimating the clutter covariance was proposed and shown to increase system performance by increasing the signal-to-noise ratio (SNR).

In this work, every sensor in the distributed network is a transceiver, and as such, observes the angle from a multitude of angular ambits that are well in excess

of a standard bistatic, or even netted radar system. This increase in *angular diversity* permits a large cross-section of angular radar cross section measurements to be taken of the target under observation, increasing the likelihood that a larger RCS reflection is captured by one of the many receiver nodes comprising the distributed sensor network. Another aim of this work is to remove the requirement to engage in waveform optimization on transmit, for any particular sensor node within the distributed sensing network. In fact, only a single tone is transmitted and received by any one transmitter within the distributed sensing network. This push to narrowband RF operation permits the dual benefit of a simpler transceiver architecture, as well as reducing the computational complexity of the associated radio-frequency hardware.

2.2.4 Adaptive Signal Processing as a Means to Increase Performance of Legacy Mono- and Bi-Static Radar Systems.

In [17] the role of adaptive signal processing in suppressing clutter and increasing the effective signal-to-noise ratio was considered. There is a rich body of literature in the area of adaptive signal processing, with particular applications in the following discussion on radar adaptive signal processing and space-time adaptive processing (see [18] for an excellent tutorial on STAP).

Adaptive signal processing is defined with respect to the transmitter or the receiver, where transmitter adaptivity involves varying the transmit waveform, and hence is more commonly referred to in the vernacular as waveform diversity; conversely, receiver adaptivity involves methodologies for processing incident signal energy impinging upon the receiver for use in target detection and parameter estimation algorithms. For waveform diversity, [19] discusses a method of space-time interference suppression for a distributed radar system possessing frequency diverse transmit waveforms, with the result that fine spatial resolution can be achieved if sufficient clutter suppression is achieved. Melvin, et. al. [20] describe recent advances in the field of adaptive signal processing to show how STAP could be implemented on an operational sensor, providing a more robust framework for implementation of STAP algorithms than those provided by the seminal results of Brennan, et. al. [21 and 22]. Exploiting mathematical theory to aid in developing solution sets to common radar problems (steering vector mismatches, sidelobe interfering signals, and signal detection in colored Gaussian noise), [23] proposes a canonical technique for adaptive radar detection using conic rejection. The basic

premise of [23] is that by reformulating the radar detection problem in the form of conic sets, the desired detector can be derived as a variation of the generalized likelihood ratio test (GLRT), and since the problem formulation simplifies to conic sets, the detector is invariant to minor mismatch errors in the receiver. Recently, there has been interest in using Bayesian methods to solve the radar detection problem; one of which is presented in [24] where a Bayesian two-step GLRT (B2SGLRT) detector is formulated based upon the need to detect a target in a Gaussian disturbance with unknown spectral properties. This B2SGLRT performs better in the presence of heterogeneous clutter than conventional radar detectors, especially for data starved scenarios.

A natural progression for adaptive signal processing is to move beyond the naïve receiver architecture and assume there is some *a priori* knowledge on the scene under illumination. This knowledge-based (KB) signal processing paradigm received a great deal of attention in recent years and is shown in a seminal work [25] to perform better, especially in challenging heterogeneous clutter scenarios. By exploiting knowledge of the scene under observation, even the B2SGLRT detector of the previous section is shown to have performance increases, achieving results that are close to the optimal detector, which assumes perfect knowledge of the clutter covariance matrix. In [26] a series of examples in which knowledge-aided (KA) signal processing strategies would be beneficial is surveyed; the need for KA/KB adaptive signal processing strategies would help to ensure more optimal performance in the heterogeneous operational environments in which sensors operate. Fusing the previous literature survey, [27] demonstrates the derivation of a KA signal processor for coherent radar detection of targets embedded in non-homogeneous environments; with the obvious result that the detector performs well for the case of target detection in dense heterogeneous environments.

Previously, the benefits of using a bistatic radar system for target detection and parameter estimation was discussed in some detail, with the generalized case of the bistatic radar-multistatic radar-being comprised of N transmitters and M geographically separate receivers. Germane to parameter estimation of an illuminated target is the detection of said target, [28] introduces a binary detector for a distributed system of sensors with [29] introducing a refined method of data fusion to increase the resolution of a multistatic radar system. In [30] the concept of netted radar sensitivity is addressed with the role of radar parameters, numbers,

locations, and specification of the transmit/receive nodes on system performance. The netted radar ambiguity function (AMBF) is discussed in [30] and the importance of sensor placement and target location are shown to affect the ambiguity regimes of the netted radar system. In order to minimize the ambiguities faced by a multistatic radar system, the transmitted waveforms need to be optimized; [31] describes waveform selection strategies for a multistatic radar system, with respect to the resultant AMBF. Finally, in [32] a more direct discussion on the role of waveform diversity in distributed radar systems is discussed, with a clear requirement for a cognitive sensor necessary to the success of a future distributed radar system.

The fusion of data emanating from so many disparate and heterogeneous systems, sensors, and data is critical to the success of any multistatic radar system, [33] discusses sensor fusion algorithms for use with heterogeneous sensor data.

Each of the previous sections deals with variations upon a theme: target detection and parameter estimation for a point-source target or over-resolved/extended target structure. However, there are two interesting cases to consider that inspired this thesis, and the eventual mathematical foundations of pre-detection fusion, and the bespoke detection and ranking algorithms of Chapters 4 and 6. The first of these two cases is that of the generalized inner product (GIP), which inspired the non-parametric algorithms of Chapter 4. Second, the concept of the low-energy coherence (LEC) optimum receiver, which inspired the algorithm development of Chapter 6, that results in the ability to detect targets at negative signal-to-noise ratios. These previous efforts have led to the results of this thesis, and aided in laying the foundational underpinnings of a mathematical framework that will serve to analyze heterogeneous sensor networks, develop pre-detection fusion rules, establish detection thresholds and assess system performances. To that end, the concepts of both LEC and the generalized inner-product (GIP) will be introduced.

In the seminal work by Hotelling [34], the concept of a generalization of the Student's T-test was introduced, which eventually was applied to the radar detection problem and became known as the GIP. The GIP improves the performance of a radar detector in the presence of non-homogeneous clutter. In [35] the GIP-based processing coherently combines the multiple returns from the doubly spread targets and adaptively rejects interference; thereby improving

performance and target parameter estimation. Previous works on the application of the GIP for extended targets can be found in [36] and [37]. Germane to each of these papers is the application of the GIP to detect an extended target structure by application of a shape template, versus the traditional route of target detection by range-Doppler bin. This approach to target detection is more effective, since the extended target will appear in range-Doppler bins to possess similar characteristics to the surround clutter.

An even more interesting case of target detection is discussed in [1], in which the target illuminated is captured by the receiver system, and a target covariance function is formed from either an imperfect basis or target signal energy that is below the noise threshold. This results in the signal energy being spread across the signal subspace (the eigen-decomposition of the maximum likelihood estimate of the target covariance matrix). Since the eigenvalue of the signal is less than, in all instances, the noise threshold, the optimal manner in which to recover the signal is to form the LEC receiver. An early work by Bucklew [21] looked at the detection of a point-source target under LEC conditions, however, for the operational environment, sensor systems comprising a distributed layered sensing paradigm will be engaging extended target structures possessing both unknown location and kinematics. The GIP has been shown [35-37] to be effective, even for the case of a mismatched target template. For a sensor system to be considered robust, the target detection will need to be invariant with respect to both the target covariance function (i.e.-both known and unknown target covariance) and the noise environment (i.e.-both white and colored Gaussian noise).

In an attempt to push the boundary on current state-of-the art, this thesis focuses on the pre-detection fusion process in combination with non-parametric detection and ranking algorithms to develop the mathematical foundation for both: heterogeneous sensor heterogeneous data fusion; and post-parametric signal processing. This latter point is extremely important for heterogeneous sensor heterogeneous data fusion, as each sensor and data type may have its own unique set of corruptive noise and clutter distributions that would have to be accounted for in current sensor fusion schemas. Under our non-parametric detection and ranking algorithms, developed within Chapter 4, there is no requirement to understand, or even have *a priori* information on the underlying corruptive processes present in the system or environment.

2.3 Of Targets and Target Models

The target backscatter is assumed to be comprised of the primary components: (1) noise; (2) clutter; (3) and target. There are also higher-order effects that are typically not assumed, though multipath is generally one that has been considered previously, and factors heavily in the formulation of bistatic radar problems [80,92] Each component of the received signal is captured by the receiver and is the result of direct excitation by the transmit beam or the thermal noise of the radar hardware and radar/target environment. Now, the clutter and target echoes-radar is essentially an echolocation device-are the result of spurious emissions, assumed negligible, and direct excitation by the impinging electromagnetic energy on the target and its surrounding environment. The impinging electromagnetic radiation energizes the clutter environment and target structure inducing surface currents on the observational environment. This radio-frequency (RF) energy propagates across the target and clutter environment and is dissipated and reflected. Dissipation occurs when the material has a complex refractive index value, as do most real-world objects. Some dielectrics, especially those that are crystalline (i.e.-sapphire) or amorphous (i.e.-glass), generally possess only a real refractive index value and cause a refraction and reflection. The imaginary component of the complex index of refraction causes absorption and loss of energy. When the electromagnetic energy encounters a discontinuity, or induces a resonant behavior a portion of the RF energy is reflected. Since this reflection of energy is dependent upon the scene under illumination by the sensor, or network of sensors, there is some level-no matter how small-that is reflected in all directions, with some portion of that being directed to the sensor receiver(s). One interpretation of this phenomenon is to consider the illuminated scene of interest as being a virtual three-dimensional antenna, comprised of heterogeneous elements from dielectric-to-metallic. Since perfect electrical conductors (PECs) are just hypothetical constructs, the illuminated scene will always reflect less energy to the receiver than that which impinges upon it, and the surrounding environment, from the transmit sensor(s)-ie a conservation of energy problem.

For this work, the target is considered weak when compared to the noise and clutter environment in which the target exists. This target may be considered a small-sized finite object that occupies a single bin, or a large in the respect that the object occupies several adjacent range bins. Further, we will only consider targets that are stationary, removing the Doppler component from the reflected

target echoes. Now, a target that is small relative to the size of a range bin is considered, theoretically, as a point-target; typically modeled, or assumed, to be an infinitely small sphere of some finite radar cross section (RCS) that may be constant, statistically varying, angularly selective, and/or frequency selective (i.e.-dispersive). Should the point target assumption be violated, we can consider the case of a target that occupies more than one adjacent range bin. We refer to this as a range-spread, or as in [1] singly-spread, case.

The implications for a target that violates the point target assumption cannot be overlooked. First, the major cornerstone of radar target detection, analysis, and mathematical foundation are considered from the standpoint of a point-target-a theoretical construct consisting of an infinitesimally small sphere of finite sized reflectivity. Indeed, to have a target that is a continuum is a challenge for the radar designer. How a large hard-body target is typically modeled at present is under another assumption referred to as the *salient feature* analogy. In this case, the *salient* feature is considered to be a point of stationary phase on the target body that is persistent for some viewing angle. This salient feature is typically modeled as a point in Cartesian coordinates with a given value of reflectivity from near-zero (an RF absorbent material) to infinity (a PEC). Additionally, for a modern radar system, the higher the signal power is when compared to the surrounding environment and noise, the easier the declaration of target present is to achieve. This is true as most methods of target detection that are in use presently are based upon a threshold test, wherein a null hypothesis is referenced to power level that is sans-target, whist the alternative hypothesis is referenced to a power level that exceeds the null hypothesis power level.

$$H_0: n(t) \tag{2.1a}$$

$$H_1: s(t) + n(t) \tag{2.1b}$$

Practically speaking, this threshold is represented by a *threshold statistic,* γ, which represents the statistical test, $\gamma \lessgtr_{H_1}^{H_0}$. Now, should the target actually occupy multiple range bins, one method to extract a point approximation of a target is to make use of the salient features of the target. These salient features are also typically the strongest, most dominate, scattering centers of the extended target object. Each scattering center is defined by a Cartesian coordinate and a complex amplitude corresponding to the associated reflectivity of that location on the given target structure. For the remainder of this work, the target considered is comprised of a trio of spheres that have an assigned Cartesian location and associated

reflectivity. The value of the reflectivity is arbitrary, and constitutes a method by the author to force a condition on the bespoke detection and ranking algorithms to determine the presence of a stronger to weaker reflector comprising the modeled extended target body. Extensions of this work will replace the arbitrary spherical point targets with dielectric spheres to assess the impact on detection and ranking efficacy. Below is a table of the target scattering centers and their associated reflectivity, and an associated plot of their generalized locations with respect to the sensor network considered in Chapters 4 and 6 is shown in Figure 4.

Table 1: Scattering Center Parameters

Scattering Center	Reflectivity Coefficient (ρ)	Scattering Center Location (x, y)
1	$\rho = 2.00$	$[5, 0]$
2	$\rho = 1.75$	$[-2.5, 4.33]$
3	$\rho = 1.50$	$[-2.5, -4.33]$

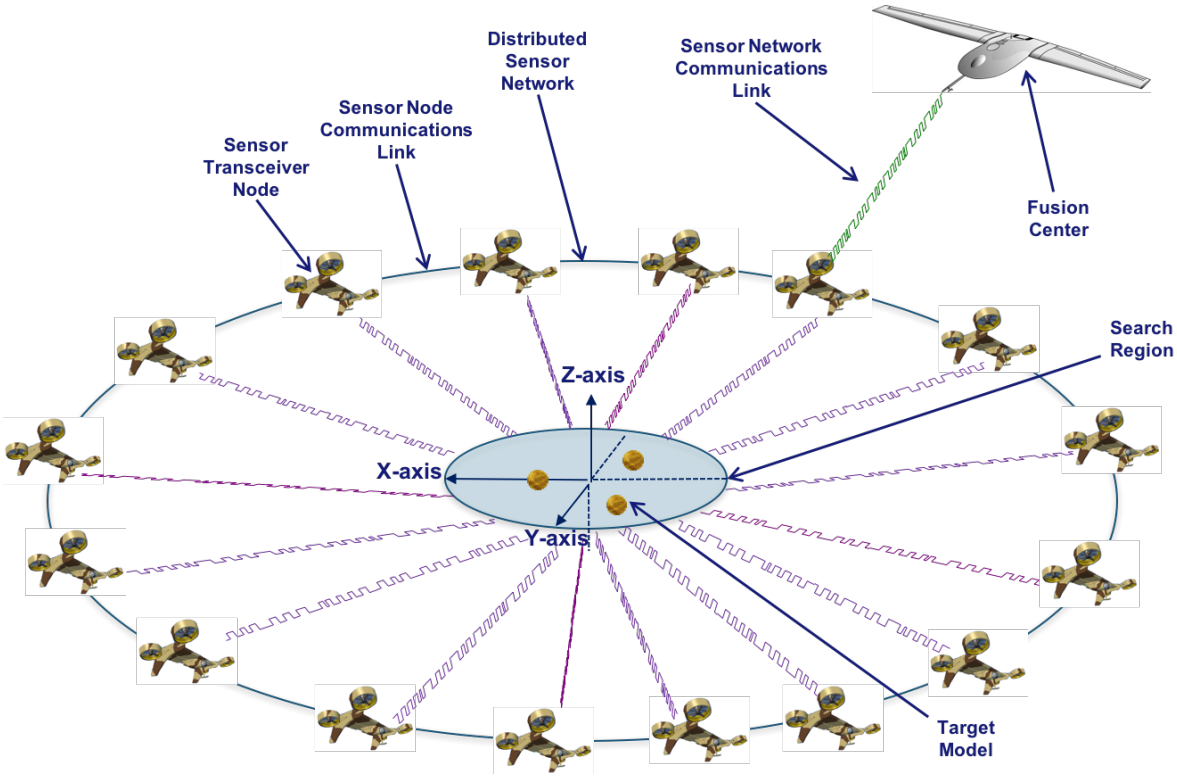

Figure 5: Generalized Distributed Sensor Network Topology

We have discussed previously the need to move beyond the requirement to have *a priori* knowledge of the target covariance in order to achieve detection performance at low-SNR levels in Section 2.2.4. Continuing on that theme, the target model considered for this work is comprised of a trio of spatially separated dielectric non-magnetic spheres; the aim of which is to simulate salient scattering features of an extended target body. This canonical target model also serves to

limit ambiguous detection results, to allow for the assessment of efficacy of proposed distributed sensor network detection algorithms. Typical target models are assumed metallic, so as to minimize the complexity of the electromagnetic waveform interaction to the surface boundary conditions. This permits ready first-order effects to be simplified into a reflective amplitude scaling of the incident electromagnetic wave in the direction of the transmitted receiver, for a spherical or flat-plat target model. Whilst not considered within this work, research has been conducted with Generalized Method of Moments code to analyze the higher order interactions of a dielectric spherical body and an impinging electromagnetic wavefront; resulting in multiple scattering and reflection phenomenologies that greatly increase the complexity beyond the surface boundary layer of the target body. This higher order interaction is more necessary for imaging (via backprojection algorithms) and target material composition (estimating the permittivity and permeability to estimate the type of dielectric present), whilst impacts on detection performance are still under investigation to date.

2.3.1 Moving Beyond the Requirement for *a priori* Knowledge

The aim of this work is to develop a *pre-detection fusion process* for a *distributed sensor network topology*, and to enable the recovery of targets that are considered to have *low signal-to-noise ratios(SNR)*-or as introduced in Chapter 6, *weak* SNRs; to that end, we seek to build upon prior work on netted radar, the low energy coherence (LEC) receiver paradigm [1], and aspects of adaptive signal processing. Further, the penultimate goal of this work is to lay the mathematical foundation for the realization of an algorithm for the fusion of heterogeneous data from heterogeneous sensors, [see Chapter 8 for further details]. We begin by considering a generalized distributed sensor network topology, epitomized by Figure 5, and build upon this architecture to realize the *pre-detection fusion algorithm*, introduced in Chapter 3. The sensor network topology of Figure 4 is that of a *ring node* structure, commonly used in telecommunications. The role of the apparent fusion center is twofold: (1) conceptually, the fusion center serves as the processor of the bespoke detection and ranking algorithms of Chapters 4 and 6; (2) practically, it serves to lower the required complexity of the sensor nodes comprising the distributed sensor network.

In this work, each sensor node is little more than a radio-frequency transceiver operating on a single tonal frequency. This serves to introduce some

realism behind the rationale for using large numbers of sensors to accomplish a germane detection and ranking process. Additionally, a tonal transceiver is easy and low-cost, which allows for the realization of this concept with attritable unmanned aerial systems (UAS), loosely coordinating with one another through a standard telecommunications network topology. In fact, multiple programs within the United States Department of Defense are investigating the potential utility of large scale, low-cost, attritable sensor systems to achieve a multitude of critical intelligence, surveillance, and reconnaissance (ISR) roles, normally reserved for more capital manned and unmanned systems. This work seeks to add another use case to the role of distributed sensor networks for the United States Air Force ISR mission.

Finally, the aim of this work is to build upon the concept of the LEC receiver concept, by enabling detection without the requirement to know the target covariance function *a priori*. Central to the role of any sensor network topology, single or otherwise, is the need to find, fix, and track targets of interest in a wide-variety of real-world environments; many of which contact potential targets of interest that are not characterized *a priori* and may require further investigation by a trained analyst. The LEC receiver concept is intriguing and germane to many USAF ISR mission sets, but the requirement to know the target covariance runs counter to practicality of that paradigm. Algorithms introduced in Chapter 4 and 6 for the detection and ranking of targets that are considered low SNR, or weak as defined in Chapter 5, permit the recovery and ranking of those targets with no requirement for *a priori* knowledge of the target objects. The efficacy of those algorithms, and their mathematical formulation lends their use to nearly all USAF mission sets, particularly those ISR scenarios in which the target(s) are challenging to find with currently fielded sensor technologies and architectures.

2.4 Relevancy of Thesis to the United States Air Force

This research is relevant to the United States Air Force within its layered sensing and cognitive radar/sensor initiatives. The asymmetric threat of the twenty-first century introduces stressing sensing conditions that may exceed the ability of traditional monostatic sensing systems to perform their required intelligence, surveillance and reconnaissance missions. In particular, there is growing interest within the United States Air Force to move beyond single sensor sensing systems,

and instead begin fielding and leveraging distributed sensing systems to overcome the inherent challenges imposed by the modern threat space.

The intended applications of this thesis research are relevant to the Air Force within its layered sensing and cognitive radar/sensor initiatives. The asymmetric threat of the twenty-first century places real-time constraints of seconds and not hours to detect and declare targets whether they are in space, air or on the ground. Images and human involvement are too slow and not feasible given our deployment on many fronts combined with the needs for space surveillance, our border patrols, home land security, and law enforcement needs.

3 Introduction to Target Detection from Monostatic Radar to Distributed Sensor Networks

3.1 Introduction

Having explored the beginnings of this work, and grounding in recent realities, it is now time to build the foundational theory necessary to understand the contents of Chapters 4 and 6. In particular, we start with the basics of radar detection theory, expanding to include how that changes when the target is no longer represented by a single isotropic-point source, and ending with an examination of Van Trees' *low-energy coherence* receiver paradigm; which strongly motivated the development of the low-signal-to-noise ratio detection and ranking algorithms of Chapters 4 and 6. The hope is that by leading the reader through familiar basics, and adding to that body of knowledge with other related mathematical principles, the bespoke algorithms of Chapters 4 and 6 are more intimately understood. In no way is this an extensive and comprehensive background theory section, but the rudiments presented henceforth should provide an adequate baseline for the interested reader to dive deeper, should they wish to, by following the trail of references throughout this section.

3.2 Radar Detection

Radar uses radio waves in the form of echo-location to detect the range of an illuminated object. The illuminated object may be a target of interest, a diverse clutter background, or some combination of both. There are number of references that cover the subject of target detection, see [1,3 and 38-41]. For most cases, the target detection problem is best described by a binary hypothesis test, which is shown below for completeness. The null hypothesis, H_0 represents the case where the received signal is comprised of noise. An alternative hypothesis, H_1 represents the case where the received signal is comprised of a signal plus noise. The role of the radar receiver is to determine if a signal is present, or not. This is equivalent to the receiver making a decision as to whether the null or alternative hypothesis is true, based upon observation of some number of samples at the receiver.

$$H_0 := n(t) \tag{3.1a}$$

$$H_1 := s(t) + n(t) \tag{3.1b}$$

The simplest detection problem is that of the single-point target in a single range cell, see Figure 6, using the binary hypothesis criterion in Equations (3.1a) and (3.1b). This also corresponds to the simple non-fluctuating, or Swerling 0 case, useful for describing the target reflectivity.

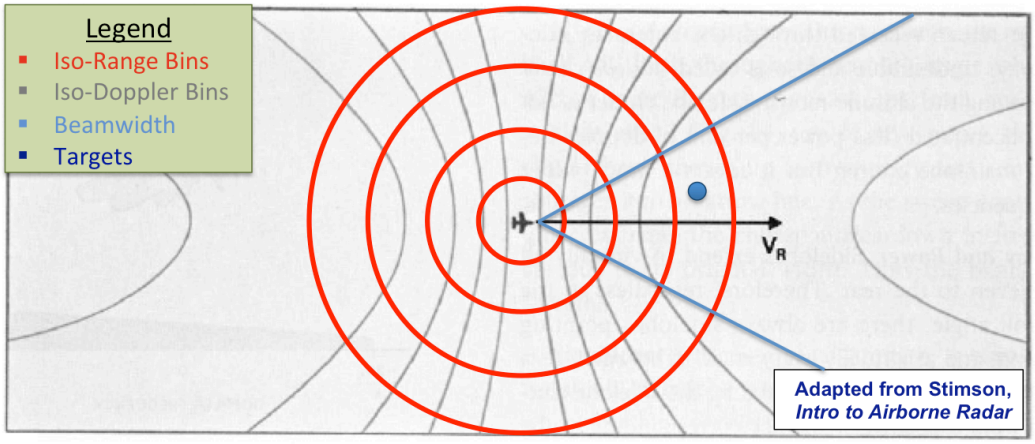

Figure 6: Single Point-Scatterer in a Single Range Bin

Traditional signal processing methodologies seek to reconcile the apparent disparity in reflectivity profiles of scene clutter and target reverberations, thereby exploiting variations in the signal-to-clutter plus noise-ratio (SCNR) to determine a target detection. However, not all targets of interest are best described as a point-source target. For the case of a system possessing a high-resolution sensor, the illuminated target under observation may more aptly be described as an extended target structure. Extended target structures occupy multiple adjacent range bins, see Figure 7.

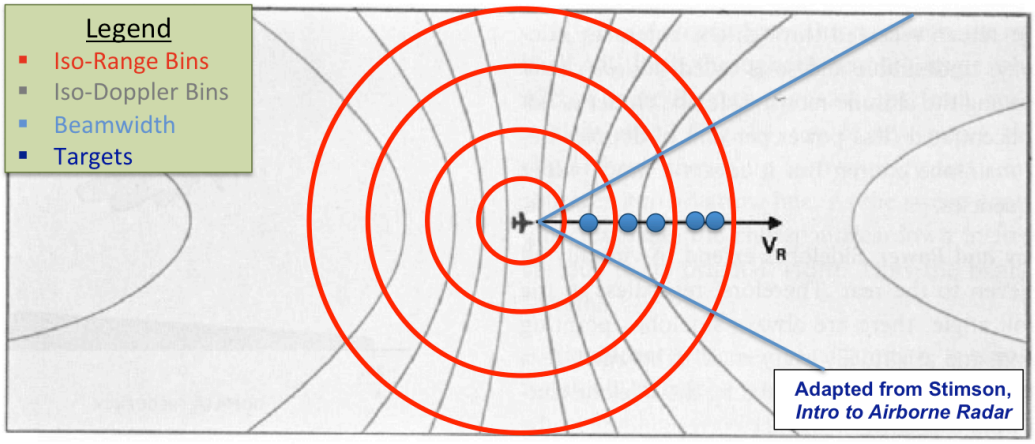

Figure 7: Range-Spread Target (Target with Multiple Scattering Centers)

In this case, the standard radar problem is understood to be one of a statistical decision-making process: a received signal is compared to some threshold with the goal to declare the presence when the threshold is exceeded, and to do the antithesis when the target is absent. From this vantage point, our detection and ranking algorithms introduced in Chapters 4 and 6 are still bounded by this fundamental statistical process. Let us re-examine the statistical decision theory behind the radar detection problem formulation.

3.3 Basics of Statistical Decision Theory

One method of approaching the detection problem is from a probabilistic framework that utilizes elements of statistical inference to make a decision as to whether a signal is present in the received signal or not. The theory of statistical inference is based on hypothesis testing. Recognizing that real-world data is corrupted to some degree by noise, hypothesis testing was improved by the incorporation of decision theory. The objective of statistical decision theory is to formulate a detection rule that operates on the received data to aid in the decision of which hypothesis is the best choice, based upon the received signal.

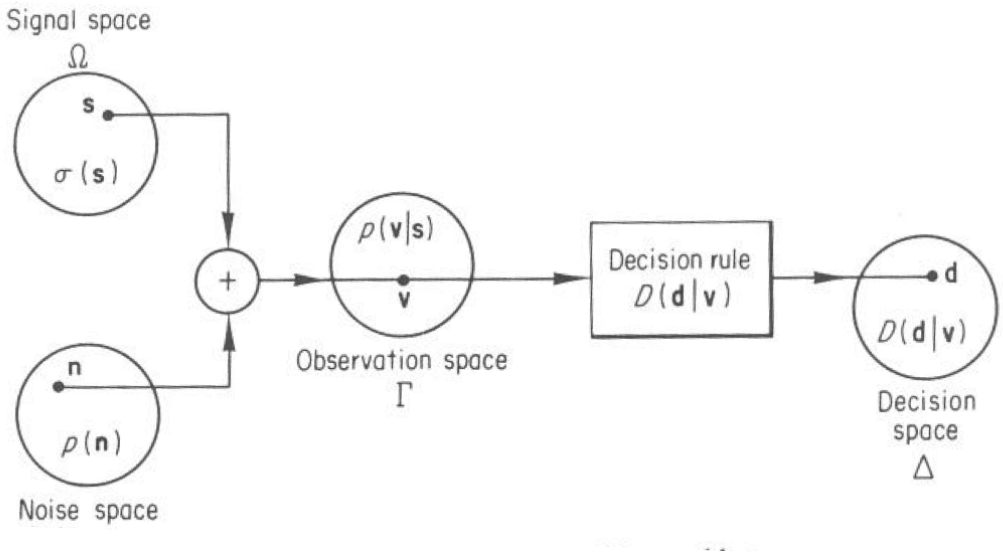

Figure 8: Statistical Decision Theory Diagram

The decision problem is best illustrated by Figure 8 shown above. The received signal arriving at the radar is the result of an echo from the environment that can be assumed to be comprised of noise and possibly a signal. The signal can be assumed to be a point in a signal space, Ω, composed of the class of all possible signal echoes, with each point in this space representing a waveform of a particular

combination of amplitude, phase, and frequency-shifting. When possible, a probability distribution, $\sigma(\boldsymbol{s})$ is assigned to a signal in Ω. Similarly, the noise space can be defined as being composed of a number of points, **n,** that describe all possible realizations of a noise process. Statistical properties of the noise are then captured by a probability distribution $p(\mathbf{n})$, much the same as in the case of the signal space.

The observed received signal, or echo, can be described by another space-dubbed the observation space, Γ-whose points **v** represent all possibly joint probability distributions of signal and noise echoes within a given period of observation. The conditional probability, $p(\mathbf{v}|\boldsymbol{s})$, is used to describe the frequency of occurrence of each of the members of the observation space. This can be shown graphically to be the equivalent of describing the traditional radar detection problem.

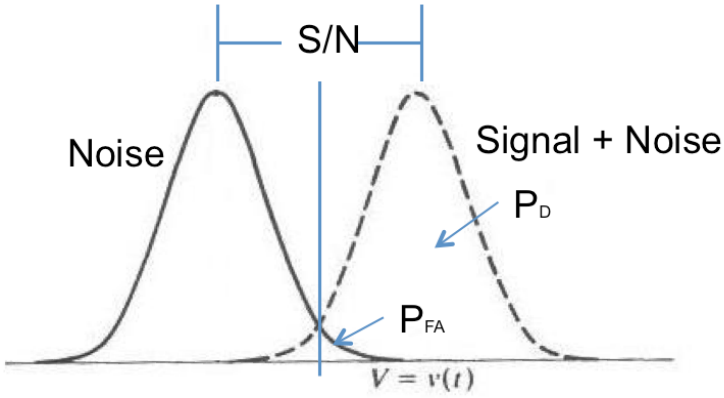

Figure 9: Traditional Radar Detection Problem

Following the observation space is the decision rule. The decision rule is a operator that maps a point in the observation space into the decision space. This operator is analytically shown to only be a function of the observed waveform, **v,** and the possible set of decisions, **d**. There is no explicit assumption of the signal, **s.** The decision rule, $D(\mathbf{d}|\mathbf{v})$, could be random or nonrandom decision rule; in most instances, the decision rule, or mapping operator is nonrandom.

After mapping the observation, **v,** from Γ into the decision space, Δ, the possible set of decisions is denoted by the variable **d.** Should the decision rule be viewed as a probability, the decision rule, $D(\mathbf{d}|\mathbf{v})$, describes the probability density of each point in Δ for each possible observed waveform **v.** In Figure, 9, the decision space essentially describes whether the observed waveform **v** is above rf below a threshold. For the detection problem, the decision space contains only two possible

points: signal present or no signal present. For the case where there may be multiple signals of interest, this decision problem can be generalized for any number, *N*, of signals of interest.

The fundamental issue for the decision problem is to determine an optimal operator to map the observation space, Ω, to the decision space, Δ. So, for the detection problem, the real challenge lies in determining some optimal decision rule, $D(\mathbf{d}|\mathbf{v})$.

In the remainder of this section, various aspects of the statistical decision theory problem are introduced. As the breadth of detection theory is quite considerable, only salient highlights are discussed.

3.3.1 Binary Detection

Binary detection is the most basic form of detection problem in which one of the two possible outcomes are possible: target present or target absent. From the previous section, there is assumed to be a signal space, Ω, and a noise space. The mapping operator for the observational space, Γ, is the hypothesis test given by the null hypothesis H_0 and the alternate hypothesis H_1,

$$H_0 := \mathbf{s} \in \Omega_0 \tag{3.2a}$$

$$H_1 := \mathbf{s} \in \Omega_1 \tag{3.2b}$$

Where the operator maps the observation space into two non-overlappoing decision space regions. From Equations (3.2a) and (3.2b), the two decision regions are spanned by Ω_0 where $\mathbf{s} = 0$, and Ω_1 where $\mathbf{s} \neq 0$. By defining the *a priori* probabilities of the observed signal, **v**, to be p for signal present and q for signal absent, the probability density function for the signal, $\sigma(\mathbf{s})$ is defined as

$$\sigma(\mathbf{s}) = \boldsymbol{q}\delta(\mathbf{s} - 0) + \boldsymbol{p}w(\mathbf{s}) \tag{3.3}$$

Now, there are four possible outcomes for a binary hypothesis test, a correct decision for signal present or signal absent, and an incorrect decision regarding the presence or absence of a signal. Declaring a signal present when the signal is absent is referred to as a false alarm, and is denoted by the symbol α. Deciding there is no signal present when there is a signal present is called a missed detection and is denoted by the symbol β. Referring to the binary detection problem from a cost function perspective, the costs of correct decisions are

$$C_{1-\alpha} = C\left(\mathbf{s}\epsilon\Omega_{0;d_0}\right) \tag{3.4a}$$

$$C_{1-\beta} = C\left(\mathbf{s}\epsilon\Omega_{1;d_1}\right) \tag{3.4b}$$

The cost function analysis of the binary detection problem is akin to creating a

decision rule operator that minimizes a cost function, which corresponds to minimizing the number of false alarms and missed detections. In this respect, the cost of a correct decision is

$$C_{1-\alpha} = C_{1-\beta} = 0 \tag{3.5}$$

The cost function for the binary detection problem is referred to as the loss function, and the goal for creating an optimal decision rule is to minimize the loss function. The loss function is found to be [42]

$$L(D,\sigma) = \int_{\Omega} L_C(D|\mathbf{s})\sigma(\mathbf{s})d\mathbf{s} \tag{3.6}$$

where the function L_C is the conditional loss function for all possible decisions **d** for any given **s** and decision rule D. Mathematically, the conditional loss function can be shown to be [42]

$$Lc\ (D|\mathbf{s}) = E_{\boldsymbol{d}|\boldsymbol{s}}\ [C\ (\mathbf{s},\mathbf{d})] \tag{3.7}$$

which can be expanded in terms of conditional probabilities such that [42]

$$L_C\ (D|\mathbf{s}) = \int_{\Gamma} p\ (\mathbf{v}|\mathbf{s})\ d\mathbf{v} \int_{\Delta} C\ (\mathbf{s},\mathbf{d})\ D\ (\mathbf{d}|\mathbf{v})\ d\mathbf{d} \tag{3.8}$$

The loss function for the binary detection problem is given by the expression [16]

$$L\ (D,\sigma) = \boldsymbol{q}\alpha C\alpha + \boldsymbol{p}\beta C\beta \tag{3.9}$$

where α is the Type I error

$$\propto = \int_{\Gamma} p(\mathbf{v}|0)\ D(d_1|\mathbf{v})d\mathbf{v} \tag{3.10}$$

and β is the Type II error

$$\beta = \int_{\Gamma} p(\mathbf{v}|\mathbf{s})_{\mathbf{s}}\ D(d_0|\mathbf{v})d\mathbf{v} \tag{3.11}$$

From Equation (3.11) the type II error probability is averaged with respect to the a priori distribution of the signal.

3.3.2 Bayes' Decision Criterion

Bayes' decision criterion results from the minimization of $L\ (D,\sigma)$ and is best known for the likelihood ratio that results from the formulation of the decision rule. This likelihood ratio decision rule is nonrandom and can be written in the form of a generalized likelihood ratio

$$\ell(\mathbf{v}) = \frac{\mathbf{p}p(\mathbf{v}|\mathbf{s})_s}{\mathbf{q}p(\mathbf{v}|0)} \tag{3.12}$$

Since the decision space, Δ, contains only two regions, the minimization of $L\ (D,\sigma)$ for the signal absent decision is

$$D_{\boldsymbol{\beta}}\ (d_0|\mathbf{v}) = 1 \tag{3.13a}$$

$$D_\beta\ (d_1|\mathbf{v})\ =\ 0 \tag{3.13b}$$

The inequality resulting from this condition is [42]

$$\mathbf{p}C_\beta p(\boldsymbol{v}|\boldsymbol{s})_\mathbf{s}\ <\ \mathbf{q}C_\alpha p(\mathbf{v}|0) \tag{3.14}$$

The minimization of *L*(D, sigma) for the signal present decision is

$$D_\beta\ (d_0|\mathbf{v})\ =\ 1 \tag{3.15a}$$

$$D_\beta\ (d_1|\mathbf{v})\ =\ 0 \tag{3.15b}$$

with the associated inequality being [42]

$$\mathbf{p}C_\beta p(\mathbf{v}|\mathbf{s})_\mathbf{s}\ >\ \mathbf{q}C_\alpha p(\mathbf{v}|0) \tag{3.16}$$

The threshold for the Bayes decision criterion in the decision space equates to

$$\gamma = \frac{C_\alpha}{C_\beta} \tag{3.17}$$

3.4 Where It All Started: Low-Energy Coherence Receiver

The concept of the low-energy coherence (LEC) receiver was first proposed by [43-45] in regards to the signal detection problem and [46-47] for use in radar astronomy. At first glance, the low-energy coherence case may seem uninteresting or of limited utility, but there are a number of scenarios in radio-frequency sensing that give rise to low-energy coherence cases; ranging from radio-astronomy, to sonar, and many salient detection problems in radar and remote sensing. In [38] the LEC receiver is developed for the case of a point and extended target, under white Gaussian noise conditions for a monostatic sensor. We propose to develop a mathematical framework for heterogeneous sensor fusion, target detection and parameter estimation that is based on the Low-Energy Coherence (LEC) optimum receiver design. This framework will serve to analyze heterogeneous sensor networks, develop pre-detection fusion rules, establish detection thresholds and assess system performances.

The low-energy coherence scenario is best understood from the standpoint of the signal subspace of the received target echo. The target detection problem is based upon a simple binary hypotheses test

$$H_0: \boldsymbol{r}(t) = \boldsymbol{n}(t) \tag{3.18a}$$

$$H_1: \boldsymbol{r}(t) = \boldsymbol{s}(t) + \boldsymbol{n}(t) \tag{3.18b}$$

Initially, an unbiased maximum likelihood estimate of the target covariance is formed from a set of received signals from a monostatic sensor, such that the target covariance is found from

$$\boldsymbol{C}(r) = \frac{1}{k-1}\sum_{i=1}^{k}(\boldsymbol{x}_i - \bar{x})(\boldsymbol{x}_i - \bar{x})^T \tag{3.19}$$

where x_i is the *i*-th observation of the *k*-dimensional random (vector) variable and $\bar{x}$ is found from

$$\bar{x} = \begin{bmatrix} \bar{x}_1 \\ \vdots \\ \bar{x}_k \end{bmatrix} = \frac{1}{k}\sum_{i=1}^{k} x_i \tag{3.20}$$

and is the sample mean. Taking the singular value decomposition of Equation (3.18a) and (3.18b), the matrix, $\boldsymbol{C}(r)$ can be factorized into the form

$$\boldsymbol{C}(r) = \boldsymbol{U}\boldsymbol{\Sigma}\boldsymbol{V}^* \tag{3.21}$$

where $\boldsymbol{U}$ is a $k \times k$ unitary matrix, $\boldsymbol{\Sigma}$ is a $k \times k$ diagonal matrix with non-negative real numbers on the diagonal, and $\boldsymbol{V}^*$ is a $k \times k$ complex transpose unitary matrix. The diagonal elements of $\boldsymbol{\Sigma}$ are known as the singular values and are analogous, under certain conditions, to the eigenvalues found from the eigendecomposition of a covariance matrix, see [2] for more details. For the LEC condition to be true, each singular value along the diagonal of $\boldsymbol{\Sigma}$ must be small, compared to the noise level. This condition is given below

$$\lambda_i^2 \ll \frac{N_0}{2}, \quad i = 1, 2, \ldots, k \tag{3.22}$$

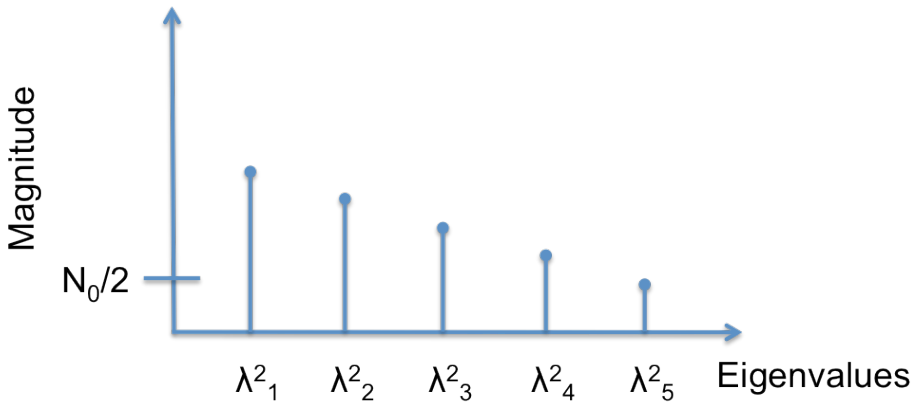

Figure 10: Eigenvalues for Positive Signal-to-Noise Ratio

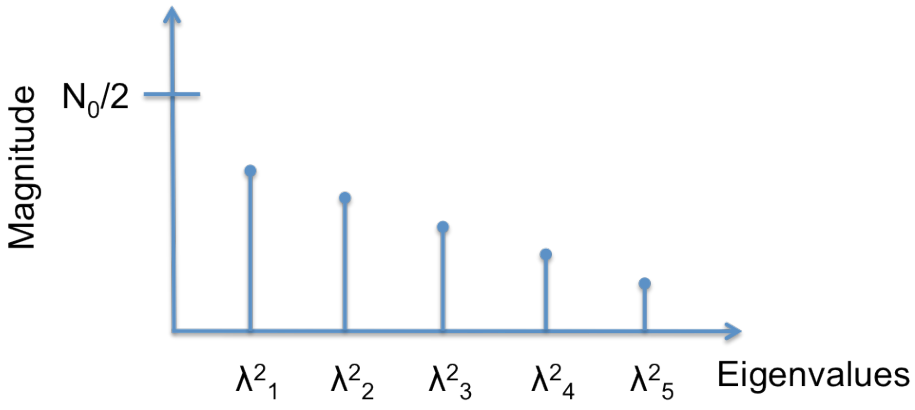

Figure 11: Eigenvalues for Negative Signal-to-Noise Ratio

Having considered the target detection problem for more classical cases where the signal is assumed larger than the noise in the observation space, attention is now focused to the detection of signals in the signal space that are weaker than the noise space variables. This additional constraint on the decision rule formulation was illustrated previously via Figure 11. Here the assumption is made that once the threshold statistic is determined, the probability of false alarm and the probability of missed detection are easily found from the following expressions

$$P_F \simeq P_F^{[1]} \triangleq e^{\left(\boldsymbol{\mu}(s)-s\boldsymbol{\mu}+\frac{\dot{x}^2\ddot{\boldsymbol{\mu}}(s)}{2}\right)}\text{erfc}_*\left(s\sqrt{\ddot{\mu}(s)}\right) \tag{3.23}$$

and

$$P_M \simeq P_M^{[1]} \triangleq e^{\left(\boldsymbol{\mu}(s)+(1-s)\dot{\boldsymbol{\mu}}(s)+\frac{(1-s)^2}{2}\ddot{\boldsymbol{\mu}}(s)\right)}\text{erfc}_*\left[(1-s)\sqrt{\ddot{\boldsymbol{\mu}}(s)}\right] \tag{3.24}$$

The function for the error function compliment, $\text{erfc}_*(x)$ is given as

$$\text{erfc}_*(X) \backsimeq \frac{1}{\sqrt{2\pi}}e^{-\frac{X^2}{2}},\ \ X \geq 2 \tag{3.25}$$

The low-energy coherence case starts with the basic binary detection problem

$$H_0: \boldsymbol{r}_i(t) = \boldsymbol{n}(t) \tag{3.26a}$$

$$H_1: \boldsymbol{r}(t) = \boldsymbol{s}(t) + \boldsymbol{n}(t) \tag{3.26b}$$

Noise, $\boldsymbol{n}(t)$, is assumed to be a white, zero-mean Gaussian process with spectral height, $\frac{N_0}{2}$, and the signal is assumed to be a zero-mean Gaussian process. The covariance function of the signal is found from

$$\boldsymbol{K}_s(t,u) = \sum_{i=1}^{\infty}\lambda_i^s\boldsymbol{\phi}_i(t)\boldsymbol{\phi}_i(u),\ \ T_i \leq t,u \leq T_f \tag{3.27}$$

The eigenvalues, λ_i^s, are the mean-square values of the i^{th} coefficient. Should the signal energy be spread across a large number of coordinates, and each of these eigenvalues are small when compared to the spectral height of the noise process, then this case is referred to as the low-energy coherence (LEC) case

$$\lambda_i^s \ll \frac{N_0}{2},\ \ i = 1,2,\ldots \tag{3.28}$$

From [38], the general decision rule gives the test

$$\frac{1}{2}\left(\frac{2}{N_0}\right)^2\iint_{T_i}^{T_f}\boldsymbol{r}(r)\boldsymbol{K}_s(t,u)\boldsymbol{r}(u)\text{d}t\text{d}u \gtrless_{H_0}^{H_1}\ \gamma \tag{3.29}$$

From the previous expression, the threshold function for the LEC case can be found to be, from [1]

$$\boldsymbol{\mu}(s) \simeq -\frac{s(1-s)}{2}\left\{\frac{1}{2}\left(\frac{2}{N_0}\right)\iint_{T_F}^{T_i}\boldsymbol{K}_s^2\,(t,u)\text{d}t\text{d}u\right\} \triangleq \boldsymbol{\mu}_{\text{LEC}}(s) \tag{3.30}$$

The bracketed term in equation (3.30) can be shown, under certain assumptions, to be the signal-to-noise ratio [1] and is defined by

$$d^2 \triangleq \frac{\left(E\left[l_R^{(1)}|H_1\right]-E\left[l_R^{(1)}|H_0\right]\right)^2}{\mathrm{Var}\left[l_R^{(1)}|H_0\right]} \tag{3.31}$$

where $l_R^{(1)}$ is found from

$$l_R^{(1)} = \frac{1}{2}\left(\frac{2}{N_0}\right)^2 \sum_{i=1}^{\infty} \lambda_i^s r_i^2 = \frac{1}{2}\left(\frac{2}{N_0}\right)^2 \iint_{T_i}^{T_f} \boldsymbol{r}(t)\boldsymbol{K}_s(t,u)\boldsymbol{r}(u)\mathrm{d}t\mathrm{d}u \tag{3.32}$$

The resultant error functions are

$$P_F \simeq \mathrm{erfc}_*\left(\frac{d}{2}+\frac{\gamma}{d}\right) \tag{3.33}$$

$$P_M \simeq \mathrm{erfc}_*\left(\frac{d}{2}-\frac{\gamma}{d}\right) \tag{3.34}$$

The receiver operator characteristics are easily found by varying the threshold parameter, γ.

3.4.1 Range-Spread Target Model

For this scenario, the target is composed of point scatterers assumed to occupy a number of adjacent range cells. This corresponds to an apparent spreading of the target returns over a number of adjacent range cells in our receiver. Under Van Trees' [1] low-energy coherence (LEC) receiver concept, a new formulation of Equation (3.35) is required to account for this range-spreading, necessitating the need for a unique implementation of the target covariance function. We begin by defining the range-spread target signal echo

$$\tilde{\boldsymbol{s}}(t) = \sqrt{E_t}\int_{-\infty}^{\infty} \tilde{\boldsymbol{f}}\,(t-\lambda)\tilde{\boldsymbol{S}}_R(\lambda)\tilde{\boldsymbol{f}}^*(u-\lambda)\mathrm{d}\lambda \tag{3.35}$$

where $\tilde{\boldsymbol{b}}_R$ is a random variable describing the spatial sample function for the range-spread target, and $\tilde{\boldsymbol{f}}(t-\lambda)$ is the time-shifted complex envelope function of the signal. Solving for the covariance function for the signal echo

$$\tilde{\boldsymbol{K}}_{\boldsymbol{s}}(t,u) = E_t\int_{-\infty}^{\infty} \tilde{\boldsymbol{f}}(t-\lambda)\tilde{\boldsymbol{S}}_R(\lambda)\,\tilde{\boldsymbol{f}}^*(u-\lambda)\mathrm{d}\lambda \tag{3.36}$$

with $\tilde{\boldsymbol{S}}_R \triangleq E\left\{\left|\tilde{\boldsymbol{b}}_R(\lambda)\right|^2\right\}$ is the target scattering function. From [1], the optimal receiver structure is shown in Figure 12.

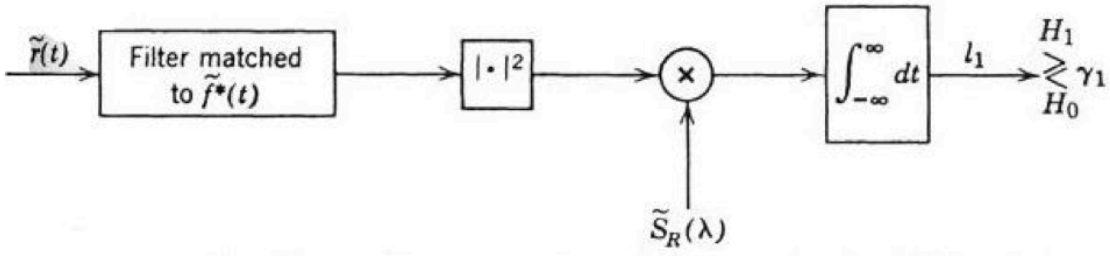

Figure 12: Optimal Receiver for Range-Spread Target

The corresponding likelihood ratio test for the range-spread target is, again from [38]

$$\ell = \frac{1}{N_0}\int_{-\infty}^{\infty} \tilde{\boldsymbol{r}}^*(t)\widetilde{\boldsymbol{h}}(t,u)\tilde{\boldsymbol{r}}(u)\mathrm{d}t\mathrm{d}u \underset{H_0}{\overset{H_1}{\gtrless}} \gamma \tag{3.37}$$

with, γ, being the threshold for the decision space. Now, under the low-energy coherence condition, the function $\widetilde{\boldsymbol{h}}(t,u)$ is replaced with the range-spread target covariance [38]

$$\widetilde{\boldsymbol{h}}(t,u) = \frac{1}{N_0}\widetilde{\boldsymbol{K}}_{\boldsymbol{s}}(t,u) \tag{3.38}$$

Substitution of Equation (3.37) into (3.26) gives the corresponding likelihood ratio test under the low-energy coherence conditions, corresponding to the optimal receiver shown in Figure 12

$$\ell = \frac{E_t}{E_0}\iiint_{-\infty}^{\infty} \tilde{\boldsymbol{r}}^*(t)\tilde{\boldsymbol{f}}\,(t-\lambda)\tilde{\boldsymbol{S}}_{\boldsymbol{R}}(\lambda)\tilde{\boldsymbol{f}}^*(u-\lambda)\tilde{\boldsymbol{r}}(u)\mathrm{d}t\mathrm{d}u\mathrm{d}u\mathrm{d}\lambda \underset{H_0}{\overset{H_1}{\gtrless}} \gamma \tag{3.39}$$

Van Trees' [1] low-energy coherence receiver is inherently limited to implementations and scenarios that are monostatic in nature. There is however; a strong desire to depart from monostatic modalities, and embrace multi-sensor configurations to better realize performance gains inherent in multistatic radar networks. In the next section, reasons for moving beyond monostatic radar sensors are discussed, along with introducing differing topologies of multistatic radar networks and their associated system performance improvements.

3.5 LEC Revisited in the Context of Standard Detection Approaches

To illustrate our motivation for an LEC based approach let us first consider a classical single radio-frequency (RF) radar system where a coherent processing interval consists of a single pulse $s(t)$ given as

$$s(t) = \sqrt{2E}\mathrm{Re}\left\{\tilde{f}(t)e^{j\omega_c t}\right\}, \quad 0 \le t \le T_d \tag{3.40}$$

where $\mathrm{Re}\{\cdot\}$ denotes the real part operator, $\tilde{f}(t)$is the complex envelope of the transmitted pulse, E and T_d are the energy and duration of the pulse, respectively, and $\omega_c = 2\pi f_c$ is the carrier frequency. Let the complex envelope of the receiver input be denoted by $\tilde{\boldsymbol{r}}(t)$. According to whether a target is absent H_0 or present H_1, the two hypotheses are presented by

$$H_0: \tilde{\boldsymbol{r}}(t) = \tilde{\boldsymbol{n}}(t) \tag{3.42a}$$

$$H_1: \tilde{\boldsymbol{r}}(t) = a\tilde{\boldsymbol{s}}(t-\tau)e^{j\omega_D t} + \tilde{\boldsymbol{n}}(t) \tag{3.42b}$$

where $\tilde{a}$ is a complex gain which accounts for propagation and scattering effects of the target and along the path between the transmitter, target and the receiver, τ

and ω_D denote total time delay and Doppler shift experienced by the transmitted signal, respectively, and $\tilde{\boldsymbol{n}}(t)$ denotes the complex envelope of the additive noise present at the receiver input. Let us assume additionally that the envelope $\tilde{\boldsymbol{n}}(t)$ is a complex Gaussian random process with zero-mean and white in quadrature components with power spectral density $\frac{N_0}{2}$. To simplify the notation we drop the symbol for complex envelope and rewrite the previous equation as

$$H_0: \boldsymbol{r}(t) = \boldsymbol{n}(t) \tag{3.43a}$$

$$H_1: \boldsymbol{r}(t) = a\boldsymbol{\phi}(t) + \boldsymbol{n}(t), \;\; T_i \le t \le T_f \tag{3.43b}$$

where $\tilde{\boldsymbol{s}}(t-\tau)e^{j\omega_D t} \rightarrow \boldsymbol{\phi}(t)$ and $T_d = T_f - T_i$. This is a well-known problem where the optimal band-pass receiver consists of a matched filter $\boldsymbol{\phi}^*(T_d - t)$ followed by a sampler. Let us now go beyond this simple single radar system with a point target case and extend it in several directions.

3.5.1 Multiple Heterogeneous RF Sensors with a Point Target

Let us consider a scenario with *N* RF sensors that utilize orthogonal waveforms. If we linearly fuse the receiver input signals to form a composite signal $\boldsymbol{r}(t) = \sum_{i=1}^{N} \boldsymbol{r}_i(t)$, our two hypotheses, assuming a point target, become

$$H_0: r(t) = \boldsymbol{n}(t) \tag{3.44a}$$

$$H_1: r(t) = \sum_{i=1}^{N} a_i \boldsymbol{\phi}_i(t) + \boldsymbol{n}(t), \;\; T_i \le t \le T_f \tag{3.44b}$$

For large *N* and under a few additional assumptions, the above formulated case becomes a LEC case. In particular, let $\boldsymbol{K}(t,u)$ be the covariance function of our composite signal in the absence of noise. It can be written as a series

$$\boldsymbol{K}(t,u) = \sum_{i=1}^{N} \lambda_i \, \boldsymbol{\phi}_i(t)\boldsymbol{\phi}_i(u), \;\; T_i \le t \le T_f \tag{3.45}$$

Thus, the energy of our composite signal is distributed along *N* coordinates.

$$\lambda \ll \frac{N_0}{2}, \;\; i = 1,2,\dots,N \tag{3.46}$$

If we are approaching the LEC case and the optimal receiver design can be based on the LEC theory (note that even when LEC conditions are not fully met, a LEC based receiver can be an adequate near-optimal receiver).

3.5.2 Over-resolved Targets

Processing becomes more challenging in the case of over-resolved targets. Namely, the target return signal does not have the form $a\boldsymbol{s}(t-\tau)e^{j\omega_D t}$ and the return signal now becomes

$$\boldsymbol{r}(t) = \int_{L_0}^{L_1} \boldsymbol{s}(t-\tau)\boldsymbol{b}(\tau)d\tau + \boldsymbol{n}(t), \;\; T_i \le t \le T \qquad (3.49)$$

where $\boldsymbol{b}(\tau)$ denotes the target's impulse response and $L = L_1 - L_0$ denotes the target range (delay) spread.

More generally, in the case of multiple homogeneous sensors the two hypotheses become:

$$H_0: \boldsymbol{r}(t) = \boldsymbol{n}(t) \qquad (3.50a)$$

$$H_1: \boldsymbol{r}(t) = \sum_{i=1}^{N} \int_{L_{0,i}}^{L_{1,i}} \boldsymbol{s}(t-\tau)\boldsymbol{b}(\tau)d\tau + \boldsymbol{n}(t), \;\; T_i \le t \le T_f \qquad (3.50b)$$

The hypothesis still distills down into the traditional problem of detecting a signal (obtained by fusing multiple homogeneous sensors) in the presence of interfering white Gaussian noise. Although the corresponding signal covariance matrix $\boldsymbol{K}(t,u)$ will now have a more complicated structure, the LEC based approach can still apply under certain conditions.

3.5.3 Multiple Heterogeneous Sensors

Let us now consider a scenario with *N heterogeneous* sensors. This time the received signals $\boldsymbol{r_i}(t) = 1,2,3,\ldots,N$, and the form of the composite signal is

$$\boldsymbol{r}(t) = \sum_{i=1}^{N} \mu_i \boldsymbol{r}_i(t) \qquad (3.51)$$

where μ_i coefficients are responsible for adequate scaling of time domain signals of a different nature. The new covariance matrix $\boldsymbol{K}(t,u)$ will possess a complex structure that will have to be ascertained based upon the observational sensors utilized and the nature of the target. However, once the sensors and target are chosen, the LEC based findings regarding the (sub)optimal receiver design can be utilized. It can be shown that the optimal LEC receiver, assuming that all conditions are perfectly met, has the implementation as shown in Figure 13.

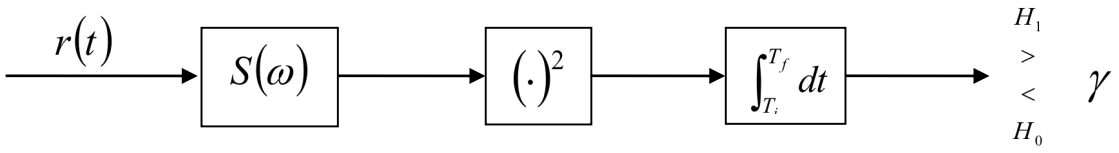

Figure 13: Optimal LEC Receiver

In Figure 13, $\boldsymbol{S}(\omega)$ denotes the power spectral density of the signal of interest whilst γ denotes the detection threshold. Thus, it is a relatively simple structure that consists of a filter, followed by a square-law operation and an integrator. The challenge in this effort is to investigate the implications that different sensor

densities and extended target bodies have on $\boldsymbol{S}(\omega)$ and the receiver structure shown above.

3.5.4 Clutter Considerations

So far, we have assumed the received signal is comprised of the signal of interest (target return) and white Gaussian noise at the sensor receiver. When considering the use of the LEC approach, this results in a fairly benign covariance function. When only the signal and white Gaussian noise are present at the receiver, the covariance of the received signal equals:

$$\boldsymbol{R}(t,u) = \boldsymbol{K}(t,u) + \frac{N_0}{2}\boldsymbol{\delta}(t-u) \tag{3.52}$$

In most practical situations, surface clutter (terrain or sea) and noise are present at the receiver(s). As a consequence, the covariance matrix of the received signal thus becomes:

$$\boldsymbol{R}(t,u) = \boldsymbol{K}(t,u) + \boldsymbol{R}_c(t,u) \tag{3.53}$$

where $\boldsymbol{R}_c(t,u)$ denotes the covariance of the received signal in the absence of target. In order to follow the LEC based approach one has to adequately pre-process the received signal so that its covariance has the form as in Equation (3.52). This is typically accomplished by pre-whitening. In the case when $\boldsymbol{R}_c(t,u)$ is known, the pre-whitening leads to a processed signal with the covariance:

$$\boldsymbol{R}'(t,u) = \boldsymbol{R}_c^{-1}\boldsymbol{K}(t,u) + \boldsymbol{\delta}(t,u) \tag{3.54}$$

In a more realistic case when the noise plus clutter covariance has to be estimated, after the whitening we obtain:

$$\boldsymbol{R}'(t,u) = \widehat{\boldsymbol{R}}_c^{-1}\boldsymbol{K}(t,u) + \widehat{\boldsymbol{R}}_c^{-1}\boldsymbol{R}_c(t,u) \tag{3.55}$$

where $\widehat{\boldsymbol{R}}_c$ is the estimate of $\boldsymbol{R}_c$ so that $\widehat{\boldsymbol{R}}_c^{-1}\boldsymbol{R}_c \approx \boldsymbol{\delta}(t,u)$. Thus, in the presence of clutter the corresponding LEC based receiver has the general form as shown in Figure 14 where $\boldsymbol{h}_w(t,u)$ is the multi-dimensional pre-whitening filter and $\boldsymbol{S}_w(\omega)$ is the power spectral density of the pre-whitened signal of interest, that is the processed signal with the covariance $\widehat{\boldsymbol{R}}_c^{-1}\boldsymbol{K}(t,u)$.

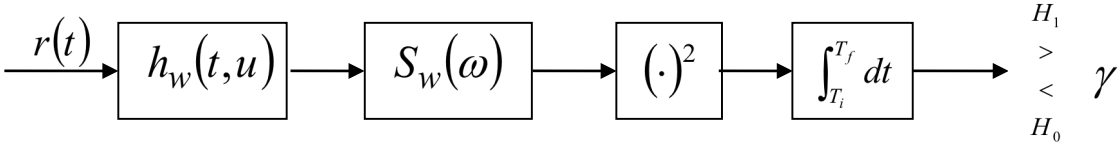

Figure 14: Optimal LEC Receiver with Pre-Whitening Filter

3.6 Moving Beyond the LEC

In the previous section the low-energy coherence (LEC) receiver concept was detailed for single and multiple sensors. One point of consideration that was not adequately addressed was the requirement for the LEC to have *a priori* knowledge of the observed target covariance in order for the receiver conditions to be satisfied. This is not a point of triviality, this is the *sell* for the LEC receiver as a method for detecting objects that are *weak*, or have extremely low signal-to-noise ratios (SNRs) at the receiver front-end. However, for most practical consideration of the United States Air Force, the nature of the target is not always known *a priori*; in fact, in most instances, the role of the radars and networks of sensors is to *find, fix, and track* objects of interest. This entails *detection* and passing *valid detection reports* to a *tracker*. The purpose of a *tracker* is to maintain cognizance of the target of interest and minimize *false alarm reports*, or so-called Type II statistical errors. Indeed, for this work, the focus is on the ability of a distributed sensing network to engage in the *detection* of a target body *without* the requirement for *a priori knowledge* of its accompanying covariance function. To that end, we focus primarily on the *detection algorithms* and leave the role of *false alarm* reduction to a follow-on, or associated, tracker algorithm.

Further, the role of our detection algorithms is to deduce the *presence* of a target, as well as *how many* are present. This later point is referred utilizes *statistical ranking* to appropriately determine the total salient scattering features that are present on the target body. Recall, that for this work, the target is considered *extended*, which refers to the fact that the target is comprised of multiple *scattering centers*. As the target body is a contrived example comprised of a trio of dielectric spheres arranged in Cartesian space, we appropriately refer to each canonical scattering center, as a *salient scattering feature*.

Before we move forward with this work, we need to derive the mathematical formulation of our *pre-detection fusion* process that forms the basis of our bespoke *depth-based* and weak SNR detection algorithms of Chapters 4 and 6, respectively.

3.7 Introduction to the Pre-Detection Fusion Process

The purpose of this section is to introduce the reader to the basic concepts of pre-detection fusion. More generally, we focus on the development and processing methodology for a distributed radio-frequency (RF) sensor network comprised of multiple transceivers that transmit and process a single tone on receive. Following a mathematical time-reversal operation, the data is sent to a single radar sensor-fusion node that is capable of implementing a *pre-detection* fusion algorithm from data transmitted by the multiple radio-frequency sensors comprising the distributed sensing network; we call this sensor-fusion node, the *fusion center*. The role of the fusion center is as simple, or as complex, as the system of systems sensing architecture demands. For example, the fusion center may apply a pre-detection fusion algorithm and re-transmit that data to a secondary network, or the data may be further processed onboard for near-real time or real-time purposes. For the duration of this chapter, it is assumed that the data is processed on board a single fusion center, with no real-world constraints being placed on the form of this sensor. In fact, for the remainder of this work, the development and application of algorithms are assumed to take place within the fusion center itself. Individual sensors comprising the distributed network are assumed capable of processing and transmitting their received information, but are not investigated further beyond this level; primary focus is on the pre-detection fusion and post-fusion algorithms and associated performance characteristics. Investigations into the phenomenology of the target are slowly introduced from a simple Born approximation to an extended target body comprised of multiple dielectric scattering centers.

3.7.1 Time-Reversal Operator for Isotropic Target Scattering Centers

In this section, the concept of the *pre-detection fusion process* is derived, starting with the scalar wave equation. The time-reversal operator that is produced by the *pre-detection fusion process* is utilized throughout the remainder of this work. We start with the simple case of point-type targets; those targets that are assumed to possess a finite reflectivity, but are volumetrically infinitesimally small. For the following simulation, the transmitters and receivers are assumed to be equally distributed on a circle surrounding the multiple scattering centers of a range-extended target body. The point targets are assumed to be in the far-field and be positioned multiple wavelengths apart-i.e. $(d \gg \lambda)$.

Let us begin by considering the propagation of some number of scalar waves in the presence of r target scattering centers (reflectors) localized within a finite-sized spatial-domain-or more simply, multiple targets in a bounded spatial domain. The local variation of the speed of propagation induced by the r^{th} reflector at a particular location in the Cartesian coordinate system, denoted by $\boldsymbol{x_j}$, is

$$v_j(\boldsymbol{x}) = \eta_j \mathbf{1}_{\Omega_j}(\boldsymbol{x} - \boldsymbol{x}_j) \tag{3.56}$$

where Ω_j is a compactly supported spatial-domain with volume l_j, and $\mathbf{1}_{\Omega_j}$ is a characteristic function of Ω_j, and η_j is the dielectric contrast (which is equivalent to the strength of the target reflector reflectivity at $\boldsymbol{x}_j$). The corresponding speed of propagation, for the scalar wave, is then shown to be of the form

$$\frac{1}{c^2(\boldsymbol{x})} = \frac{1}{c_0^2}\left(1 + \sum_{j=1}^{r} V_j(\boldsymbol{x})\right) \tag{3.57}$$

with c_0 denoting the known propagation speed ($3\times10^8\ {}^{m}/_{S}$ in a vacuum), which corresponds to the local variation in the speed of light constant. Let's also assume that a time-harmonic point source acts at the location $\boldsymbol{z}$ with frequency ω. The resulting field in the presence of the r target reflectors is the solution to the following transmission problem $\hat{u}(\cdot, \boldsymbol{z})$

$$\Delta_{\boldsymbol{x}}\, \hat{u} + \frac{\omega^2}{c^2(\boldsymbol{x})}\hat{u} = -\delta_{\boldsymbol{z}}(\boldsymbol{x}) \tag{3.58}$$

with the radiation condition imposed on $\hat{u}$. The transmitter array of M sources and the receiver array of N elements are located at (all in relation to the Cartesian coordinate system)

$$M := \{\boldsymbol{z}_1, \ldots, \boldsymbol{z}_M\} \tag{3.59a}$$

$$N := \{\boldsymbol{y}_1, \ldots, \boldsymbol{y}_N\} \tag{3.59b}$$

The field received by the n^{th} receiving element (radar receiver) $\mathbf{y}_n$ when the wave is emitted from the m^{th} transmitter element (radar transmitter) $\mathbf{z_m}$ is $\hat{u}(\boldsymbol{y}_N, \boldsymbol{z}_M)$. If the incident field is removed, then the $(n,m)^{th}$ entry of the corresponding time-reversal operator is obtained

$$\mathsf{A}_{nm} = \hat{u}(\boldsymbol{y}_n, \boldsymbol{z}_m) - \hat{G}(\omega, \boldsymbol{y}_n, \boldsymbol{z}_m) \tag{3.60}$$

The incident field is the homogeneous Green's function given by $G(\omega, \boldsymbol{x}, \boldsymbol{y})$ of the wave equation, which for two-dimensions is given by

$$\hat{G}(\omega, \boldsymbol{x}, \boldsymbol{y}) = \frac{i}{4} H_0^{(1)}\left(\frac{\omega}{c_0}|\boldsymbol{y} - \boldsymbol{x}|\right) \tag{3.61}$$

with $H_0^{(1)}$ representing a Hankel function of the first-kind, zeroth-order. For the remainder of this work, the focus is on a planar Cartesian coordinate system, a

limitation that is readily moved to three-dimensional space via utilization of an alternate form of the Green's function.

In the Born approximation, the volume for $\Omega_j, j = 1, \ldots, r$ goes to zero, and the measured field is approximated by the expression

$$\hat{u}(\boldsymbol{y}_n, \boldsymbol{z}_m) = \hat{G}(\omega, \boldsymbol{y}_n, \boldsymbol{z}_m) + \sum_{j=1}^{r} \rho_j \, \hat{G}\left(\omega, \boldsymbol{y}_n, \boldsymbol{x}_j\right)\hat{G}\left(\omega, \boldsymbol{x}_j, \boldsymbol{z}_m\right) \quad (3.62)$$

for all transmitter and receiver locations $\boldsymbol{y}_N$ and $\boldsymbol{z}_M$. The coefficient ρ_j is the reflection coefficient for a given target body and is defined by the quantity

$$\rho_j = \frac{\omega^2}{c_0^2}\eta_j l_j^2 \quad (3.63)$$

We determine the singular value from the expression

$$\sigma_j := \rho_j \left(\sum_{n=1}^{N}\left|\hat{G}\left(\omega, \boldsymbol{x}_j, \boldsymbol{y}_n\right)\right|^2\right)^{\frac{1}{2}} \left(\sum_{m=1}^{M}\left|\hat{G}\left(\omega, \boldsymbol{x}_j, \boldsymbol{z}_m\right)\right|\right)^{\frac{1}{2}} \quad (3.64)$$

where $\hat{G}\left(\omega, \boldsymbol{x}_j, \boldsymbol{y}_n\right)$ is the general form of the radar sensor receiver array Green's functions and $\hat{G}\left(\omega, \boldsymbol{x}_j, \boldsymbol{z}_m\right)$ is the general form of the radar sensor transmitter array Green's functions. To formulate the time-reversal operator, it is also necessary to calculate the normalized vector of Green's functions for the radar sensor transmitter and receiver array. The normalized vector of Green's functions for the receiver array to the reflector point specified by $\boldsymbol{x}$ is given by

$$\boldsymbol{u}(\boldsymbol{x}) := \frac{1}{\left(\sum_{l=1}^{N}|\hat{G}(\omega, \boldsymbol{x}, \boldsymbol{y}_l)|^2\right)^{\frac{1}{2}}}\left(\hat{G}(\omega, \boldsymbol{x}, \boldsymbol{y}_n)\right)_{n=1,\ldots N} \quad (3.65)$$

The normalized vector of Green's functions for the radar sensor transmitter array from the reflector point specified by $\boldsymbol{x}$ is given by

$$\boldsymbol{v}(\boldsymbol{x}) := \frac{1}{\left(\sum_{l=1}^{M}|\hat{G}(\omega, \boldsymbol{x}, \boldsymbol{z}_l)|^2\right)^{\frac{1}{2}}}\left(\hat{G}(\omega, \boldsymbol{x}, \boldsymbol{z}_n)\right)_{m=1,\ldots,M} \quad (3.66)$$

Having solved for the target reflector singular value and the normalized vector of Green's functions for the radar sensor transmitter and receiver array, the associated time-reversal operator is determined from the following

$$\mathbf{A} = \sum_{j=1}^{r} \sigma_j \boldsymbol{u}\left(\boldsymbol{x}_j\right)\boldsymbol{v}\left(\boldsymbol{x}_j\right)^* \quad (3.67)$$

We note that Equation (3.67) is of rank r and *positive semidefinite*. This latter point is of critical importance as we venture from positive-to-negative signal-to-noise ratios, see Chapter 5 for further details. Equation (3.67) is the ultimate form of our pre-detection fusion process, resulting in the formation of the target time-reversal operator. Finally, the idea of using the time-reversal operator to preserve our target data in a higher dimensional space-an outer product space-is a unique contribution of this data fusion process, and one that contributes to the efficacy of the detection and ranking algorithms presented in Chapters 4 and 6.

3.7.2 Inclusion of Additive Measurement Noise

It is assumed that all measurements contain some element of additive noise (ie-receiver thermal noise, environmental, etc), represented by **W**, which is considered a matrix of independent and identically distributed complex entries with Gaussian statistics, $\mathbf{W}_{i,j} \in \mathcal{CN}(0, \sigma^2)$. The resultant measured time-reversal operator is then

$$\mathbf{B} = \mathbf{A} + \frac{1}{\sqrt{M}}\mathbf{W} \tag{3.68}$$

Equation (3.67) is valid for the non-trivial asymptotic regimes in the limit $M \to \infty$, where the scaling factor $\frac{1}{\sqrt{M}}$ is appropriate. The challenge is to first detect the presence of a signal, then rank the number of signals, to determine the ultimate number of target reflectors-ie target scattering centers-within the scene of interest. For most detection algorithms, a single target is assumed present, resulting in a singular metric for the determination of target present/absent. In stark contrast, range-extended targets, possessing multiple-scattering centers, result in a non-singular metric for determination of target present/absent-necessitating the requirement for an iterative detection methodology. This *iterative detection methodology*, in the form of statistical ranking, is developed and demonstrated for each detection algorithm present in this thesis.

3.7.3 Clutter Considerations

Corruption noise is assumed comprised of environment noise and clutter, as well as thermal receiver noise from each radar sensor forming the distributed radio-frequency sensor network. In order to keep the number of variables to a minimum, clutter is not presently considered, only receiver thermal and environmental noise processes are considered. Following the completion of this initial investigation, challenges associated with the incorporation of clutter will be considered; however, at this stage in algorithm development, clutter introduces an additional variable that is manifest as a secondary bounded perturbation on the time-reversal operator; above and beyond that of the bounded rank perturbation from the target objects within the scene under illumination by our multistatic radar sensor network. The challenges associated with separating the clutter rank from the signal rank are well known, as are effective mathematics for minimizing its deleterious impact on radar sensor network detection performance [48-49]. Should a desire exist to

incorporate clutter into the performance predictions for the depth-based detector, the process is rather straightforward; though, clutter models would be excessively complicated by the dimensionality of the multistatic radar sensor geometries-particularly for three-dimensional cases! Assume, no matter how simplistic this view is in reality, that clutter is an additive corruptive process. Further, assume this clutter corruptive process is characterized by a series of measurements that is unique to each radar sensor, and to each point in the observational space of the multistatic network. Finally, without particular concern for the naivety of the following assumption, assume the clutter corruptive process is complex, and comprised of a unique complex valued reflectivity that may-or may not-conform to any of the known uni-, bi-, or multi-variate random processes. The clutter corruptive process is now found in much the same manner as the time-reversal operator comprised of range-extended target reflectivity information. Of note, is the fact that the formulation of the *clutter* time-reversal operator is very much in keeping with the process of determining the *target* time-reversal operator for a *partially-coherent target*-or a target that is has an *angular* dependence on the *observed* target *reflectivity*. In Chapter 5, the *partially-coherent* range-extended target structure is composed of multiple scattering centers *with each* scatterer having a reflectivity value that is based upon the *observational angle* of the radar sensor.

Start by considering the apparent *clutter reflectivity* observed by each radar sensor comprising the multistatic network.

$$\psi = \frac{\omega^2}{c_0^2}\eta l^2 \tag{3.69}$$

Next, extend the monostatic observation into a general observed clutter reflectivity variable

$$\psi_j = \frac{\omega^2}{c_0^2}\eta_j l_j^2, \;\; j \in [1,2,\dots r] \tag{3.70}$$

Now, assuming the clutter variable conforms to a complex distribution (uni-, bi-, multi-variate), $\mathcal{P}$, the general form of the clutter additive corruptive noise process is $\mathbf{P}_{i,j} \in \mathbb{C}\mathcal{P}\left(\mu_j, \sigma_j^2, \dots\right)$; where the notation, $\{\dots\}$, refers to higher order moments of the general clutter distribution, $\mathcal{P}$. Solving for the respective time-reversal operator of the *observed* clutter reflectivity singular values, we have

$$\Psi_j := \psi_j \left(\sum_{n=1}^{N}\left|\hat{G}\left(\omega, \boldsymbol{x}_j, \boldsymbol{y}_n\right)\right|^2\right)^{\frac{1}{2}} \left(\sum_{m=1}^{M}\left|\hat{G}\left(\omega, \boldsymbol{x}_j, \boldsymbol{z}_m\right)\right|\right)^{\frac{1}{2}} \tag{3.71}$$

The respective time-reversal operator of the *observed* clutter reflectivity, and again ignoring the naivety of the additive assumption, we have general form of the clutter corruptive noise process

$$\mathbf{P} = \sum_{j=1}^{r} \Psi_j \boldsymbol{u}(\boldsymbol{x}_j)\boldsymbol{v}(\boldsymbol{x}_j)^* \tag{3.72}$$

Again, whilst the study of clutter and associated impacts on radar performance (mono-, bi-, or multistatic) is of ongoing importance to the radar community, clutter considerations are a bit beyond the scope of this work, though is an active area of investigation, see Chapter 7 for further discussion.

3.8 Summary

In this section, we have introduced the rudiments of radar detection, statistical decision theory, and the low-energy coherence (LEC) receiver. We then walked through the derivation of the LEC receiver paradigm from a monostatic to multistatic formulation. In each instance of the LEC receiver construct, there is a requirement to know the target covariance *a priori*. This is indeed the underlying assumption required for use of the LEC under varying noise and clutter conditions. However, the goal of this work is to permit distributed sensor network detection algorithms to be implemented under two conditions: the first is that the data collected from each sensor is fused prior to detection, our so-called pre-detection fusion process; and second, that the fused data is then processed through a detection, and later ranking, algorithm that *does not* require any *a priori* knowledge of the target or target covariance. To that end, we conclude this section with an overview of the *pre-detection fusion* process that serves as the basis for the bespoke detection, and ranking, algorithms of Chapters 4 and 6. The pre-detection fusion process is derived from first principles, and extended to include corruptive noise and clutter processes. Going forward, corruptive clutter is left to follow-on work, see Chapter 8, whilst the emphasis for Chapters 4 and 6 is the recovery of targets via additive corruptive noise. This serves to deepen the understanding, and permit comparison, of the bespoke detection and ranking algorithms of Chapters 4 and 6 with each other, and those commonly used in academia and industry.

In the next chapter, the basis of the nonparametric detection and ranking algorithm is introduced for a distributed radio-frequency sensor network.

4 Nonparametric Detection and Ranking for a Distributed Radio-Frequency Sensor Network

4.1 Overview

In this Chapter, we introduce a novel non-parametric depth-based method for the target detection and ranking problem in noisy environments under nominal signal-to-noise ratios. Specifically, a distributed sensor network comprised of multiple transceivers is considered. Each sensor is able to transmit and receive a single tone; which is passed to a fusion center where the data is formed into a time-reversal operator via a pre-detection fusion algorithm. An algorithm is introduced for the determination of the presence of a target(s) in the background medium. The detection performance versus signal-to-noise ratio is developed for a given false alarm rate and compared to a typical monostatic sensor. After detection, a critical challenge in sensing is determining the number of targets present in the scene of interest. With this challenge in mind, an algorithm is introduced to determine the effective rank of the time-reversal operator; this algorithm is developed via depth-based methods and is shown to be robust when the P_D is above 90%.

4.2 Introduction Non-Parametric Detection via Statistical Data Depth

One challenge in formulating predicted detection performance for a multi-sensor system, especially one incorporating waveform diversity, is that traditional assumptions of Gaussianity are no longer valid. During the 1940's British mathematicians were able to show with a continuous wave radar that the measurements did indeed follow a Normal distribution (were Gaussian); or Rayleigh in the case of a magnitude detector. However, since those early days of radar, a plethora of waveforms have been developed, proposed, and implemented; not all of these waveforms have been shown-mathematically-to conform to the normality assumption.

Further, when the underlying corruptive noise processes begin to stray from mono- and bivariate populations, classical approaches begin to break down, leading to uncertainty of the detection process. When coupled with the desire for sensor systems to operate in evermore challenging environments, we begin to appreciate the requirement for nonparametric methods for multivariate populations

of corruptive noise. Any proposed nonparametric detection algorithm should also perform amicably under bivariate populations of corruptive noise processes-i.e. those that are readily characterized through second-moment methods, such as the covariance matrix. In this work, a novel non-parametric depth-based method for detecting an object in a background medium comprised of noise emanating from either a bi-or multi-variate population is presented. A distributed sensor network comprised of multiple transceivers is specifically considered. Each sensor, or node, is able to transmit and receive a single tone; with the output of the receiver from each node feeding into a central fusion center. This *fusion center* applies a pre-detection fusion algorithm to the received data to form a common time-reversal operator, upon which a variety of processing tasks may be accomplished. In particular, an algorithm is introduced for determining the presence of a bounded rank perturbation of the resultant time-reversal operator. The detection performance is further enhanced by the inclusion of the Neyman-Pearson criterion for the depth-based detector. The detection performance versus signal-to-noise ratio (SNR) is compared to that of a single pulse and envelop detector, as well as a newer random matrix theoretic detection statistics introduced in [50]. We demonstrate, for the case in which the noise is assumed Gaussian, the performance of the depth-based detector is significantly better than the single pulse and envelope detector.

Further, we introduce a method of *statistical* ranking, whereby the overall rank of the perturbation to determine the effective number of signals present in our time-reversal operator is quantified. The ability to introduce statistical ranking into our detection algorithm greatly increased the overall utility of this proposed nonparametric approach.

When the bounded rank perturbation is greater than unity, the depth-based detection algorithm is able to account for the presence or absence of a target(s), but not the number of targets present. We next introduce a *ranking* algorithm to permit the estimation of the effective rank of the perturbation. The ability to introduce statistical ranking into our detection algorithm greatly increases the overall utility of this proposed nonparametric depth-based approach for detection. This allows the distributed sensor network to both detect and estimate the number objects within the scene under illumination. A series of Monte Carlo simulations are considered for a variety of signal-to-noise ratios, and the robustness of the ranking algorithm is determined in reference to set the probability of detection.

Due to the nonparametric foundation of our detection and ranking algorithms, we are unable to directly compare the anticipated performance once the underlying corruptive noise process is multivariate. In an effort to show efficacy, we compare the performance of the depth-based detector against a general class of monostatic detector. In an effort to quantify the lower-bound of detectability with our depth-based detector, we also consider the multivariate corruptive noise process to be initially known *a priori*-the clairvoyant case-which permits the detection threshold to be characterized through a Monte Carlo simulation to great precision; we follow this with the case in which a second multivariate process- the unknown case-is used to estimate the detection threshold under limited sample support; the results for both cases are compared. Due to the underlying uncertainty surrounding general classes of multivariate processes, especially those that are not completely characterized *a priori*, our depth-based detector performance, while applicable to any corruptive noise process, will have a detection performance that varies from multivariate population to multivariate population. Owing to the better detection performance versus classical detection schemas, we anticipate the benefits of utilizing the depth-based detector for challenging corruptive noise processes will outweigh any performance uncertainty that may come from detection and ranking under multivariate conditions with regards to the false alarm rate versus probability of detection.

The detection performance versus signal-to-noise ratio is developed and compared to that of a typical monostatic radar. To control the effective false-alarm rate of the detection statistic, the depth-based detection algorithm is formulated as a Neyman-Pearson detector, so that the false-alarm rate can be set to a constant value while determining the probability of detection versus signal-to-noise ratio.

4.2.1 Introduction to Half-Space Depth and Associated Properties

Given k multivariate populations $\pi_i = \pi(P_i)$ on $\mathbb{R}^d, d > 1$, with absolutely continuous distributions P_i, defined on random variables X_i for $i = 1,2,\dots,k$ we propose a procedure for selecting the "most dispersed" member from a group k populations. We define our measure of dispersion in terms of the depth-based scale curve introduced by Liu, et al. in [51]. The scale curves if $\mathcal{P}$ is the collection of probability distributions, we may consider a depth function to be any bounded, nonnegative mapping $D(\cdot;\cdot)\colon \mathbb{R}^d \times \mathcal{P} \longrightarrow \mathbb{R}$ that provides a probability based center-

outward ordering of points in $\mathbb{R}^d$. For the center-outward ranking, we will make use of Tukey's Half-Space Depth [52-53]

$$D(x;P) = \inf\{P(H)|x \in H, H \text{ is a closed half-space}\} \quad (1.1)$$

where $x \in \mathbb{R}$. This half-space depth has four primary properties that provide insight into the power and utility of depth-based measures, these properties were proposed in [54]

1. $D(Ax+b;\ P_{Ax+b}) = D(x;P_x)$ for any random vector $X \in \mathbb{R}^d$, and $d \times x$ nonsingular matrix A, and any $d \times 1$ vector b.
2. For any $P \in \mathcal{P}$ with center Θ, then $D(\Theta;P) = sup_x(x;P)$.
3. If Θ is the deepest point for any $P \in \mathcal{P}$, then $D(x;P) \leq D(\Theta + \alpha(x-\Theta);P)$ for $\alpha \in [0,1]$.
4. $D(x;P) \to 0$ as $\|x\| \to \infty$ for any $P \times \mathcal{P}$.

4.2.2 Depth-Regions and Measures of Dispersion

Application of property (1) allows for the definition of *α-trimmed depth-regions* of P,

$$D^\alpha(P) = \{x \in \mathbb{R}^d | D(x;P) \geq \alpha\} \quad (4.2)$$

If we solve for the volume of a particular *α-trimmed depth-regions*, we have *de facto* solved for the dispersion of that same region. In order to compare the dispersion of one population with that of a second population, we introduce the concept of a *scale curve*. The scale curve is the volume, or dispersion, and is defined as

$$V^p = \inf\{\text{Volume}(D^\alpha(P)) | P(D^\alpha(P))) \geq p, 0 < \alpha < \alpha^*\} \quad (4.3)$$

with $p \in (0,1)$ and where $\alpha^* = sup_{x \in \mathbb{R}^d} D(x;P)$.

Definition 1. *For $p \in (0,1)$, we say that π_i is more dispersed, or more concentrated, than π_j (at level p), if $V_i^p \geq V_j^p$ is the volume from the population π_i.*

If P is absolutely continuous, according to [54], the collections of $D^\alpha(P)$ based on the half-space depth are affine equivariant, nested, connected, and compact for $p \in (0,1)$.

4.2.3 Empirical Distribution

For any given set of data, let $X_{i,1}, X_{i,2}, \dots, X_{i,n}$ be a random sample from P_i for a random variable X_i, and B be a Borel set, the empirical distribution is defined as

$$P_{i,n}(B) = \frac{1}{n}\sum_{j=1}^{n} I_B\left(X_{i,j}\right) \tag{4.4}$$

with $I_B(x)$ being an indicator function for B.

4.2.4 Depth-Based Detection

In order to formulate the hypothesis test, we need to first define the two populations that are to be compared. The first population is that of a general class of arbitrary distribution, representative of the background medium-i.e. Gaussian noise. The second population is a measured time-reversal operator consisting of a bounded rank signal perturbation with additive noise; in which the noise is scaled to simulate a set of signal-to-noise sample values. From these two populations, we define a new depth-based detection statistic, but first let us revisit the binary hypothesis test utilized for our example.

$$H_0 := \boldsymbol{n}(t) \tag{4.5a}$$

$$H_1 := \boldsymbol{s}(t) + \boldsymbol{n}(t) \tag{4.5b}$$

Typically, we measure a component of the received signal and compare this value to a pre-determined, or adaptive, threshold that allows us to transform equation (4.5a) and (4.5b) into

$$\delta_{\text{Threshold}} \underset{>H_1}{\overset{\leq H_0}{}} \tag{4.6}$$

with the null hypothesis indicating the absence of a signal. The depth-based detection method is also based on a threshold statistic, determined from a ratio of two dispersion values

$$\frac{\hat{V}_{[i]}}{\hat{V}_{[\text{Threshold}]}} = \delta \tag{4.7}$$

in which $\hat{V}_{[i]}$ and $\hat{V}_{[\text{Threshold}]}$ are the differential dispersion values for the populations of the measured time-reversal operator and noise matrix with arbitrary distribution, respectively. Differential dispersion values are derived from the difference of two dispersion values, as shown below

$$\hat{V}_{[\text{Threshold}]} = \hat{V}^{\beta}_{\text{Threshold}} - \hat{V}^{p}_{\text{Threshold}} \tag{4.8}$$

The differential dispersion is the difference between the volume defined by the contour β, and that of the volume of a second contour p. Typically, we define $\beta \simeq 1$, to ensure we incorporate all of the population values in our depth functional; the

second dispersion is found from a smaller contour defined by $p \in (0,1)$. In this instance, we have defined $p = [0.5,0.75,0.9]$. The difference between these two contours defines the volume of an annular region, $\hat{V}_{[\text{Threshold}]}$; with an increase in the annular region being attributed to the presence of a signal. We compare the differential dispersion of the assume noise threshold, with that of the measured data. In this manner, the second differential dispersion value in the threshold statistic is given as

$$\hat{V}_i = \hat{V}_i^{\beta} - \hat{V}_i^{p} \tag{4.9}$$

The depth-based detection binary hypothesis test is now akin to

$$\delta \underset{>H_1}{\overset{\leq H_0}{}} \delta_{\text{Threshold}} \tag{4.10}$$

where the $\delta_{\text{Threshold}}$ is determined for a given class of measurement noise. For the purpose of this thesis, the threshold is found empirically through a Monte Carlo simulation; a large number of noise realizations were created, for two population groups of white Gaussian noise comprised of 124 singular values, to determine the empirical volume of the annular region bounded by the contour D^p and D^{β}; this Monte Carlo simulation was repeated several times to ensure a consistent estimator for the empirical mean μ and standard deviation σ. For each instance, the empirical volume is calculated for the annulus by subtracting the volume of the $p = [0.5,0.75,0.9]$ contours from the $p_{\text{max}} = 1$ contour. The mean and variance for the volume of the annular region is listed in Table 2

Table 2: Empirical Thresholds

$V_{p^{th}}$ **Annulus**	$\bar{\mu}$	$\bar{\sigma}$	$V_{\text{Empirical}}$
90%	0.0016	$3.2e^{-4}$	$\bar{\mu} + k\bar{\sigma}$
75%	0.0011	$3.2e^{-4}$	$\bar{\mu} + k\bar{\sigma}$
50%	$4.3e^{-4}$	$2.3e^{-4}$	$\bar{\mu} + k\bar{\sigma}$

From Chebyshev's Inequality, we know that for any distribution in which the standard deviation is defined, the variables that fall within a certain number of standard deviations from the defined mean, $k\sigma$, is *at least as much as* [55]

Table 3: Empirical Threshold Table

Minimum Population from the Mean	Number of Standard Deviations *k*
50%	$\sqrt{2}$
75%	2
89%	3
94%	4
96%	5
97%	6
$1-\frac{1}{k^2}$	*k*

From Table 3, we see that for an empirical false alarm rate of 6%, we would require the $\hat{V}_{Threshold}$, $\mu + k\sigma$, to be equivalent to $\mu + 4\sigma$; likewise, for an empirical false alarm rate of 4% and 3%, we require the $\hat{V}_{Threshold}$ to be $\mu + 5\sigma$ and $\mu + 6\sigma$, respectively. Further, the dispersion resulting from the addition of a signal in the measured noise is manifest from the outlying nature of the signal singular values, when compared to the body of the measured noise plus *a priori* noise distribution data depth functional [56]; which is true for nominal signal-to-noise ratios (SNR). This is due to the fact that the singular values associated with the signal exhibit a level of eigenvalue repulsion, allowing them to be separate from the body of the data depth functional, see Figure 15. As the SNR decreases, this 'eigenvalue' repulsive force becomes weaker and the signal singular values become distributed on the outer contour of the data depth functional. From this vantage point, we are not seeking the point of deepest depth for signal detection, but the values for which the singular values are most outlying, and result in an increase in volume for a given annular contour bounded by $p^{th} \in (p, 1)$. Since we have defined the metric as the ratio of scale curves, and the false alarm rate is controlled by the empirical $\hat{V}_{Threshold}$, in this manner the threshold is actually equivalent to unity, $\delta_{Threshold} = 1$. The Chebyshev Inequality represents a more severe constraint on the detection statistic, and should be more robust, though may result in lower P_D versus SNR for a given P_{FA}.

Having introduced the depth-based detection algorithm, a summary of the procedures for implementing the algorithm are listed in the table below for Algorithm 4.1.

Algorithm 4.1: Depth-Based Detection Algorithm
1a: Calculate $\boldsymbol{N}$ Versions of the target-free time-reversal operator from target-free training data, $\widehat{\mathbf{B}}_{\boldsymbol{N};\text{Threshold}}$
1b: Calculate the time-reversal operator under test, $\widehat{\mathbf{B}}$
2: Set the desired values for contour $\boldsymbol{D^{\beta}}$ and $\boldsymbol{D^{p}}$
3a: Calculate the differential volumes from the annulus of each of the $\boldsymbol{N}$ target-free time-reversal operator formed by the contours of $\boldsymbol{D^{\beta}}$ and $\boldsymbol{D^{p}}$ $$\widehat{\boldsymbol{V}}_{\boldsymbol{N};\text{Threshold}} = \widehat{\boldsymbol{V}}^{\boldsymbol{\beta}}_{\boldsymbol{N};\text{Threshold}} - \widehat{\boldsymbol{V}}^{\boldsymbol{p}}_{\boldsymbol{N};\text{Threshold}}$$
3b: Calculate the differential volumes from the annulus of the time-reversal operator under test formed by the contours of $\boldsymbol{D^{\beta}}$ and $\boldsymbol{D^{p}}$ $$\widehat{\boldsymbol{V}}_{\boldsymbol{i}} = \widehat{\boldsymbol{V}}^{\boldsymbol{\beta}}_{\boldsymbol{i}} - \widehat{\boldsymbol{V}}^{\boldsymbol{p}}_{\boldsymbol{i}}$$
4a: Calculate the mean, $\boldsymbol{\mu}$, and standard deviation, $\boldsymbol{\sigma}$ of the target-free differential volumes, $$\widehat{\boldsymbol{V}}_{\text{Threshold}}$$
4b: Set the desired false alarm rate, $\boldsymbol{k}$, to form $\widehat{\boldsymbol{V}}_{\text{Threshold}} = \boldsymbol{\mu} + \boldsymbol{k\sigma}$
4c: Calculate the nonparametric threshold value for the binary hypothesis test $$\delta_{\text{Threshold}} = \frac{\widehat{V}_{\boldsymbol{Threshold};\,\boldsymbol{\mu}+\boldsymbol{k\sigma}}}{\widehat{V}_{\boldsymbol{Threshold};\,\boldsymbol{\mu}+\boldsymbol{k\sigma}}} = 1$$
5: Calculate the ratio of differential volumes for the threshold and time-reversal operator under test $$\delta = \frac{\widehat{V}_{\boldsymbol{i}}}{\widehat{V}_{\boldsymbol{Threshold}}}$$
6: Determine the outcome of the binary hypothesis test $$\delta \underset{>H_1}{\overset{\leq H_0}{}} \delta_{\text{Threshold}}$$

Having determined the empirical threshold statistic for the hypothesis testing, the proceeding section is dedicated to a demonstration of efficacy of the depth-based detection algorithm for a range-spread target comprised of three scattering centers corrupted by measurement noise.

4.3 Depth-Based Detection Examples

In this example, there are three isotropic scattering centers comprising an over-resolved (ie-range-extended) target that are within the scene under illumination by the distributed sensor network. Since the Born approximation was utilized to develop the time-reversal operator, the reflectivity of the target scattering centers are fixed, with an associated volume of zero. The surrounding background medium is assumed to be that of a standard Gaussian noise type. We further approximate the form of the noise to be white Gaussian noise, $\mathcal{N}(0, \sigma^2)$, with the variance fixed

at a value of unity. The signal-to-noise ratio is varied from $-3dB$ to $10\ dB$ in order to capture a broad range of conditions resulting from the sensor network pre-detection fusion process. The resulting signal subspace rank is then three, with all other rank components being associated with the random noise process. As the noise is increased, the eigenvalue repulsion between the noise and signal weakens; this weakening results in missed detections and the potential for false alarms. This later statement implies a fundamental limit of efficacy for the depth-based detection algorithm for a given range of signal-to-noise ratio values, that is addressed and overcome in Chapter 6.

Fundamentally, there is no set constraint on the underlying statistical distribution for either the signal or the noise; white Gaussian noise was chosen so that the results of this novel depth-based detection method are readily comparable against traditional monostatic receiver operating characteristics-ie single pulse and envelope detectors.

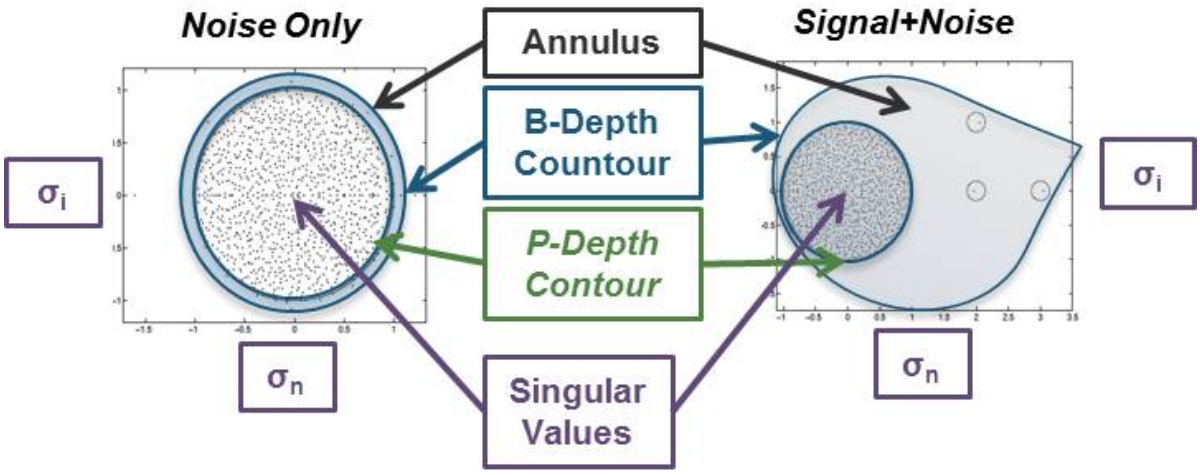

Figure 15: Data Depth Functional Annular Volume Comparison for Noise Only vs Signal+Noise

4.3.1 Depth-Based Detector Performance: Non-Parametric Case

In order to develop an adequate probability of detection curve, a Monte Carlo simulation was performed at each signal-to-noise ratio (SNR) sample. The number of Monte Carlo runs per SNR increment was large enough to ensure a representative sample point was captured that would be free from spurious statistical anomalies arising from the random noise process. At present, the depth-based detector is not optimized to run on a parallel processing computing architecture, so is single-threaded, and computationally inefficient. As computational efficiency was not an initial goal of this effort, this was an acceptable trade for initial demonstration of efficacy of the depth-based methods for detection

and ranking. Thus, the number of Monte Carlo simulations were kept to a statistically significant value, but not increased to a number that would effectively *smooth* the generated receiver operating characteristic figures. For the remainder of this section, oscillations and/or jitters present in the receiver operating characteristic figures should be attributed to smaller number of effective Monte Carlo simulations run for each example. A follow-on effort is underway to investigate computationally efficient implementations for depth-based methods, to make them more relevant for real-time sensing systems. A detection was recorded if, and only if, the annular volume increased sufficiently to exceed the detection threshold. For each $p^{th} = 0.5$ contour, the probability of detection was recorded for false alarm rates of 6% through 0.01%. The role of any detection algorithm is to ensure a sufficient balance is struck between suppressing Type I and Type II statistical errors within the detection hypothesis test to warrant their use; the role of the associated tracking algorithm-should one be utilized-is to drive the false alarm rate as low as possible.

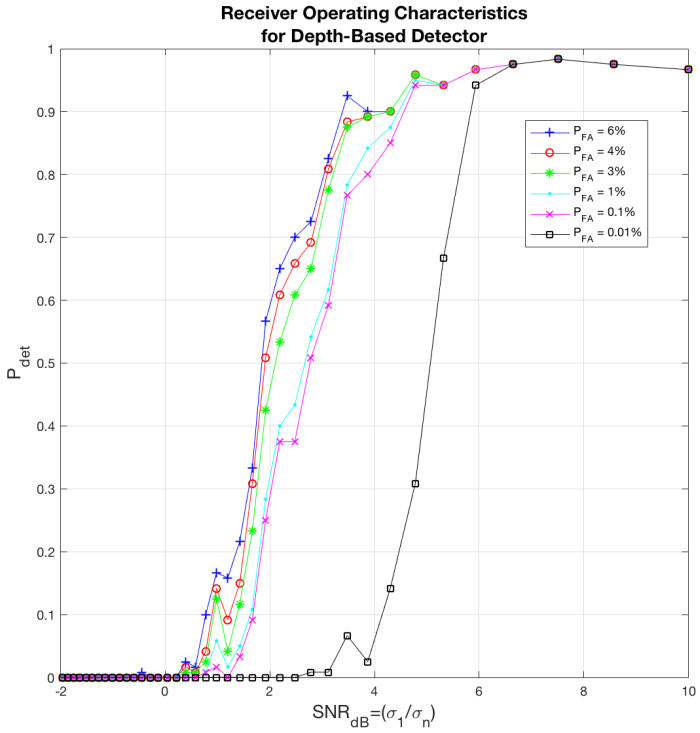

Figure 16: Probability of Detection vs SNR for Depth-Based Detection Statistic

From Figure 16 the receiver operating characteristic (ROC) curves only appear for false alarm values of, $P_{FA} = 6\%$ to $P_{FA} = 0.01\%$, owing to the restrictive form of the Type I error control used in the depth-based detector. For comparison, if we assume a standard form of a radar detector, as found in [39], a performance comparison is possible for a single-pulse detector (no integration within the

receiver) for noise corruption described by a normal Gaussian distribution. The form of the detector is shown below

$$P_D = \frac{1}{2} - \Phi\left(x - \sqrt{2\times \text{SNR}}\right) \tag{4.11}$$

where *x* is the detection threshold (ie-3 times the noise power) and ϕ is the error function. The performance of the depth-based detector does indeed outperform the classical single-pulse detector, as shown in Table 4, particularly as the probability of false alarm decreases.

Table 4: Probability of Detection Comparison with Chebyshev Inequality

P_{FA}	*x*	Required SNR for Classical Detector	Required SNR for Depth-Based Detector	Improvement Factor of Depth-Based Detector
6%	1.88	3.2 dB	3.6 dB	-0.4 dB
4%	2.05	4.2 dB	3.7 dB	+0.7 dB
3%	2.17	4.5 dB	3.8 dB	+1.3 dB
1%	2.33	5.1 dB	4.5 dB	+0.6 dB
0.1%	3.08	7.7 dB	4.6 dB	+3.1 dB
0.01%	3.62	10 dB	6.0 dB	+4.0 dB

4.3.2 Knowledge-Aided Depth-Based Detector

The Chebyshev Inequality is a more restrictive detection criterion; which was deliberately chosen to ensure the depth-based detection algorithm is general for any given class of distribution-both known and unknown. We would expect the detection probabilities are less than that of Equation (4.11), in which the function is derived from a normal Gaussian noise process assumption. In our example, the corruptive noise distribution is also assumed to be normal Gaussian; so, if we choose to re-run the same simulation by assuming our depth-function has complete *a priori* knowledge of the corruptive noise distribution, then the following false-alarm rates in Table 5 are more appropriate, and are found from the error function. We note, that owing to the conservative nature of the Chebyshev Inequality, the equivalent false-alarm rate-assuming Gaussian noise-for values greater than $P_{FA} \geq 10^{-2}$ are significantly better than those shown in Table 5, but are purposefully kept to $(P_{FA} = 10^{-9})$ and $(x = 6.23)$ for more relative comparisons of performance.

Table 5: Probability of False Alarm for Knowledge-Aided Depth-Based Detector vs Classical Detector

Chebyshev's Inequality, P_{FA}	$k\sigma$	x	Equivalent P_{FA} for Gaussian Noise
6%	4σ	3.62	10^{-4}
4%	5σ	4.75	10^{-6}
3%	6σ	5.61	10^{-8}
1%	9σ	$x \gg 6.23$	$P_{FA} \ll 10^{-9}$
0.1%	10σ	$x \gg 6.23$	$P_{FA} \ll 10^{-9}$
0.01%	32σ	$x \gg 6.23$	$P_{FA} \ll 10^{-9}$

For reliable detection performance, the probability of detection was set to $P_D = 0.9$. The Knowledge-Aided Depth-Based (KA-DB) detector in comparison with the classical single-pulse detector of Equation (4.11) is given in Table 6; which does show significantly better performance; especially when the false alarm rate is low- i.e. $P_{FA} \leq 10^{-4}$.

Table 6: Probability of Detection Comparison for Knowledge-Aided Depth-Based Detector vs Classical Detector

$k\sigma$	Required SNR for Classical Detector	Required SNR for Depth-Based Detector	Improvement Factor of Depth-Based Detector
3σ	10 dB	3.6 dB	+6.4 dB
4σ	15.6 dB	3.7 dB	+11.9 dB
6σ	20.8 dB	3.8 dB	+17.0 dB
9σ	$SNR \gg 25\ dB$	4.5 dB	<+20.5 dB
10σ	$SNR \gg 25\ dB$	4.6 dB	<+20.4 dB
32σ	$SNR \gg 25\ dB$	6.0 dB	<+19.0 dB

4.3.3 Depth-Based and Knowledge-Aided Depth-Based Detector Performance vs. Envelop Detector

More realistically, a radar sensor utilizes the envelope of the received signal to perform a binary hypothesis test. If we assume a general form of the envelope detector [39]

$$\text{SNR} = \text{A} + 0.12\text{AB} + 1.7\text{B} \tag{4.12}$$

with $\text{A} = \ln\left(\frac{0.62}{P_{FA}}\right)$ and $\text{B} = \ln\left(\frac{P_D}{1-P_D}\right)$, then the depth-based and knowledge-aided depth-based detector performance is found in table Table 7 and 8, respectively. When knowledge of the underlying noise distribution was assumed, the depth-

based methods were shown to improve on the classical single-pulse magnitude threshold detector and classical envelope detector by a factor of up to $> +20dB$ for the case of a P_{FA} of less than 1%.

Table 7: Probability of Detection Comparison for Depth-Based Detector vs Envelope Detector

P_{FA}	Required SNR for Envelope Detector	Required SNR for Depth-Based Detector	Improvement Factor of Depth-Based Detector
6%	6.7 dB	3.6 dB	+3.1 dB
4%	7.2 dB	3.7 dB	+3.5 dB
3%	7.6 dB	3.8 dB	+3.8 dB
1%	9.0 dB	4.5 dB	+4.5 dB
0.1%	11.9 dB	4.6 dB	+7.3 dB
0.01%	14.8 dB	6.0 dB	+8.8 dB

Table 8: Probability of Detection Comparison for Knowledge-Aided Depth-Based Detector vs Envelope Detector

$k\sigma$	Required SNR for Envelope Detector	Required SNR for Depth-Based Detector	Improvement Factor of Depth-Based Detector
4σ	12.5 dB	3.6 dB	+8.9 dB
5σ	17.9 dB	3.7 dB	+14.2 dB
6σ	23.3 dB	3.8 dB	+19.5 dB
9σ	$SNR \gg 26.0\ dB$	4.5 dB	>+21.5 dB
10σ	$SNR \gg 26.0\ dB$	4.6 dB	>+21.4 dB
32σ	$SNR \gg 26.0\ dB$	6.0 dB	>+20.0 dB

One benefit of the depth-based detector is the basis of its nonparametric formulation, which does not rely on the underlying corruptive noise process to conform to a univariate or bivariate distribution; in fact, the depth-based detector should be more optimal for cases in which the underlying noise process is multivariate and not adequately described by a second-order moment method.

4.4 Introduction to Depth-Based Ranking

In the previous formulation of the depth-based detector, knowledge-based or otherwise, there is no due consideration given to the fact there may be more than one scattering center present in the scene under illumination by the distributed sensor network. This is actually a rather glaring omission, as the example clearly

dictated the inclusion of multiple scattering centers. Now, in an effort to correct this omission, a ranking algorithm is introduced to permit the sensor network to determine the effective number of scattering centers within any given observational scene of interest. Second only to detection, is the germane process of determining the number of scattering centers in the background medium. In [57] the authors made use of a ranking and selection algorithm to select the number of components in principal components analysis via the defining of a preference zone based on the ratios of two some of eigenvalues. A series of publications by Chen, [11, 58-60] detailed methods for determining the effective number of signals (ie-scattering centers) based on an asymptotic approach via a confidence interval of the number of principal components. Since the perturbations to the time-reversal operator resulting from the scattering centers are finite and bounded, we propose the use of a confidence interval for the selection and ranking of the measured time-reversal operator. This confidence interval has previously been introduced as the method for minimizing Type I errors in the nonparametric depth-based detector. Applying this minimization of the Type I error recursively allows for the establishment of the confidence interval and ability to apply a statistical selection and ranking algorithm for the determination of the number of signals (ie-scattering centers) present. Recall previously that the false-alarm control was developed for the depth-based detector to be both nonparametric and defined for any statistical probability in which the mean and standard deviation is defined.

From the depth-based detector, singular values lower than the effective rank of the time-reversal operator cause the annulus to collapse; signifying only noise is present. Since the Type I error control forms the basis of the confidence interface, the confidence interval can be selected based upon the desired level of minimization of the false alarm rate. This allows for both a conservative and liberal confidence interval bound to be determined. Recall that the annulus collapses when the signal rank is exceeded. In this manner, as successive signal singular values are removed from the depth-based ranking algorithm via a recursive detection procedure, which incorporates a Type I error control, the proper selection and ranking of the perturbation signals to be recovered is accomplished in a nonparametric fashion.

4.4.1 Depth-Based Ranking Approach

We begin by considering two populations: one comprised of white Gaussian noise, $\mathcal{N}(0,\sigma^2)$, with variance equivalent to unity; and a second population consisting of a bounded rank perturbation with additive white Gaussian noise, in which the measurement noise is assumed statistically similar to the noise population. To fully develop the depth-based ranking algorithm, initially the standard binary hypothesis test is considered

$$H_0 := n(t) \tag{4.13a}$$

$$H_1 := s(t) + n(t) \tag{4.13b}$$

However, Equations (4.13a) and (4.13b) do not properly account for the iterative testing that is to be accomplished via the ranking algorithm; specifically, the binary hypothesis test is more properly written as

$$H_0^j := n(t) \tag{4.14a}$$

$$H_1^j := s^j(t) + n(t) \tag{4.14b}$$

where the superscript j denotes the rank value of the time-reversal operator under test, and is chosen from the sequence of real numbers formed by, $j = [1,2,3,\dots,n]$, and is assumed for all further instances of the superscript j in this chapter. Traditionally, the selection of the null or alternative hypothesis is chosen based upon a pre-determined, or adaptive, threshold that transforms Equation (4.14a) and (4.14b) into

$$\delta_{\text{Threshold}}^j \underset{H_1^j}{\overset{H_0^j}{\lessgtr}} \tag{4.15}$$

which requires a threshold. Previously we showed this to be a non-parametrically derived quantity represented by a volume in *n*-dimensional space. This quantity may be determined with training data or empirically as is the case with this work. This quantity is then used as the approximate of the noise bounds on the time-reversal operator. Each scattering center manifests as a bounded perturbation on the target covariance function, and owing to its localized phenomenology, is isolated to a single and unique singular value; this stands in stark contrast to thermal/environmental noise that is always full-rank, indicating a diffuse statistical process; and clutter that is never tightly bound, but partial or full-rank, indicative of a simple or complex statistical process, respectively. This bounded phenomenology is the principal reason detection and ranking is possible. Rather than attempting to determine which selection procedure could choose the correct partial-to-full rank of a clutter or noise process, the selection algorithm only has to

contend with one or more finite bounded perturbations isolated to a single singular value. Now, admittedly our object model is a collection of finite-sized target scattering centers, but even complex extended targets are modeled as collections of scattering centers; and more importantly phenomenologically appear as discrete or diffuse collection of point-scatterers (point-scatterer clouds).

Differential dispersion values are determined from the difference of the volume defined by the contour, D^{β^j}, and that of the volume of a second contour, D^p. Previously, β, was defined as unity, and that definition holds true here, where we are attempting to ascertain the effective rank of the target time-reversal operator function non-parametrically. The value of unity for contour, D^{β^j}, encompasses all population values for an assumed rank of our target time-reversal operator, in our depth functional. The value of contour, D^p, is between the values of $p \in (0,1)$, and constitutes the inner radius of the annulus that is comprised of our annular volumetric parameter used for our recursive binary hypothesis test. For this case, whilst the value of p has previously been defined as, $p \in [0.5,0.75,0.5]$, we initially fix the value at $p = 0.5$; thus, maximizing the possible annular volume of our depth functional, and ensures the collapse of this annular volume is due to the absence of a signal; as the singular values for our corruptive noise process is, $\mathcal{N}(0,\sigma^2)$, with $\sigma^2 = 1$; thereby ensuring a clustering of noise singular values that are far removed from signal singular values.

As our example consists of a finite number of dielectric scattering centers of the singly-spread target-or rather, the *range-extended* target, as there is no assumed motion smearing the resultant echoed received signal-the ranking algorithm does not need to run any longer than the computational time required to find the effective rank of the corruptive noise process; defined as the rank value at which point the binary hypothesis test choose H_0. For each step in our recursive algorithm, the contours, D^{β^j} and D^p are defined. Each contour is effectively the boundary for a value for our depth functional $D^{\beta^j} := \hat{V}^{\beta^j}$ and $D^p := \hat{V}^p$. Having defined the depth function values, the differential dispersion is calculated from

$$\hat{V}^j_{[i]} = \hat{V}^{\beta^j}_{[i]} - \hat{V}^p_{[i]} \tag{4.16}$$

The threshold value is derived from signal-free training data comprised of only the underlying corruptive noise process. Similarly, we calculate the annular volume of the corruptive noise process by choosing $\beta = 1$ and $p = 0.5$.

$$\hat{V}^j_{\text{Threshold}} = \hat{V}^{\beta^j}_{\text{Threshold}} - \hat{V}^p_{\text{Threshold}} \tag{4.17}$$

where the normalized threshold statistic is found from

$$\delta^{j}_{\text{Threshold}} = \frac{\hat{V}^{j}_{\text{Threshold}}}{\hat{V}^{j}_{\text{Threshold}}} \tag{4.18}$$

In this manner, regardless of the actual measurement noise, the threshold for determination of the binary hypothesis test is non-parametrically derived. Before we can jump into ranking, a method of false alarm control is required. As was the case for depth-based detection, the Chebyshev Inequality is applied to our nonparametric threshold annular region, in an effort to minimize Type II errors. A number of $\hat{V}^{j}_{\text{Threshold}}$ values are calculated based on target-free training data, and the mean and standard deviation of the vectorized quantities are determined. The Chebyshev Inequality is valid for any population, provided a mean and standard deviation exist. We choose the false alarm rate by varying a single parameter, k in the expression

$$\hat{V}^{j}_{\text{Threshold}} = \mu^{j} + k\sigma^{j} \tag{4.19}$$

where μ^{j} and σ^{j} were previously derived from training data. k is the effective number of standard deviations that are required to encompass a minimum population mean of $\left(1 - \frac{1}{k^2}\right)$. In our case, for a desired false alarm rate of 6%, k is required to be set at $k = 4$; whereas for a desired false alarm rate of 4% or 3%, k is 5 and 6 respectively. The threshold for the binary hypothesis test is equivalent to

$$\delta^{j}_{\text{Threshold}} = \frac{\hat{V}^{j}_{\text{Threshold; }\mu^{j}+k\sigma^{j}}}{V^{j}_{\text{Threshold; }\mu^{j}+k\sigma^{j}}} \Rightarrow 1 \tag{4.20}$$

which is to say, unity. This is a nonparametrically derived quantity that ensures the applicability of the binary hypothesis test over a wide-range of corruptive noise processes, without compromising the integrity of the depth-based detector.

Determination of the confidence interval is based on the estimate of the annular volume between the $\hat{V}^{\beta}$ and $\hat{V}^{p}$; as the annulus region contracts with each recursive contraction of contour, $V^{\beta^{j}}$, there is a point at which the annulus of the signal-free is volumetrically equivalent to the annulus of the time-reversal operator under test. It is important to note that whilst noise-thermal, environmental or otherwise-is full-rank, there is a bounded perturbation resulting from the presence of scattering center reflection(s) that is manifest as a localized singular value(s) in the time-reversal operator; this offset has previously been described as arising from Newton's Third Law, but is more colloquially referred to as *eigenvalue*

repulsion. Now, one the rank of the echoing scattering center(s) is exceeded, the singular values of the time-reversal operator under test collapses to values that are essentially equivalent to the signal-free time-reversal operator, derived from signal-free training data. Since the values under test differ only in statistical variability, the Chebyshev inequality derived threshold value, $\delta_{\text{Threshold}}$ should eclipse the volumetric bounds of noise-on-noise annular volumes, and result in a null hypothesis being chosen for the binary hypothesis test, see Equation (4.13a) and (4.13b). In this manner, the differential volume serves as the confidence bounds for our depth-based ranking algorithm. To conclude the depth-based ranking algorithm, the final binary hypothesis test is then

$$\delta^j \underset{H_1^j}{\overset{H_0^j}{\lessgtr}} \delta^j_{\text{Threshold}} \tag{4.21}$$

where j has previously been defined as the rank value under test, and is a sequence of real numbers formed by, $j = [1,2,3,\dots,n]$. The value of j, or the effective rank of the time-reversal response matrix under test, for which the test last hypothesis determines alternative hypothesis, H_1, is true also determines the final rank value of the matrix; thus, the first value at which H_0 is determined true, terminates the recursive depth-based ranking algorithm, and also indicates the point at which the annular region of the differential volume collapses, and only contains noisy singular values.

In this section, a bespoke depth-based ranking algorithm was introduced, along with a method for controlling the Type II error of the nonparametric binary hypothesis test. For the succeeding section, a series of examples are presented, focused on a common scenario, and the results of the depth-based ranking algorithm are determined based upon a receiver-operating characteristic curve (ROC).

4.4.2 Depth-Based Ranking Examples

Whereas the Section 4.3 focused on demonstrating the efficacy of the depth-based *detector*, this section is primarily focused on the development of receiver-operating characteristic (ROC) curves that highlight the virtue of the depth-based *ranking* algorithm of Section 4.4. In an effort to maintain consistency between Section 4.3, each of the three scattering centers considered for demonstration of the depth-based ranking algorithm has a discrete reflectivity and location within the scene of under observation by the distributed network. Thus, allowing for each of the three

scattering centers to be uniquely detected, ensuring there is no potential ambiguity in the ranking results. Below is a table highlighting the specific parameters assigned to each scattering center using for the subsequent examples.

Table 9: Scattering Center Parameters

Scattering Center	Dielectric Coefficient (ρ)	Scattering Center Location (x, y)
1	$\rho = 2.00$	$[5, 0]$
2	$\rho = 1.75$	$[-2.5, 4.33]$
3	$\rho = 1.50$	$[-2.5, 4.33]$

Each of the three scattering centers is placed approximately equidistant from the origin of the scene under illumination. Further, the location of each scattering center is chosen to maximize the distance between each remaining scattering center, creating an equilateral triangle, ensuring no two scattering centers overlap. Whilst the Born approximation does not allow for a particular dielectric property to be characterized, the reflectivity values are chosen, such that, their values are approximations of dielectric permittivities equivalent to dielectric spheres of finite size-in this case, variations of glass and crystalline materials. This last point is nuance, and does not drastically alter the results, other than to prepare the reader for a discussion on reflectivity recovery-post-detection and post-ranking-see Chapter 8 for further discussion.

Initially, the results are seemingly a repeat of Section 4.3, in that we are concerned principally with the results for the ranking algorithm with an assumed initial rank of unity; not very interesting, to be sure, but a necessary first step when Equation (4.21)-the iterative binary ranking hypothesis test-is utilized. When the term *rank* is applied to a sensing problem, the point is not to rank, in any particular order, the scattering centers within the illuminated scene, but to place a confidence bound on the actual number of scattering centers present. Whilst this previous statement may, again, feel like the origins of a semantic argument, ranking is more of a *bounding* operation, as opposed to a mathematical treatment to determine the particular location and makings of the scattering centers within the distributed sensor network's area of concern. Enough of nuance and semantics, let us now consider the outcome of Equation (4.21) for the case in which the rank is initially considered to be unity. For all results in this section, the assumed required probability of detection is, $P_D = 0.9$, with the false alarm rates of concern fixed to $P_{FA} \in [6\%, 4\%, 3\%, 1\%, 0.1\%, 0.01\%]$.

As previous discussed in Section 4.3.1, the performance of any receiver operating characteristic curve needs to be compared to a baseline in order to have any relative meaning. Considered in isolation, results are easily analyzed, but there is no weight to the results without a suitable comparison. For this section, the depth-based ranking algorithm results are compared against a very traditional sensor receiver architecture-that of the envelope detector, see Equation (4.12). Now, Equation (4.12) is not concerned in any manner with the concept of allowing a confidence bound to be formed for the purposes of *ranking*, but rather for the simple purpose of determining a simple binary output: scattering center present, or scattering center absent.

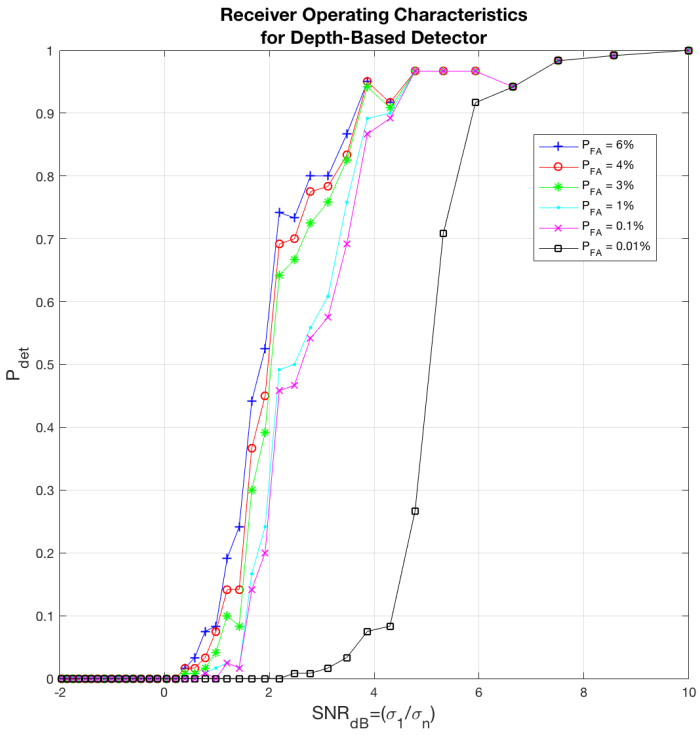

Figure 17: Probability of Detection vs SNR for Depth-Based Rank (j = 1)

Thus, any attempt to compare the results of the depth-based ranking algorithm should be approached from the considered stand-point that we are attempting to determine if the ranking algorithm enhances the quality of information gleaned following post-depth-based detection. Under this framework, the depth-based ranking algorithm should produce ROC curves that perform *on par*, or exceed the performance of the envelope detector, and demonstrate equivalent performance to the depth-based detector. Having described the desired outcome from the proceeding examples, depth-based ranking receiver-operating characteristic curve for a unity rank approximation is shown in Figure 17.

Table 10: Unity Rank Comparison for Depth-Based Ranking Algorithm vs Envelope Detector

P_{FA}	Required SNR for Envelope Detector	Required SNR for Depth Based Detector $(j = 1)$	Improvement Factor
6%	6.7 dB	3.6 dB	+3.1 dB
4%	7.2 dB	3.7 dB	+3.5 dB
3%	7.6 dB	3.8 dB	+3.8 dB
1%	9.0 dB	4.5 dB	+4.5 dB
0.1%	11.9 dB	4.6 dB	+7.3 dB
0.01%	14.8 dB	6.0 dB	+8.8 dB

As expected, the results track closely with those of the standard depth-based detector approach. Further, the results are typically an average of $+3dB$ better than the standard envelope detector. That is all well and good, however, the relative merit of the depth-based ranking algorithm is a bit lost for a unity rank time-reversal operator. Now initially, the problem considered the presence of 3 target scattering centers; thus, allowing for more in-depth investigation and demonstration of the efficacy of the depth-based ranking approach. Having exhausted discussion on the unity rank binary hypothesis test, let us move the depth-based ranking test to an assumed rank 2 time-reversal operator, see figure 18.

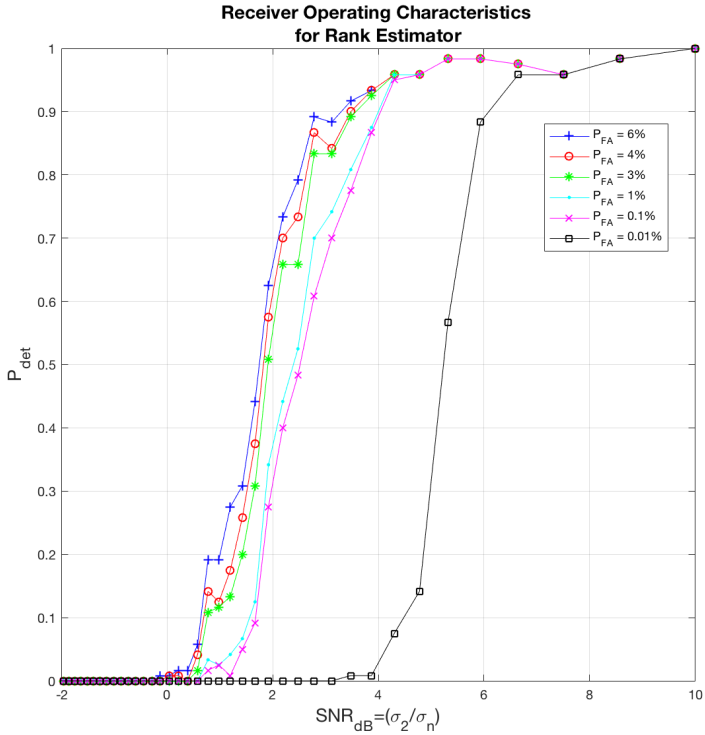

Figure 18: Probability of Detection vs SNR for Depth-Based Ranking (j=2)

Most noticeable in Figure 6 and Figure 7 is the trend towards higher required signal-to-noise ratio in order to determine the outcome of the Equation (4.21) for $j = 2$. Just how much is shown in table Table 11, though for all intents and purposes, the results track closely with those of receiver operating characteristic curves of the unity rank test, $j = 1$ for Equation (4.21). What exactly does this mean? More precisely, does this trend towards higher signal-to-noise result in a detriment or enhancement to our post-depth-based detection depth-based ranking algorithm? Realistically speaking, small variations in required signal-to-noise are not a detriment, but a consequence of any data processing approach dealing with simulated-or real-data; thus, we do not consider any fluctuation resulting in an improvement over the classical single-pulse envelope detector to result in detrimental performance. In fact, even though the results in table Table 11 are similarly as impressive as the unity rank test in table Table 10, there is but a small variation in resultant average performance of $-0.1dB$, in which the improvement factor is around $+2.9dB$ for the rank $j = 2$ for equation (4.21).

Table 11: Rank (j=2) Comparison for Depth-Based Ranking Algorithm vs Envelope Detector

P_{FA}	Required SNR for Envelope Detector	Required SNR for Depth-Based Detector $(j = 2)$	Improvement Factor
6%	6.7 dB	3.8 dB	+2.9 dB
4%	7.2 dB	4.3 dB	+2.9 dB
3%	7.6 dB	4.3 dB	+3.3 dB
1%	9.0 dB	4.4 dB	+4.6 dB
0.1%	11.9 dB	4.5 dB	+7.4 dB
0.01%	14.8 dB	6.2 dB	+8.6 dB

Thusly, the value for the depth-based ranking test moves from $j = 2$ to $j = 3$, and the receiver operating characteristic curves generated for the outcome of ranking binary hypothesis test for a variety of signal-to-noise ratios from $-3dB$ to $10dB$. For the cases in this section, the detection performance is assumed acceptable for $P_D = 0.9$, with the false alarm rates of concern being, $P_{FA} \in [6\%, 4\%, 3\%, 1\%, 0.1\%, 0.01\%]$. The results for the depth-based ranking algorithm for $j = 3$ are shown below in Figure 19

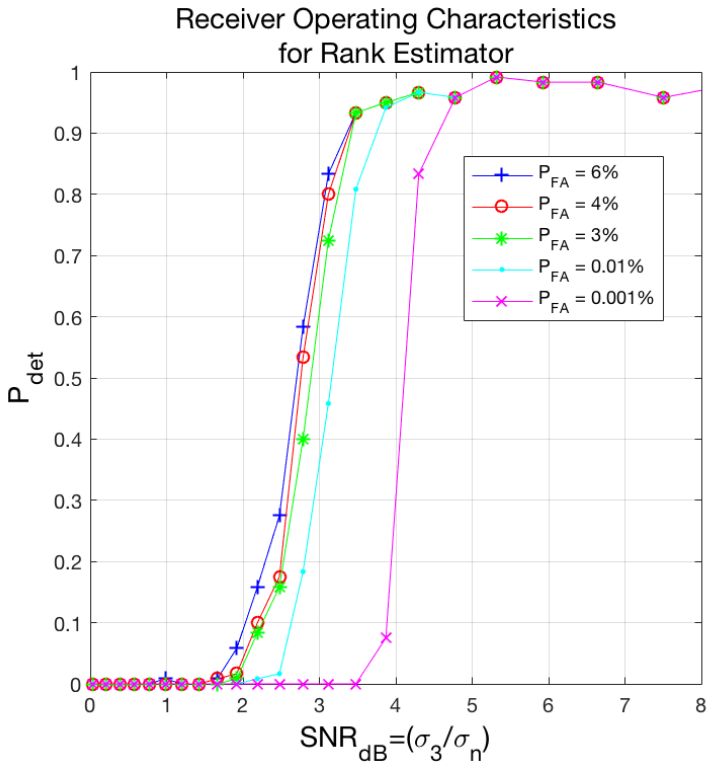

Figure 19: Probability of Detection vs SNR for Depth-Based Ranking (j=3)

Again, the particular values for the required signal-to-noise ratios to determine the presence of a rank 3 signal in the target time-reversal operator is not the primary concern, as long as the signal-to-noise ratio exceeds the performance of the single-pulse envelope detector, and is approximately equivalent to the depth-based detector; wherein the results are stated to exhibit an enhancement in information post-depth based detection, by providing new information on the confidence bound of the rank of the signal embedded within the target time-reversal operator. Indeed, even for an assumed rank of $j = 3$, the results are quite telling-see Table 12-and further demonstrate the efficacy of the depth-based ranking algorithm for their determination of the number of scattering centers within a scene of interest under illumination by the distributed sensor network.

Table 12: Rank (j=3) Comparison for Depth-Based Ranking Algorithm vs Envelope Detector

P_{FA}	Required SNR for Envelope Detector	Required SNR for Depth-Based Ranking $(j = 3)$	Improvement Factor
6%	6.7 dB	3.2 dB	+3.5 dB
4%	7.2 dB	3.3 dB	+3.9 dB
3%	7.6 dB	3.4 dB	+4.2 dB
1%	9.0 dB	3.7 dB	+5.3 dB
0.1%	11.9 dB	3.7 dB	+8.2 dB
0.01%	14.8 dB	4.5 dB	+10.3 dB

In summary, this particular section showcased the results for the post-depth-based detector depth-based ranking algorithm. The results for the depth-based detector were compared to those of a classical single-pulse envelope detector; wherein the performance of the envelope detector was assumed as the minimum floor of performance in which the depth-based detector is declared an enhancement to, or the detriment of, the information gleaned post-depth-based detector. In each of the three cases considered: $j \in [1,2,3]$, the results tabulated in Table 10, Table 11, and Table 12 demonstrated the performance improvement was on the order of $+3.0\ dB$ better than the classical single-pulse envelope detector; the significance of which is that the depth-based ranking algorithm was declared a value-added enhancement to the depth-based detector, by providing a confidence bound of the effective rank of the measured target time-reversal operator.

4.5 Summary

In this chapter, we have introduced a depth-based method for range-extended target scattering center detection in noisy environments, based on a pre-detection fusion algorithm. The performance of the detector was determined for differing levels of noise and compared to a classical single-pulse detector. The results demonstrated the benefits of utilizing a distributed sensor network and depth-based algorithms for the detection of a target scattering center obfuscated by a noisy measurement environment. When knowledge of the underlying noise distribution was assumed, the depth-based methods were shown to improve on the classical single pulse magnitude threshold detector and a classical envelope detector by a factor of over $+20.0\ dB$. Additionally, the depth-based detector is nonparametric, and does not rely on the underlying corruptive noise process to conform to a univariate or bivariate distribution-as is the case with traditional parametric detectors.

Future efforts are focused on the extension of this depth-based detector to broader classes of corruptive noise distribution; including those distributions that are not adequately described by second-order moment methods. The real benefit of this depth-based approach is that no form of the underlying corruptive noise is required to be known *a priori*, and the very fact that the depth-based detection and

depth-based ranking algorithms are nonparametric, means they are applicable to broad ranges of distributions-both characterized and unknown.

4.6 Conclusion

Depth-based methods lie at the intersection of mathematical statistics and computational geometry and have emerged over the past decade as a promising candidate for dealing with high-dimensionality nonparametric multivariate data. Whilst there have been several publications detailing depth-based methods and applications, there are currently no publications that focus on sensing related challenges that could benefit from the incorporation of the depth-based algorithms. In this chapter, the author demonstrated the more salient task of a sensing system-detection-and the detection improvement afforded by the tandem use of a distributed sensor network and a depth-based detection algorithm. A broad range of sensing modalities are currently being explored that would benefit from this emerging field of mathematical statistics and anticipate further examples of depth-based methodologies to emerge as part of this broader research effort.

5 Introduction to Weak Signal-to-Noise Ratio Regimes: Using a Distributed Sensor Network to Overcome Traditional Barriers to Sensing

5.1 Motivation

Previously, we introduced a novel non-parametric depth-based method for the target detection and ranking problem in noisy environments under nominal signal-to-noise ratios. In this chapter, we seek to expand our performance bounds, and introduce detection and ranking in the negative signal-to-noise ratio (SNR) regime. There are many ways to look at the extreme bounds of performance, and there are most assuredly many more than could possibly be covered in this work; instead we look at the overall theoretical performance bound from the microcosm of the detection threshold. Without detailing specifics of any particular distributed sensor system, modality, and associated waveforms and parametrics, we seek to understand at what point the maximum efficiency for detection performance is achieved. An interesting set of publications [48-49, 61-62], explored the problem via summations of individual radar monostatic sensor estimated covariance matrices. Theoretical detection performance was achieved with signal-to-noise ratios (SNR) as low as $-34dB$ [48, 61], and approximately $-30dB$ signal-to-clutter-plus-noise ratios (SCNR) [49, 62]. How is this possible?

The answer lies at the intersection of *big data* and distributed sensor networks. More importantly, the ability to achieving practical detection performance in the negative SNR regime is due to the generalization of classical *communicative probability* to *non-communicative probability*. From communicative probability, random variables are typically called *observations* and denoted by the variable x which is found from a probability distribution $P(x)$, and the expectation is called the *first moment* or *mean* and represented by the symbol, $\langle f(x)\rangle$ or $E\{f(x)\}$, and is found from

$$\langle f(x)\rangle = \sum_x f(x)P(x) \tag{5.1}$$

or more generally,

$$E\{x\} = x_1p_1 + x_2p_2 + \cdots + x_np_n \tag{5.2}$$

with the sum of $p_1 + \cdots + p_n = 1$. In non-communicative probability, matrices or operators take the place of scalar random variables and the trace function serves as the expectation. Non-communicative probability is a generalization of classical

probability-as discussed previously is possible due to *free-probability*. This serves two fundamental purposes, one of which has already been mentioned twice:

1. Quantities build from the algebra of random variables and their associated expectations, such as the trace of a, $n \times n$, random matrices are typically very stable in the large n limit; this is in spite of the fact the associated sample space and event space may vary with n [63].
2. Free-probability is an abstract formalism, which allows the generalization of classical commutative theory of probability to the theory of non-commutative probability, which does not have any associated sample or event space.

More importantly, non-commutative probability has as special cases (see [63])

1. Classical probability
2. Spectral theory, where matrices or operators take on the role of random variables and the trace function assumes the role of the expectation of random variables
3. Random matrix theory, which is viewed as a combination of classical probability with spectrum theory
4. Quantum mechanics, where the physical observables are the random variables and the expectation is the expected value on a given observable being in a particular state

In free-probability, the goal is to have the *algebra* serve as the basis of the theory, as opposed to foundations built upon sets, categories, etc. Whilst free-probability is the enabling theorem upon which this chapter is based (the algebra is the foundation), the particular phenomenon that is responsible for the ability of a distributed sensor network to make observations and detections in negative signal-to-noise ratio regimes is called *concentration of measure*. In the next section, the theoretical foundation for sensing in negative SNR regimes under big data scenarios is introduced.

5.2 Concentration of Measure

Typically, detection algorithms seek to reduce the dimensionality of the collected data to enable a single variable to be manipulated for the purpose making of a binary decision versus a threshold variable. In this thesis, the concept of *big data* has been discussed and shown to benefit salient modalities of sensing-such as detection. The so-called *curse of dimensionality*, is actually a blessing: increases in dimensionality often aid in mathematical analysis, see references [48-49], and [61-62] for examples. In particular, reference [61] details a method to reduce

interference from clutter sources on the sample covariance matrix through the use of reproducing kernel Hilbert spaces; which increased the dimensionality of the sample covariance matrix, and reduced the impact of clutter interference by *spreading* the corruptive clutter energy over a larger number of basis functions. The *blessing of dimensionality* is the subject of this chapter, and is studied from the vantage point of concentration of measure-as examined through Talagrand's inequality. Many complicated and high-dimensional quantities are more readily analyzed by assuming they exhibit behaviour that is consist with Lipschitz functions, which are smoothly varying functions and are handled within the framework of Talagrand's inequality.

Talagrand stated, one probabilistic aspect of measure of concentration, that a random variable that depends-*in a smooth way*-on the influence of many independent variables is essentially constant [64]. Therefore, due to concentration of measure, a Lipschitz function is nearly constant. The resultant tail bounds behave, no worse than, a scalar Gaussian random variable with absolutely controlled mean and variance [63]. One key differentiator of convex optimization problems and those characterized by concentration of measure under Talagrand's inequality is convex optimization assumed the following conditions are true:

1. Linearity
2. Convexity

To move from standard probabilistic views on probability inequalities, especially those relying on law of large numbers theorems, to the probabilistic concentration of measure phenomenon the following is assumed true:

1. Convexity
2. Lipschitz

From [63], the theory of concentration inequality tries to determine from a random vector, $\boldsymbol{x}$, from a measurable space, $\boldsymbol{\chi}$, and a measurable map, $f : \chi \to \mathbb{R}$, what is the explicit bound on $\mathbb{P}(f(\boldsymbol{x}) - \mathrm{E}[f(\boldsymbol{x})]| \geq t)$. In this chapter, the application of concentration of measure is on matrices, not random vectors-which is due to free-probability. However, under free-probability, the emphasis is on a probability based upon a foundation of *algebra* not *spaces*. So, with that thought in mind, let us explore an example of the application of concentration of measure to a sequence of random variables. Let $X_1, X_2, \ldots X_n$ be a sequence of independent random variables assuming the values of ± 1 with equal probability, or $p_{0,1} = 0.5$.

$$S_n = X_1 + \cdots + X_n \tag{5.3}$$

The law of large numbers, under classical probability theory, would state that the quantity S_n is essentially constant and equal to zero. Under the central limit theorem, the fluctuations of S_n would be $\sqrt{(n)}$, which is not equal to zero. Now, from [64], as the value of n in S_n increases and approaches ∞, that is the appropriate value at which S_n should be measured. Following the approach by Ledoux in [64], we find from the concentration of measure the classical exponential bound

$$\mathbb{P}\left(\left\{\frac{|S_n|}{n} \geq t\right\}\right) \leq 2e^{\frac{-2nt^2}{2}}, t \geq 0 \tag{5.4}$$

which is equivalent to $\frac{S_n}{n} \simeq 0$. Concentration of measure is readily generalized by [63]

1. Replacing linear functionals, such as sums of random variables, by Lipschitz functions of the samples
2. Considering measures that are not of product form

By replacing the sums of random variables with sums of random matrices, we arrive at the application of concentration of measure to free-probability, and the fundamental mathematical foundation for detection under low signal-to-noise ratio regimes by a distributed sensor network.

5.3 Concentration of Measure for Eigenvalues

In the previous section, the phenomenon of concentration of measure was briefly introduced. For the interested reader, [64] is an excellent exposition on the topic. In this section, the concept of concentration of measure is extended to eigenvalues of random matrices, or more importantly sums of random matrices. In order to extend concentration of measure, eigenvalues and their associated functionals should be shown to be Lipschitz functions, so that Talagrand's inequality is applicable. For this chapter, only those concentration inequalities for relevant random variables are discussed; recall in free-probability, random variables are matrices. For the remainder of this section, the extension of concentration of measure to eigenvalues and their functionals closely follows portions of Chapter 4 of [63], whose contents were motivated by the research funding provided by the Air Force Office of Scientific Research under grant FA8650-11-RY-09COR and was co-authored by thesis advisor Dr. Michael Wicks.

Application of concentration of measure to eigenvalues is focused on two core connections: Lipschitz mappings of eigenvalues, and smoothness and

convexity of the eigenvalues of a matrix and traces of matrices. The latter is particularly important, as the trace function is a linear functional, greatly simplifying the mathematics involving multiple complex random matrices. Once the eigenvalues and functionals are shown to be Lipschitz and convex, theoretical tail bounds are found for Wigner random matrices and compared to those of the sample covariance matrix for a traditional monostatic radar system.

5.3.1 Lipschitz Mappings of Eigenvalues

From [65], let G denote the Gaussian distribution on $\mathbb{R}^n$ with density

$$\frac{dF(\boldsymbol{x})}{d\boldsymbol{x}} = \frac{1}{(2\pi\sigma^2)^n} e^{\left(-\frac{\|\boldsymbol{x}\|^2}{2\sigma^2}\right)} \tag{5.5}$$

and $\|\boldsymbol{x}\|^2 = x_1^2 + x_2^2 + \cdots + x_n^2$ is the Euclidean norm of $\boldsymbol{x}$. For a K-Lipschitz function $F: \mathbb{R}^n \to \mathbb{R}$, we have

$$|F(\boldsymbol{x}) - F(\boldsymbol{y})| \leq K\|\boldsymbol{x} - \boldsymbol{y}\|, \ \boldsymbol{x}, \boldsymbol{y} \in \mathbb{R}^n \tag{5.6}$$

for a positive Lipschitz function K. Now, for any positive number t, it can be shown that

$$G(\{\boldsymbol{x} \in \mathbb{R}^n : |F(\boldsymbol{x}) - F(\boldsymbol{y})| > t\}) \leq 2e^{\left(-\frac{ct^2}{K^2\sigma^2}\right)} \tag{5.7}$$

with $\mathbb{E}\big(F(\boldsymbol{x})\big) = \int_{\mathbb{R}^n} F(\boldsymbol{x}) dG(\boldsymbol{x})$, and $c = \frac{2}{\pi^2}$. In [66] the $\sigma = 1$ case is proven. More generally, the mapping $\boldsymbol{x} \mapsto \sigma\boldsymbol{x}: \mathbb{R}^n \mapsto \mathbb{R}$, the resultant composed function $\boldsymbol{x} \mapsto F(\sigma\boldsymbol{x})$ satisfies a Lipschitz condition with constant $K\sigma$, [63]. Having shown the Lipschitz mapping of eigenvalues for a random matrix comprised of independent identically distributed entries, the next step is showing the smoothness and convexity of eigenvalues and traces of matrices.

5.3.2 Smoothness and Convexity of the Eigenvalues of a Matrix and Traces of Matrices

There were two conditions that must be met in order to move from the classical probabilistic framework to a probabilistic concentration of measure phenomena: Lipschitz and convexity. In the previous section, the Lipschitz mapping of eigenvalues was shown. The second and final step in ensuring the probabilistic framework provided by the concentration of measure phenomenon is to demonstrate the convexity of eigenvalues. For this section, we closely follow the exposition of [63]. Recall that

$$\mathrm{Tr}\big(f(\mathbf{A})\big) = \sum_{i=1}^{n} f\big(\lambda_i(\mathbf{A})\big) \tag{5.8}$$

with $\lambda_i(\mathbf{A})$ being the eigenvalues of matrix **A**. Now, consider a Hermitian $n \times n$ matrix **A**. Let f be a real-valued function on $\mathbb{R}$, and the function of the Hermitian matrix be $f(\mathbf{A})$. If we assume the matrix decomposition of **A** is $\mathbf{A} = \mathbf{UDU}^*$, and $\boldsymbol{D}$ is a diagonal real matrix denoted by $\mathbf{D} = \mathrm{diag}(\lambda_1, \lambda_2, \dots, \lambda_n)$, and **U** is a unitary matrix, then

$$f(\mathbf{A}) = \mathbf{U} f(\mathbf{D}) \mathbf{U}^* \tag{5.9}$$

with $f(\mathbf{D})$ being a diagonal matrix with entries $f(\lambda_1), f(\lambda_2), \dots, f(\lambda_n)$and $*$ denotes the conjugate transpose operation. In order to show the convexity and smoothness, we rely on the following Lemma [67]

Lemma 5.1, (Guionnet and Zeitoumi 2000)

1. If f is a real-valued convex function on $\mathbb{R}$, it holds that $\mathrm{Tr}\big(f(\mathbf{A})\big) = \sum_{i=1}^{n} f\big(\lambda_i(\mathbf{A})\big)$ is convex.
2. If f is a Lipschitz function on $\mathbb{R}$, $\mathbf{A} \mapsto \mathrm{Tr}\big(f(\mathbf{A})\big)$ is a Lipschitz function on $\mathbb{R}^{n^2}$ with Lipschitz constant bounded by $\sqrt{n}|f|_\ell$

with $|f|_\ell$ being the Lipschitz constant and defined by

$$|f|_\ell = \sup \frac{|f(\boldsymbol{x}) - f(\boldsymbol{y})|}{\|\boldsymbol{x} - \boldsymbol{y}\|} \tag{5.10}$$

where $\|\cdot\|$denotes the Euclidean norm on $\mathbb{R}^k$. From **Lemma 5.1.1** we find that the trace of a Hermitian square matrix is indeed convex, which is expected as the trace functional is linear. We also require that the function on the Hermitian matrix or eigenvalues be monotonically increasing, see [61] for a novel method of limiting the impact of clutter on the detection algorithm via monotonically increasing functions and kernel trick methods. Further, we show the smoothness criterion through **Lemma 5.1.2** with the Lipschitz constant, $|f|_\ell$, being finite, smoothly varying, and bounded.

Having showed the eigenvalues of a matrix and traces of matrices-particularly Hermitian matrices-are Lipschitz and convex, we now demonstrate the tail bounds for salient forms of matrices that will serve as the basis for the examples of this chapter, and as a comparison to conventional radar signal processing. We start by examining the sample covariance matrix, which serves as the foundation of modern statistical signal processing.

5.3.3 Concentration of Measure for Sample Covariance Matrices

Nearly all modern detection algorithms rely on variations of detection with sample covariance estimates, whether they be from

$$\mathbb{P}\{\|\mathbf{A}\| \geq 2\sqrt{n}(1+t)\} \leq Ce^{\left(-\frac{n^{3/2}}{C}\right)} \tag{5.11}$$

where $\|\mathbf{A}\|$ represents the Euclidean norm. One immediate observation from Equation (5.11) is that the sample covariance matrix is slow to converge to a constant value, and requires a very large number of observations, n to achieve this stability. This is why many sample covariance matrix based algorithms attempt to achieve homogeneity in sample observations, either through whitening (see [2-3]), adaptive matched filtering (see [68-69]), or non-homogeneity detection (see [70]). The ability to choose random variables from a similar probability distribution is akin to selecting n observations from a sample space or event space that is well-behaved-a difficult and impractical task for most sensing applications, hence the reason the signal-to-noise ratio must be positive to achieve acceptable detection performance.

5.3.4 Concentration of Measure for Wigner Random Matrices

A Wigner matrix is any $n \times n$ matrix $\mathbf{H}=\left(h_{ij}\right)_{1\leq i\leq j\leq n}$, such that

$$h_{ij} = \frac{1}{\sqrt{n}}\left(x_{ij} + y_{ij}\right) \forall\ 1 \leq i \leq j \leq n \tag{5.12}$$

where $\{x_{ij}, y_{ij}\}$ are real independent, identically distributed (IID) random variables, with an expectation, $\mathrm{E}[x_{ij}] = 0$, and variance, $\mathrm{Var}(x_{ij}) = \mathrm{E}[x_{ij}^2] - \left(\mathrm{E}[x_{ij}]^2\right) = \frac{1}{2}$. Alternatively, the Wigner matrix may also be defined as

$$h_{ii} = \frac{1}{\sqrt{n}}x_{ii} \forall\ 1 \leq i \leq n \tag{5.13}$$

where $\{x_{ii}\}$ are assumed to be real, IID random variables, with the first moment $\mathrm{E}[x_{ii}] = 0$ and second moment $\mathrm{E}[(x_{ii} - \mathrm{E}[x_{ii}])^2] = 1$. Typically, the entries of the Wigner matrix, $\mathbb{H}$, will scale with the dimensionality, to ensure in the limit, $n \to \infty$, all eigenvalues of **H** remain bounded. An example is shown below; recall that the trace function is linear, and we are attempting to show the bounded nature of the eigenvalues in the asymptotic limit

$$\mathrm{E}\sum_{k=1}^{n}\lambda_k^2 = \mathrm{E}[Tr\boldsymbol{H}^2] = \mathrm{E}\sum_{i=1}^{n}\sum_{i=1}^{n}|h_{ii}|^2 = n^2\mathrm{E}[|h_{ii}|^2] \tag{5.14}$$

where λ_k are the eigenvalues of **H**. Obvious from Equation (5.14) is the implicit assumption that the trace of the eigenvalues is not infinite as $n \to \infty$; this implies

that $\mathrm{E}\left[\mathrm{Tr}\mathbf{H}^2\right] \simeq n$, and hence $\mathrm{E}[|h_{ii}|^2] \simeq \frac{1}{n}$. Free probability and concentration of measure are the reason detection in the negative signal-to-noise ratio is possible. Whilst not necessarily apparent just yet, but as this section progresses, the conceptual theory for why this is true-in comparison to sample covariance matrix based methods-will become apparent quite soon. First, let us introduce the following theorem from [67]

Theorem 5.1. Suppose that the laws of the entries $\{\mathrm{x_{ij}}, \mathrm{y_{ij}}, \mathrm{x_{ii}}\}$ satisfies the logarithmic Sobolev inequality with constant $\mathrm{c} > 0$. Then, for any Lipschitz function $\mathrm{f}: \mathbb{R} \to \mathbb{C}$, with Lipschitz constant $|\mathrm{f}|_\ell$ and $\mathrm{t} > 0$, we have that

$$\mathbb{P}\left(\left|\frac{1}{t}\mathrm{Tr}f(\mathbf{H}) - \mathrm{E}\left[\frac{1}{n}\mathrm{Tr}f(\mathbf{H})\right]\right| \geq t\right) \leq 2\mathrm{e}^{-\frac{n^2t^2}{4c|f|_l^2}} \tag{5.15}$$

where $|\mathrm{f}|_\ell^2$ represents the Lipschitz constant.

From the concentration of measure inequality, a remarkable difference between Equations (5.15) and (5.11) is noticeable-the bound on the concentration of measure exponent converges significantly faster for Equation (5.15), that of the sample covariance matrix exponent in Equation (5.11)! This is one of the most significant theorems and comparison that differentiates conventional statistical signal processing form this new foundation built upon the theories of free probability and concentration of measure. First, in order to prove **Theorem 5.1**, we need to introduce the following theorem from Herbst, see [71]

Theorem 5.2. Suppose that $\mathbb{P}$ satisfies the log-Sobolev inequalities on $\mathbb{R}^n$ with constant c. Let $g: \mathbb{R}^n \to \mathbb{R}$ be a Lipschitz function with constant $|G|_\ell$. Then, for every $t > 0$,

$$\mathbb{P}(|g(\boldsymbol{x}) - \mathrm{E}[g(\boldsymbol{x})]| \geq t) \leq 2e^{-\frac{t^2}{2c|G|_\ell}} \tag{5.16}$$

This observation from Herbst shows that Lipschitz functions of random matrices satisfy the log-Sobolev inequality and exhibit Gaussian concentration, [71].

Proof of Theorem 451. Let $\boldsymbol{X} = \left(\{x_{ij}, y_{ij}, x_{ii}\}\right) \in \mathbb{R}^{n^2}$. Let $G(\mathbb{X}) = \mathrm{Tr}f\left(\mathbf{H}(\mathbf{X})\right)$. Then the matrix function G is Lipschitz with constant $\sqrt{2}|f|_\ell$. By **Theorem 5.2**, it can be shown that

$$\mathbb{P}\left(\left|\frac{1}{n}\mathrm{Tr}f(\mathbf{H})-\mathrm{E}\left[\frac{1}{n}\mathrm{Tr}f(\mathbf{H})\right]\right|\geq t\right)\leq 2e^{-\frac{n^2t^2}{4c|f|_\ell}} \tag{5.17}$$

Examining the proof of **Theorem 5.1**, there is an explicit focus on the use of the linear trace functional. There is a reason the trace function is so utilized under our proposed mathematical framework for the low signal-to-noise ratio detection algorithm, and that is due to both the linearity of the trace functional-as discussed previously-and the fact that relying on eigenvalues yields a less sharp concentration of measure inequality, as shown in the next example, from

Example 5.1. We start by considering the following inequality of Hoffman and Wielandt, see [72]. *Let* **A**, **B** *be* $n\times n$ *matrices with eigenvalues*

$$\sum_{i=1}^{n}|\lambda_i(\mathbf{A})-\lambda_i(\mathbf{B})|^2\leq \mathrm{Tr}(\boldsymbol{A}-\boldsymbol{B})^2 \tag{5.18}$$

This simple inequality can then be used to show the concentration of measure inequality for eigenvalues, as opposed to the trace functional, as is shown below

$$\mathbb{P}(|f(\lambda_k)-\mathrm{E}[f(\lambda_k)]|\geq t)\leq 2e^{-\frac{nt^2}{4c|f|_\ell^2}} \tag{5.19}$$

where the matrix function, $G(\boldsymbol{x})=f(\lambda_k)$, with the Lipschitz constant, $\sqrt{\frac{2}{n}}|f|_\ell$.

The bound for the trace functional converges with the square of the order of the square matrix, n, whereas the use of eigenvalues is marginally better than the current state-of-the-art in statistical signal processing-the sample covariance matrix.

5.3.5 Applications to Distributed Sensor Networks

In [62] a Wishart matrix is used to achieve detection of weak signals, under signal-to-noise ratios as low as $-34dB$. Now, in the previous section, the concentration of moment inequality showed a tailbound of $2e^{-\frac{n^2t^2}{4c|f|_\ell^2}}$ for a Wigner matrix; however, it can be shown that for a Wishart matrix, the tailbound is $2e^{-\frac{n^2t^2}{4c}}$, which is equivalent to the Wigner matrix in which the Lipschitz function has a value of unity. In many ways, the right-hand side of the concentration of measure inequality can be viewed as a Gaussian tail, with the power of the exponent representing the effective *variance*. In slightly clearer context, the exponential power for the k^{th} eigenvalue has a variance of $\sigma^2=\frac{2c}{n}$, whilst that of the trace function has a

variance of $\sigma^2 = \frac{2c}{n^2}$. For example, assuming a square Wishart matrix of size $n = 100$, the variance of the normalized trace function is 0.01 that of the k^{th} eigenvalue. To put this in context, for a square Wishart matrix of size $n = 100$, the normalized trace function-which is viewed as a statistical average of n eigenvalues-has a reduction in variance of $20dB$ over the k^{th} eigenvalue tailbound. This aids in the understanding of how detection is achievable under weak signal-to-noise ratios (see Figure 20).

In most typical application of a detection metric, a threshold value is chosen based upon some criteria, and compared to a value that is based upon measured data. Since the threshold value is fixed, the measured data value varies over the sample period. Methods of dimensionality reduction (see [2], [68-69]) attempt to reduce the sample covariance matrix to a single eigenvalue for the statistic metric. However, the sample covariance matrix still has a higher variance than the k^{th} eigenvalue statistic metric, and is much more than that tailbound on the variance of the normalized trace function statistics metric (see Figure 21).

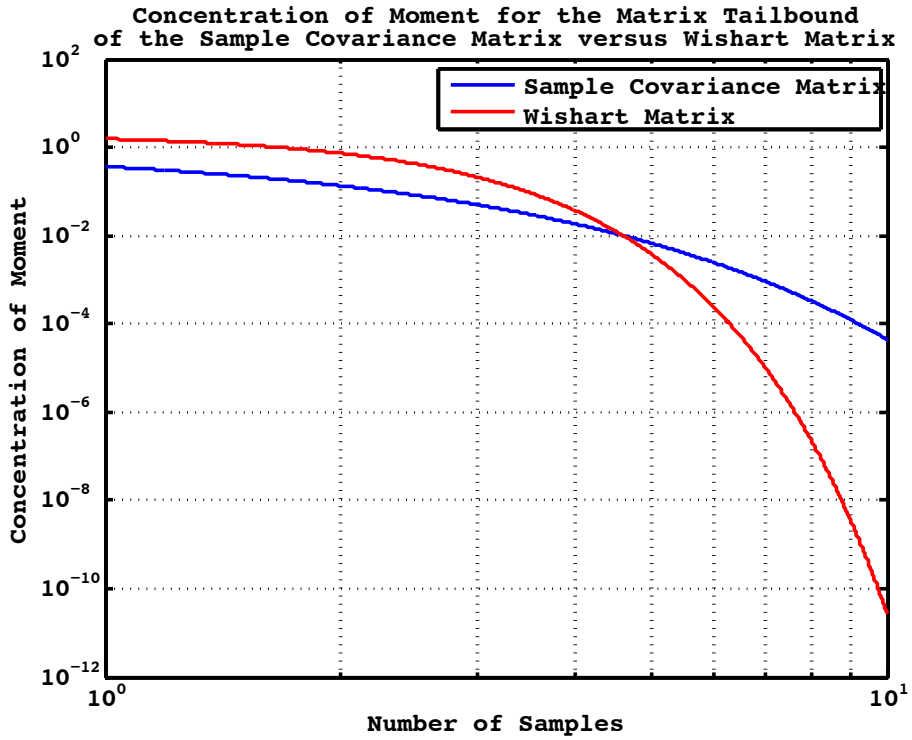

Figure 20: Concentration of Measure for Sample Covariance vs Wishart Matrix

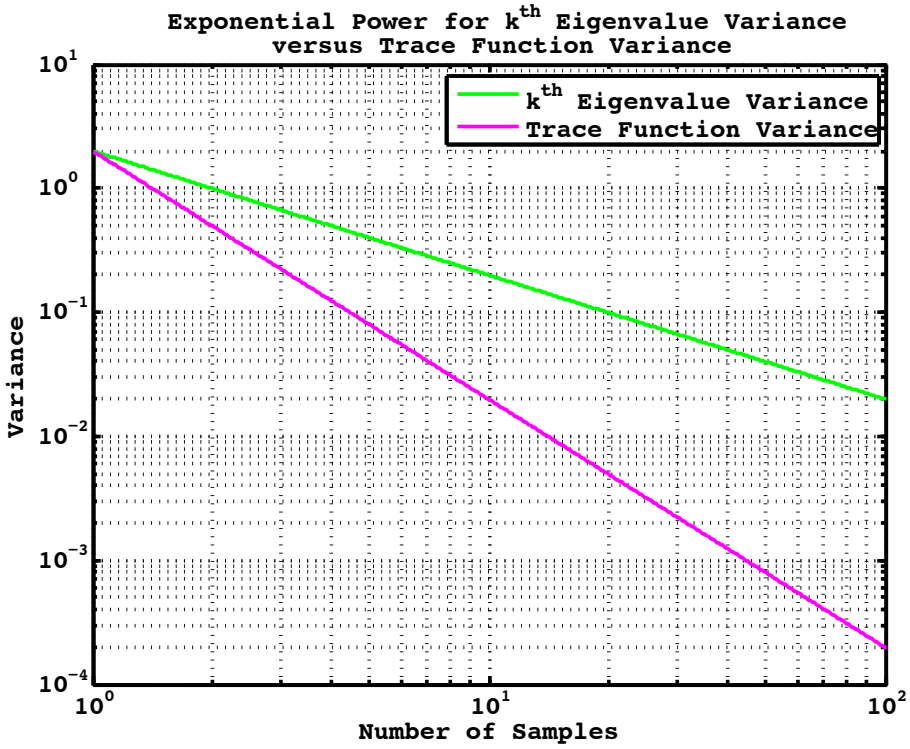

Figure 21: Eigenvalue vs Trace Function Variance

From [62], the normalized trace function was shown to be optimal, in that the detection performance at weak signal-to-noise ratios was consistent and clearly outperformed any modern statistical signal processing approach. The prime motivation for the development of this chapter was to thread the story that wove the various and disparate lemmas, theories and proofs that were instrumental in explaining how and why weak-signal-to-noise ratio detection algorithms work, and are based upon a strong foundation of recent mathematical results. The framework provided by free probability, concentration of measure, and the normalized trace function are a new mathematical foundation for the development of an entire class of innovative signal processing algorithms, that take detection and detection performance into the 21^{st} century. It is the belief of the author that in the coming years, this new framework developed will usher in a new era of signal processing possibilities, which are only now just being explored with this initial foray into weak signal detection.

In the previous chapter, the metric used for detection involves the use of a nonparametric hypothesis test, based upon the volume of an annular data depth contour. This was shown to be quite effective at low, but positive signal-to-noise ratios. For the weak SNR case, the variance variability of the threshold statistic needs to be controlled, and ensured to be of sufficient utility that hypothesis testing yields favorable probabilities of detection, for a set false alarm rate (Neyman-

Pearson criterion). For the remainder of this chapter, the statistical metric used for the hypothesis testing is found from the normalized trace function. Further, the detection performance-under free probability-is compared for a single random variable (ie-the time-reversal operator, see Chapter 4) and for a sum of random variables. Finally, the detection performance versus various types of corruptive noise processes is considered, and compared to that of Gaussian IID noise. Implicit in any detection performance results is the ability of the multistatic radar network to conduct weak scatterer detection for both a single point-type targets and extended targets comprised of multiple scattering centers.

5.4 Weak-SNR Regimes

What is meant when we say: *weak-SNR*? In [1], the low-energy coherence receiver is developed to aid in the detection of targets that were both spread (multiple scattering centers in Range-Doppler space) and *weak*; however, this terminology is not explicitly defined, leaving the signal-to-noise ratio (SNR) regime that constitutes *weak* up to the interpretation of the interested reader. The particular meaning of the term *weak* is the question that is answered in this section. In an effort to define the limit in which weak signal-to-noise ratio is reached, let us start with an informal proposition, based upon the non-parametric depth-based detector introduced in Chapter 3.

Proposition 5.1-Lower-Bound of Detectability. For nominal, positive, SNRs, Newton's Third law leads to a natural repulsion between the signal eigenvalues and the noise eigenvalues of the target time-reversal operator; leading to ready detectability of the signal, or more specifically, to better selection of the signal rankings. As the SNR begins to decrease, this natural eigenvalue repulsion begins to weaken, to the point that the signal eigenvalues become entangled in the outer convex hull of the data depth functional; however, in keeping with the third law, the signal eigenvalues are still repelled by the *bulk* of the noise eigenvalues in the data depth functional. Further, whilst the positive SNR leads to particular *signal only* regions that isolated from the noise eigenvalues, when the SNR decreases towards the negative, the signal eigenvalues are thrown about over the outer convex hull of the data depth functional. Thus, in order to conduct adequate ranking and selection to a suitable false alarm rate, in keeping with Neyman-Pearson criterion, we are forced to ascertain methods that can distinguish, in the

outlying regions of the data depth functional, those eigenvalues that are associated with the noise, and those that are associated with the signal. In this limit, the lower-bound of detectability is the point at which the signal becomes entangled in the annulus of the $0.9\ p^{th}$ contour; to the point at which there is no currently deduced method for formulating a ranking and selection criteria that will have meaningful probability of detection performance. This phenomenon, is the currently assumed limit for weak-SNR detection utilizing data depth functionals for a distributed sensor network.

In Figure 22, we demonstrate this phenomena by examining the data depth functional for a network of 60 sensors. The convex hull for a rank 3 time-reversal operator is shown below. Note how the rank of the data depth functional is readily visualized, and indicates the outlying nature of the high-SNR eigenvalues on the formation of the data depth functional using the convex hulling method.

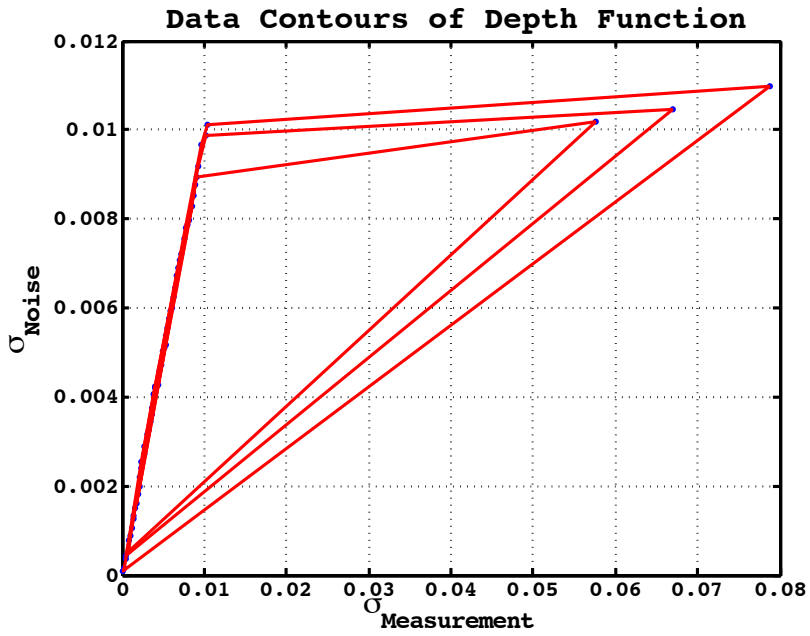

Figure 22: Data Depth Functional for 60 Sensor Network (High-SNR)

In Figure 23, the SNR is decreased, sufficiently enough that the apparent rank of the data depth functional is 2. One of the signal eigenvalues has become weak enough that it becomes entangled in the outer convex hull of the $0.9\ p^{th}$ contour. This becomes a demonstration of a moderate-SNR, one in which the highest SNR eignevalues are readily recovered, but not those eigenvalues that begin to equivalent to the noise eigenvalues.

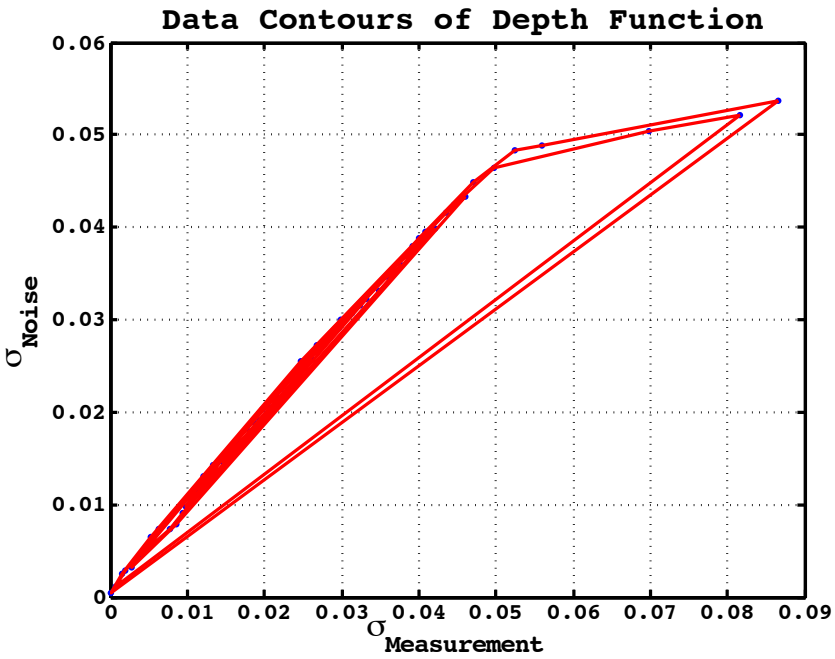

Figure 23: Data Depth Functional for 60 Sensor Network (Moderate SNR)

Our final example of the data depth functional for a network of 60 sensors demonstrates the phenomena of weak-SNR, see Figure 24. Thereby, each target eigenvalue is low enough that they are approximately equivalent to the largest noise eigenvalues. The rank of the data depth functional is not apparent, and represents visually, the concept of the weak-SNR regime.

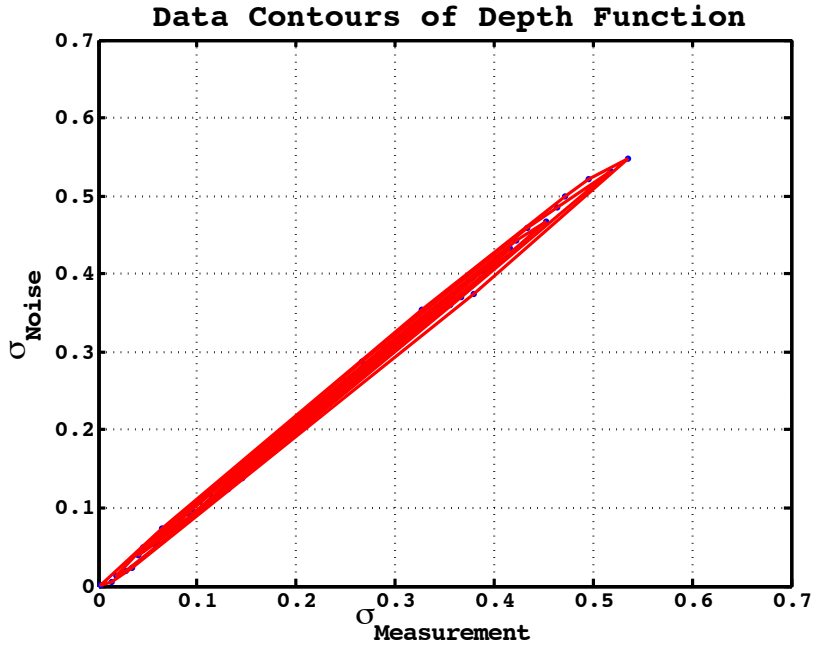

Figure 24: Data Depth Functional for 60 Sensor Network (Weak-SNR)

5.4.1 A More Formal Definition

Whilst **Proposition 5.1** is a good first step in defining the low signal-to-noise ratio regime, a more formal definition that will determine the bounds at which our low-SNR detection algorithm is implemented is required. The depth-based method has fundamental limits at which the detection performance is acceptable, meaning has a high probability of detection with a defined low false-alarm rate.

Theorem-Matrix Congruency. Let **A**, **B** be operators on a Hilbert Space $\mathcal{H}$. We say that **A** is *congurent* to **B**, and write **A**~**B**, if there exists an invertible operator **X** on $\mathcal{H}$ such that $\mathbf{B} = \mathbf{X}^{*}\mathbf{A}\mathbf{X}$. Congruence is an equivalence relation on a linear operator of a Hilbert space, represented by $\mathcal{L}(\mathcal{H})$. If **X** is unitary, we say **A** is *unitarily equivalent* to **B**, and write $\mathbf{A} \simeq \mathbf{B}$.

The previous theorem describes a fairly broad methodology for determine the congruency of two matrices on a Hilbert space, but does not necessarily give us a readily quantifiable metric for declaring two matrices congruent. This leads to a difficult inverse problem, in which the form of the operator needs to be deduced from matrices **A** and **B**. In an effort to reduce this computation, we use a more explicit form of the definition for matrix congruency, which relies on the concept of matrix *inertia*. One important point to note, is whilst we are making use of formal definitions for matrices as we develop a working definition for the weak-SNR regime, we are not necessarily limited to only those matrix types. Now, with that caveat in mind, let us press forward with a more practical definition of matrix *inertia*.

Definition 5.1- Matrix Inertia. If **A** is Hermetian, the *inertia* of **A** is the triple of non-negative integers

$$\mathrm{In}(\mathbf{A})=[\pi(\mathbf{A}),\zeta(\mathbf{A}),\nu(\mathbf{A})] \tag{5.20}$$

where $\pi(\mathbf{A}),\zeta(\mathbf{A}),\nu(\mathbf{A})$ are the numbers of positive, zero, and negative eigenvalues of **A**, counted with multiplicity. Since the concept of matrix *inertia* leaves us with three very tangible variables, this leads to our accepted definition for matrix congruency, which is readily found for any matrix

Theorem 5.3-Sylvester's Law of Inertia. Assume that $\mathrm{In}(\mathbf{A})$ is a complete invariant for congruence on the set of Hermetian matrices; this could be phrased as two Hermetian matrices are congruent iff they have the same inertia

$$\mathbf{A} \simeq \mathbf{B}, \text{iff } \ln(\mathbf{A}) = \ln(\mathbf{B}) \tag{5.21}$$

This leads to a more formal proposition that form the basis of our boundary for determining the signal-to-noise ratio that serves as the transition point from nominal to weak signal-to-noise ratio regimes

Proposition 5.2-Observation on Congruency: Let $\mathbf{A} \in \mathbb{R}^n$ be the time-reversal operator whose rank is much less than n, $\text{rank}(\mathbf{A}) \ll n$, and the elements of $\mathbf{W}_{ij} \in \mathcal{N}(0, \sigma^2)$ be the measurement noise time-reversal operator, comprised of normal Gaussian noise. If we assume that the observed measured time-reversal operator is $\mathbf{B} = \mathbf{A} + c_n\mathbf{W}$, with $[0 < c_n < \infty)$, and further assume that $\text{Tr}(\mathbf{B}) > \text{Tr}(\mathbf{W})$, and $\mathbf{B} < \mathbf{A}$ then as $c_n \to \infty$

$$\ln[\pi(\mathbf{B}), \zeta(\mathbf{B}), \nu(\mathbf{B})] \simeq \ln[\pi(\mathbf{W}), \zeta(\mathbf{W}), \nu(\mathbf{W})] \tag{5.22}$$

Thus, the measured time-reversal operator, **B**, is said to be congruent to the measurement noise time-reversal operator, **W**. The point at which this weak-SNR cross-over occurs is shown in Figure 26.

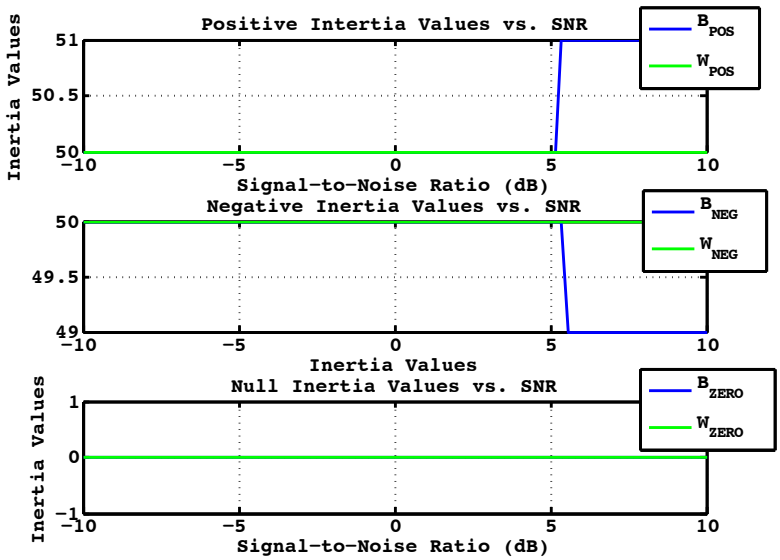

Figure 25: Low-SNR Cross-Over point: Inertia Values vs SNR

Figure 25 was generated using a simulation averaging the inertia values for the noise and measured time-reversal operators using 100 sensor nodes and $10{,}000$ Monte Carlo trials. The values were re-run for distributed sensor networks comprised of 20,40, 60, 80, 120, 140, 160, and 180 sensor nodes to determine the impact on sensor density with the cross-over point for the inertia values into the weak-SNR regime. Those results are tabulated below and demonstrate the

variability of the weak-SNR cross-over point with respect to the density of the distributed sensor network. In Figure 26, the trend shows the weak-SNR cross-over point moving lower as the density of the sensor network is increased. There is clear $\sim 12dB$ separation from a sparse network of 4 sensor nodes, to that of a dense sensor network with over 100 nodes. An asymptotic lower limit of $\sim 1dB$ is observed as the density of the sensor network increases past 200 nodes.

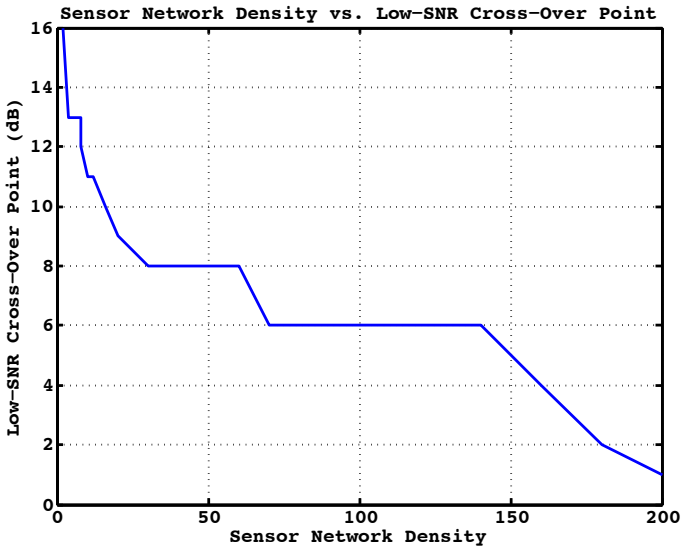

Figure 26: Sensor Network Density vs Weak-SNR Cross-Over Point

Interestingly, Figure 26 also shows a general trend for the benefit of higher dimensional sensor networks, under the proposed fusion framework; particularly, there is a clear connection between a standard monostatic benchmark of $\sim 13dB$ for a single-pulse detection threshold value [39]. As the density of the sensor network decreases, the single-pulse time-reversal operator tends to show a weak signal-to-noise (SNR) cross-over point of approximately $\sim 6dB$ above the monostatic benchmark single-pulse detection SNR of $13dB$. More importantly, Figure 26 could be used as a graphical method for optimizing the design of a sensor network to meet a required SNR for detection, or vice-a-versa.

This definition of the weak signal-to-noise cross-over point leads to an important topic of consideration: how do we recover a scatterer in the weak signal-to-noise ratio regime? Since we have assumed the definition for the weak signal-to-noise ratio regime is matrix congruency between the measured and noise time-reversal operator, it would seem there is little chance of ascertaining a suitable hypothesis test for detection-let alone ranking, should an extended object be present; this is actually not an accurate assertion. The matrix inertia simply allows us to define the transition point between the nominal and weak-signal-to-noise ratio

regimes, permitting us to switch detection algorithms without the need for an excessively complicated adaptive process. In this manner, three variables dictate the algorithm choice between the nominal depth-based detector and the weak-SNR variant-to be introduced shortly. However, to solve for the inertia of the time-reversal operator, we require a noise and signal-plus-noise measured time-reversal operator. Since both matrices look the same under weak-SNR conditions, we need to formulate a method of recovering the inertia from a sample limited time-reversal operator. This problem is shared with modern statistical signal processing approaches, which rely on the formation of the sample covariance matrix, and is greatly complicated by limited sample-support; as evidenced by the concentration of measure tailbounds for the sample covariance matrix.

5.5 Summary

In this chapter, we introduced an extension of the mathematical basis of the bespoke depth-based detector in classical communicative probability, to that of non-communicative probability. More importantly, concentration of measure was discussed and its role in determining the tailbounds for our pre-detection fusion time-reversal operator. The trace functional was introduced and suggested as suitable threshold metric for use in a detection algorithm. Finally, the concept of *weak signal-to-noise ratio regimes* was discussed, as well as an empirical cross-over point from nominal to weak-signal-to-noise ratio (SNR) regimes. This later point serves as the mathematical transition point upon which a given fusion center would move from applying the depth-based detector of Chapter 4, to that of the low-SNR detector, which is introduced in the subsequent chapter.

5.6 Conclusion

Leveraging the intersection of *big data* and distributed sensor networks, we have introduced mathematical concepts for assessing practical detection performance in weak-SNR regimes. The generalization of classical *communicative probability* to *non-communicative probability* was shown the be a critical mathematical concept to understanding the SNR *boundary point* between nominal and low-SNR regimes. The algorithms of Chapter 4 and 6 play an important part in permitting detection performance *beyond traditional sensing domains*.

6 Detection and Ranking Under Weak-Signal-to-Noise-Ratio Conditions for a Distributed Sensor Network

6.1 Introduction

Previously we showed the theoretical bounds of performance for the distributed sensor network; it is actually a function of the number of radio-frequency sensors, a mathematical framework based upon free probability and concentration of measure; and was shown to quite readily outperform its contemporary statistical signal processing-based sample covariance matrices approaches. Until now, noise limited detection scenarios have proved vexing, and many interesting signal processing tricks have been formulated to increase the bounds of detectability; however, they all suffer from a fundamental limit that is beyond the control of the system or associated algorithms, see Equation (5.11). The variance on the tailbound was previously shown to be most well behaved when using the normalized trace function, per Equation (5.15). In this section, the application of the normalized trace function is on the detection of point and extended object structures under weak signal-to-noise ratios (SNR). The SNR considered for this section onward is primarily negative and focuses on a lower-bound of detectability, which is found from a series of Monte Carlo simulations.

6.2 Declaration of Scattering Centers Under Weak-SNR Conditions

We begin by considering the standard binary hypothesis test shown below

$$H_0 := N \tag{6.1a}$$

$$H_1 := S + N \tag{6.1b}$$

In (6.1a,b) the noise, N, and signal, S, variables are replaced by operators (matrices) **W** and **A**, respectively. In instances where the measured operator is a mixture of signal-plus-noise, the notation **B** is used. A general operator is typically denoted by ρ and satisfies the following:

1. ρ has trace equal to one, or $\mathrm{Tr}\rho = 1$.
2. **Positivity**: ρ is a positive operator, or $\rho \geq 0$.

In this section, the $\mathrm{Tr}\rho$ is assumed positive (not necessarily equal to 1), whilst the positivity requirement is satisfied through the assumption that each operator is semi-definite positive (SDP); which are convex [73]. From (Chapter 3), the pre-detection fusion time-reversal operator satisfies the above requirements. Going

forward, the notation for the ρ is relaxed a bit, with the operator described as positive definite (PD). Expanding Equation (6.1a,b) to include the proper operator notation, the revised hypothesis test for this chapter is now

$$H_0 := \mathbf{W} \tag{6.2a}$$

$$H_1 := \mathbf{B} \tag{6.2b}$$

Recall that under free-probability, each matrix is now assumed a random variable. Convexity assures the uniqueness of the hypothesis testing results, whilst the use of the trace functional ensures linearity and enables the mathematics for the weak-SNR detection to be more readily implemented in a processor; as in the matrix mathematics simplifies to a set of adders and multipliers. In the next section, the trivial weak signal-to-noise detection algorithm is introduced for the known noise time-reversal operator. This initial algorithm serves as a motivational example for the unknown noise case. A ranking algorithm is introduced for the determination of the number of scattering centers present for a given range-extended target. Moving to the unknown corruptive noise time-reversal operator, an algorithm is introduced for the determination of a range-extended target comprised of multiple scattering centers; which is based upon an estimate of the asymptotic form of the finite-sample target time-reversal operator

6.2.1 The Time-Reversal Operator for Weak-SNR Regimes

For the trivial case in which the statistical form of the noise time-reversal operator is known *a priori*, the weak signal-to-noise detection algorithm is found from the following expression

$$\mathbf{A} = \sum_{i=1}^{r} \mathbf{u}(\mathbf{x}_j)\mathbf{v}(\mathbf{x}_j)^* \tag{6.3}$$

which is the familiar form of the pre-detection fusion process introduced in Chapter 3. Of particular note in Equation (6.3) is the fact the target time-reversal operator is an outer product of the *tensor product* of the transmit vector, **v**, and receive vector, **u**. This expression could also be written as a special case of the Kronecker product

$$\mathbf{A} = \sum_{i=1}^{r} \mathbf{u}(\mathbf{x}_j) \otimes \mathbf{v}(\mathbf{x}_j) \tag{6.4}$$

For the case in which the scene under illumination has a single scattering center present, $r = 1$, and

$$\mathbf{A} = \sigma_1 \mathbf{u}(\mathbf{x}_1) \otimes \mathbf{v}(\mathbf{x}_1) \tag{6.5}$$

For this work, the concept is broadened to range-extended targets, which are comprised of a multiple scatterers; this results in the form of the target time-reversal operator introduced in Chapter 3

$$\mathbf{A} = \sum_{j=1}^{r} \sigma_j \odot \mathbf{u}(\mathbf{x}_j) \otimes \mathbf{v}(\mathbf{x}_j) \tag{6.6}$$

where the dot product, $\odot$, is used to denote the mathematical relationship between the individual scatterers comprising the compound extended object, and the time-reversal operator. Immediately obvious, is the fact that the target time-reversal operator is a unique product of the individual scatterers and their associated material properties. Eigenvalue repulsion ensures each scatterer is recoverable from the underlying additive corruptive noise process. Recall from Chapter 3 that the scatterer target time-reversal operator was denoted by, **A**, the corruptive noise process by, **W**, and the measured time-reversal operator by, **B**. For the remainder of this chapter, the focus is on the development of a detection algorithm that permits recovery of the range-extended target in weak signal-to-noise ratio regimes, and hence the previous formal definition of the measurement time-reversal operator changes from $\mathbf{B} = \mathbf{A} + \frac{1}{\sqrt{M}}\mathbf{W}$, to $\mathbf{B} = \mathbf{A} + \frac{c_n}{\sqrt{M}}\mathbf{W}$; which is appropriate considering the SNR regime is weak (possibly negative) and the noise is dominant, but bounded by $c_n \in [0, \infty)$. The scaling of the noise in the negative signal-to-noise ratio regime is appropriate, as the signal time-reversal operator is always assumed to be dominated by the much stronger measurement noise time-reversal operator. In this case, we initially consider the case in which the signal (target) time-reversal operator, **A** is majorized by **W**; this point is revisited shortly in the context of the proposed detection algorithm.

$$\sigma_i(\mathbf{A}) \prec \sigma_i(\mathbf{W}), \forall\, j = 1,2,\dots,k \tag{6.7}$$

In Equation (6.7), the expression denotes that the singular values of the signal time-reversal operator are *majorized* by the corruptive noise time-reversal operator; and as the rank of the noise time-reversal operator is full, this statement is true for all singular values comprising both **A** and **W**.

6.3 Weak-SNR Detection Algorithm

Many modern statistical signal processing detection problems rely on the formation of the sample covariance matrix as crucial to the success of the adaptive algorithm [2, 69]. Likewise, the proper convergence for the time-reversal operator, or time-reversal operator random variable (under free-probability) is critical to the success

of our weak-SNR detection algorithm. For both previous instances cited, sample support limitations can cause serious issues and lead to detectors of limited operational utility. To address this issue for sample covariance matrices, a method for estimating the asymptotic form of the sample covariance matrix, based upon a shrinkage algorithm, was introduced in [74-75]. The point of introducing this algorithm is to demonstrate our method for recovering the signal time-reversal operator from the weak-signal-to-noise ratio measured time-reversal operator; which is dominated by the measurement environmental noise, and congruent with the actual receiver thermal noise-assumed Gaussian in both instances of the purpose of this work. In [74] a covariance estimation approach, based upon minimum mean-squared error (MMSE) for Gaussian samples under finite sample support is considered. A shrinkage method is introduced to aid in the recovery of the high-dimensional covariance matrix, under limited sample support scenarios. In particular in [75], the estimation algorithm was extended for elliptical distributions, which are also known as spherically invariant random vector models (SIRV). Since SIRV models encompasses heavy-tailed distributions, such as *k*-distributed, this algorithm has wide-ranging application in statistical signal processing.

The oracle approximation shrinkage (OAS) estimator seeks to find the asymptotic form-or oracle-of a finite-sample covariance matrix. For this section, we make use of the *oracle estimator* found in [74] to derive the asymptotic form of the covariance matrix, based upon a nonrandom coefficient that minimizes the mean-square error. For the OAS estimator, $\widehat{\mathbf{\Sigma}}$, uses a nonrandom coefficient to minimize the mean-square error, which is the solution to the following expression

$$\min_{\rho} \mathrm{E}\left\{\left\|\widehat{\mathbf{\Sigma}} - \mathbf{R}_x\right\|_{\mathrm{F}}^2\right\} \text{s.t.} \widehat{\mathbf{\Sigma}} = (1-\rho)\widehat{\mathbf{R}}_x + \rho\widehat{\mathbf{F}} \tag{6.8}$$

where $\widehat{\mathbf{R}}_x \in \mathbb{R}^n$ is the sample covariance matrix. The matrix $\widehat{\mathbf{F}}$ is referred to as the shrinkage target, defined as

$$\widehat{\mathbf{F}} = \frac{\mathrm{Tr}(\widehat{\mathbf{R}}_x)}{L}\mathbf{I} \tag{6.9}$$

where $\mathbf{I}$ is a L-dimensional unitary matrix. The shrinkage coefficient $\rho \in (0,1)$ in $\mathbb{R}^n$ and is used to minimize the mean square error.

The OAS initializes the estimator iteration with an initial guess of $\mathbf{R}_x$. The iteration procedure is continued until a convergence is reach, which is defined by

$$\hat{\rho}_{j+1} = \frac{\left(1-\frac{2}{L}\right)\mathrm{Tr}\left(\widehat{\mathbf{\Sigma}}_j\widehat{\mathbf{R}}_x\right)+\mathrm{Tr}^2\left(\widehat{\mathbf{\Sigma}}_j\right)}{\left(N+1-\frac{2}{L}\right)\mathrm{Tr}\left(\widehat{\mathbf{\Sigma}}_j\widehat{\mathbf{R}}_x\right)+\left(1-\frac{N}{L}\right)\mathrm{Tr}^2\left(\widehat{\mathbf{\Sigma}}_j\right)} \tag{6.10}$$

The initial guess $\widehat{\boldsymbol{\Sigma}}_0$ could be the sample covariance matrix $\widehat{\mathbf{R}}_x$, with the initial guess of being bounded by $(0 < \hat{\rho}_0 < 1)$. When the iteration convergences, the value of $\hat{\rho}_{\text{OAS}}$ can be shown to be of the form

$$\hat{\rho}_{\text{OAS}} = \min\left(\frac{\left(1-\frac{2}{L}\right)\text{Tr}\left(\widehat{\mathbf{R}}_x^2\right)+\text{Tr}^2\left(\widehat{\mathbf{R}}_x\right)}{\left(N+1-\frac{2}{L}\right)\left[\text{Tr}\left(\widehat{\mathbf{R}}_X^2\right)-\frac{\text{Tr}^2\left(\widehat{\mathbf{R}}_x\right)}{L}\right]}, 1\right) \tag{6.11}$$

After using $\hat{\rho}_{\text{OAS}}$ to substitute for ρ in 6.10, we can get the estimated covariance matrix as

$$\widehat{\boldsymbol{\Sigma}}_{\text{OAS}} = (1 - \hat{\rho}_{\text{OAS}})\widehat{\mathbf{R}}_x + \hat{\rho}_{\text{OAS}}\widehat{\mathbf{F}} \tag{6.12}$$

Proposition 6.1-OAS Inequality. The OAS inequality states that the estimate of the oracle is almost surely (a.s.) weakly majorized by the singular values of the original finite-sample covariance matrix used for the OAS estimate.

Let $\mathbf{B} \in \mathbb{R}^n$ be the observed measured time-reversal operator, and $\widehat{\boldsymbol{\Sigma}}_{\text{OAS}} \in \mathbb{R}^n$ be the estimated asymptotic form of $\mathbf{B}$. We first order the singular values of $\mathbf{B}$ and $\widehat{\boldsymbol{\Sigma}}_{\text{OAS}}$ in descending order, as follows

$$\sigma\left(\widehat{\boldsymbol{\Sigma}}_{\text{OAS}}\right)^{\downarrow} := \left(\sigma_1^{\downarrow}, \sigma_2^{\downarrow}, \ldots, \sigma_n^{\downarrow}\right) \tag{6.13a}$$

$$\sigma(\boldsymbol{B})^{\downarrow} := \left(\sigma_1^{\downarrow}, \sigma_2^{\downarrow}, \ldots, \sigma_n^{\downarrow}\right) \tag{6.13b}$$

Then for $j \in (1, k)$ and $k \leq n$, we have

$$\sigma\left(\widehat{\boldsymbol{\Sigma}}_{\text{OAS}}\right)_j^{\downarrow} \prec_w \sigma(\boldsymbol{B})_j^{\downarrow}, \forall\, 1 \leq k \leq n \tag{6.14}$$

The observed low-SNR noisy time-reversal operator $\mathbf{B}$ is thus used to estimate the oracle of $\mathbf{B}_{\text{OAS}}$, where $\mathbf{B}$ is originally said to be *congruent* with $\mathbf{W}$. Majorization of $\mathbf{B}_{\text{OAS}}$ is important and plays a pivotal role in the development of our weak-SNR detection algorithm.

6.3.1 Weak-SNR Detection for Known Noise Time-Reversal Operator

Under the *clairvoyant case*, the measured time-reversal operator and measurement additive corruptive noise time-reversal operator is assumed known. Whilst not practical for any *real-use* cases, it does serve as a suitable starting point and benchmarking exercise to determine the underlying efficacy of the proposed approach for weak signal-to-noise detection.

Now, assume $\mathbf{A}$,$\mathbf{B} \in C\mathbb{M}_M$ whose elements are contained in $\mathbf{A}_{ij} \in \mathbb{R}^+$. Further, assume that $\mathbf{B} = \mathbf{A} + c_n\mathbf{W}$, where $\mathbf{W} \in C\mathbb{M}_M$ and whose elements are

independent and identically distributed (IID) and are $\mathbf{W}_{ij} \in \mathcal{CN}(0, \sigma^2)$, and the scaling factor $c_n \in \mathbb{R}^+$ and is bounded by $0 < c_n < \infty$. Let **A** represent the known scattering center noise-free time-reversal operator for the scene under illumination, and let **B** represent the noisy measurement time-reversal operator, described previously.

For a known noisy measurement time-reversal operator $\text{Tr}(\mathbf{B}) > \text{Tr}(\mathbf{W})$, assuming the scaling factor is non-infinite, $c_n \ll \infty$. As the variable $c_n \to \infty$, then $\text{Tr}(\mathbf{B}) \simeq \text{Tr}(\mathbf{W})$. Now, by making use of the oracle approximation shrinkage (OAS) algorithm-or making use of *a priori* knowledge-we can determine the signal and noise time-reversal operators, $\mathbf{A}_{\text{OAS}}$ and $\mathbf{W}_{\text{OAS}}$, from the noisy measurement time-reversal operator, **B**, we can represent the trivial weak-SNR detection inequality as

$$\frac{\text{Tr}(\mathbf{A}_{\text{OAS}}+\mathbf{W}_{\text{OAS}})^2}{\text{Tr}(\mathbf{A}_{\text{OAS}}+\mathbf{W}_{\text{OAS}})} \leq \frac{\text{Tr}(\mathbf{A}_{\text{OAS}}^2)}{\text{Tr}(\mathbf{A}_{\text{OAS}})} + \frac{\text{Tr}(\mathbf{W}_{\text{OAS}}^2)}{\text{Tr}(\mathbf{W}_{\text{OAS}})} \tag{6.15}$$

Implicit in Equation (6.15) is value of the threshold for declaration via binary hypothesis testing. To more explicitly denote the weak-SNR algorithm, the notation is altered to directly state the threshold value that is used for detection declaration, $\gamma_{\text{Threshold}}$

$$\gamma_{\text{Threshold}} = \frac{\text{Tr}(\boldsymbol{A}_{OAS}+\boldsymbol{W}_{OAS})^2}{\text{Tr}(\mathbf{A}_{\text{OAS}}+\mathbf{W}_{\text{OAS}})} \tag{6.16}$$

The right side of Equation (6.16) is the quantity that must exceed the threshold in order for detection to be declared; however, the threshold value is currently defined in terms of a signal and noise measurement time-reversal operator. This is incorrect and needs to be rectified. In order to correct the threshold value, the signal time-reversal operator is removed, making the threshold a value defined by the noise time-reversal operator, hence, the weak-SNR threshold value is more properly written as

$$\gamma_{\text{Threshold}} = \frac{\text{Tr}(\mathbf{W}_{\text{OAS}})^2}{\text{Tr}(\mathbf{W}_{\text{OAS}})}$$

Having properly defined the value of the threshold and pegged the determination of this value with the measurement noise time-reversal operator, the weak-SNR detection algorithm is defined as

$$\gamma_{\text{Threshold}} \underset{>H_0}{\overset{\leq H_1}{}} \frac{\text{Tr}(\mathbf{A}_{\text{OAS}}^2)}{\text{Tr}(\mathbf{A}_{\text{OAS}})} + \frac{\text{Tr}(\mathbf{W}_{\text{OAS}}^2)}{\text{Tr}(\mathbf{W}_{\text{OAS}})} \tag{6.17}$$

Equation (6.16) represents the trivial weak-SNR detection algorithm, and is technically only limited in its ability to discriminate noise from a signal+noise by the precision of the detector (64-bit for the case of computer simulation, and 12 or more

bits for an actual radar signal processor analog-to-digital converter (ADC)). This does pose a rather vexing problem, in that the ability of this algorithm to work is only based upon the quantization level resolution of the detector, hence the ability of Equation (6.17) to work at SNR values as low as -30dB of more (when measured as $\frac{\sigma_1}{\sigma_n}$). The values for the oracle approximation estimation are more realistically based upon a noisy measurement time-reversal operator, of **B**, whilst that of the threshold is found from an estimate of the noise measurement time-reversal operator, $\widehat{\mathbf{W}}$. Further, from Figure 21 we see the variance on the trace function decreases as the number of samples increase. This gives credence to the use of training data for the estimation of the noise time-reversal operator, $\widehat{\mathbf{W}}$, and for a more refined estimate of the noisy measurement time-reversal operator, giving rise to the following corrections in the low-SNR detection algorithm in (6.18):

$$\gamma_{\text{Threshold}} = \frac{\text{Tr}\left(\sum_{n=1}^{N} \widehat{\mathbf{W}}\right)^2}{\text{Tr}\left(\sum_{n=1}^{N} \widehat{\mathbf{W}}\right)} \tag{6.18}$$

where N is the total number of samples to be integrated to minimize the variance on the trace estimate. Minimizing the variance on the trace function is critical for practical implementation of the weak-SNR detection algorithm outside of a controlled simulation environment (and within such an environment for the purposes of Monte Carlo). Excess variance leads to too much variability in the results of the algorithm, and inconclusive results. As with the estimate of the noise time-reversal operator, the variance of the trace function must also be controlled for the noisy measurement time-reversal operator as well; which is accomplished through integration of multiple samples of the same signal over time; akin to integration of a low-probability-of-intercept signal to increase the signal-to-noise ratio, see [76]. Unlike standard pulse integration for a radar system, the intent is not to increase the power of the correlated signal over time, whilst allowing for destructive interference of uncorrelated measurement noise, but rather to integrate in an effort to minimize the value of the variance on the trace function to prevent fluctuations of noise values from negating the benefit of the low-SNR detection algorithm. As with the threshold value, multiple noisy measurement time-reversal operators are captured, **B**, and each one passed through the oracle approximation estimation algorithm to determine the effective signal and noise time-reversal operators, $\mathbf{A}_{\text{OAS}}$ and $\mathbf{W}_{\text{OAS}}$ respectively. Hence, the new trivial weak-SNR detection algorithm is expressed as

$$\gamma_{\text{Threshold}} \underset{>H_0}{\overset{\leq H_1}{}} \frac{\text{Tr}\left(\left(\sum_{n=1}^{N} \mathbf{A}_{\text{OAS}}\right)^2\right)}{\text{Tr}\left(\left(\sum_{n=1}^{N} \mathbf{A}_{\text{OAS}}\right)\right)} + \frac{\text{Tr}\left(\left(\sum_{n=1}^{N} \mathbf{W}_{\text{OAS}}\right)^2\right)}{\text{Tr}\left(\sum_{n=1}^{N} \boldsymbol{W}_{OAS}\right)} \tag{6.19}$$

Equation (6.19) implies that the number of samples to be integrated does not need to be consistent amongst the estimate of the noise and the noisy measurement time-reversal operators. This is true, and an open area for investigation and for optimization. For the purpose of the examples to follow; however, the value of N and M are assumed the same; which is due to the fact we want to minimize the trace function variance to the same precision to minimize ambiguities in the simulated Monte Carlo results.

Now, another manner of expressing the inequality of Equation (6.15) is to analyze the singular values along the trace of the noise and noisy measurement time-reversal operators. Specifically, if $\mathbf{A}_{\text{OAS}}$, $\mathbf{W}_{\text{OAS}}$, $\widehat{\mathbf{W}}$, $\mathbf{B} \in C\mathbb{M}_{\boldsymbol{M}}$ and comprised of complex elements, and if $\mathbf{W}_{\text{OAS}}$ and $\widehat{\mathbf{W}}$ are comprised of m-length vectors of Gaussian elements, $\mathbf{W}_{\text{OAS}_{ij}}$ and $\widehat{\mathbf{W}} \in C\mathcal{N}(0, \sigma^2)$, then for any $\mathbf{A}_{OAS} + c_n \mathbf{W}_{OAS}$, where $c_n \in [0, \infty)$, or more generally, $c_n \in \mathbb{R}^+$

$$\sigma_i(\mathbf{A}_{\text{OAS}} + \mathbf{W}_{\text{OAS}}) \prec_w \sigma_i(A_{\text{OAS}}) + \sigma_i(\mathbf{W}_{\text{OAS}}), \forall\, i = 1,2, \dots, k \tag{6.20}$$

where $k < M$. Essentially, Equation (6.20) is stating that the eigenvalues comprising the threshold value of Equation (6.18) is *weakly majorized* by the eigenvalues on the right-hand side of Equation (6.15); which is true for all eigenvalues of the trace, or the so-called k^{th}-eigenvalue.

$$|d_i(\mathbf{A})| \prec_w \sigma_i(\mathbf{A}), \forall\, i = 1,2, \dots, k \tag{6.21}$$

d_i refers to the diagonal elements of target time-reversal operator $\mathbf{A}$. Equation (6.21) is more typically written in terms of the eigenvalues (singular values, in our case) as

$$|\lambda_i(\mathbf{A})| \prec_w \sigma_i(\mathbf{A}), k \ll M \tag{6.22}$$

which is true, as typically the signal rank of target time-reversal operator $\mathbf{A}$ is much less than that of the full rank of time-reversal operator $\mathbf{B}$. Alternatively, we could express Equation (6.21) in shorthand as

$$|\lambda_i(\mathbf{A})| \prec_w \sigma_i(\mathbf{A}) \tag{6.23}$$

where again, $k < n$.

In summary, assuming the measurement time-reversal operator has been generated by the fusion center pre-detection algorithm, the oracle approximation of the signal and corruptive noise time-reversal operators exists, and there is an estimate of the noise environment-operators $\mathbf{B}$, $\mathbf{A}_{\text{OAS}}$, $\mathbf{W}_{\text{OAS}}$, and $\widehat{\mathbf{W}}$ exist-the

trivial weak-SNR detection algorithm is now formulated based upon a simple multi-step process:

Algorithm 6.1: **Trivial Weak-SNR Binary Hypothesis Test** Fusion Center Weak-SNR Detection Algorithm
1a: Form the Target Time-Reversal Operator: $\mathrm{A} = \sum_{j=1}^{r} \boldsymbol{\sigma_j \mu}(\mathrm{x}_j)\, \boldsymbol{v}(\boldsymbol{x}_j)^*$
1b: Form the Corruptive Measurement Noise Time-Reversal Operator: $\mathrm{W} = \frac{\mathbf{1}}{\sqrt{\boldsymbol{M}}}\left(\boldsymbol{C}\mathbb{M}_{\boldsymbol{M}} \in \boldsymbol{C\mathcal{N}}(\mathbf{0}, \boldsymbol{\sigma}^2)\right)$
1c: Generate the Measured Time-Reversal Operator: $\mathrm{B} = \sum_{n=1}^{N} (\mathrm{A} + \boldsymbol{c}_n \mathrm{W})$
2: Calculate the OAS Estimate, $\widehat{\boldsymbol{\Sigma}}_{\mathbf{OAS}}$, **of** B
3: Determine $\mathrm{A}_{\mathbf{OAS}}$ and $\mathrm{W}_{\mathbf{OAS}}$
4: Calculate the Corruptive Noise Measurement Time-Reversal Operator: $\widehat{\mathrm{W}} = \sum_{n=1}^{N} \left(\frac{\boldsymbol{c}_n}{\sqrt{\boldsymbol{M}}} \left(\boldsymbol{C}\mathbb{M}_{\boldsymbol{M}} \in \boldsymbol{C\mathcal{N}}(\mathbf{0}, \boldsymbol{\sigma}^2) \right) \right)$
5: Determine the threshold statistic, $\boldsymbol{\gamma}$, from $\frac{\mathbf{Tr}(\widehat{\mathrm{W}})^2}{\mathbf{Tr}(\widehat{\mathrm{W}})}$
6: Determine the Outcome of the Binary Hypothesis Test: $\boldsymbol{\gamma}_{\mathbf{Threshold}} \underset{H_0}{\overset{H_1}{\lessgtr}} \frac{\mathbf{Tr}(\mathrm{A}_{\mathbf{OAS}}^2)}{\mathbf{Tr}(\mathrm{A}_{\mathbf{OAS}})} + \frac{\mathbf{Tr}(\mathrm{W}_{\mathbf{OAS}}^2)}{\mathbf{Tr}(\mathrm{W}_{\mathbf{OAS}})}$

6.3.2 Weak-SNR Detection: Real-World Case

The challenge for the weak-signal-to-noise ration (SNR) detection algorithm is in determining an effective mechanism for estimating the measurement noise time-reversal operator, $\widehat{\mathbf{W}}$, from prior measurements. Typically, we could look to adjacent range bins, for traditional monostatic radar for an acceptable estimate of the measurement noise, see [39]. A more appropriate form of training data is found from target-free time-reversal operators, which are formed on a regular interval by the distributed sensor network. Assuming the use of a *non-homogeneity detector*, [77], for preservation of similar state training data, we would expect, under free-probability, approximately four or more measurement noise time-reversal operators would be required for a sufficient estimate of $\widehat{\mathbf{W}}$-assuming relatively homogeneous, and target-free data; as opposed to the sample-covariance, which would optimally require on the order of 120 or more samples to generate a statistically-significant approximation to the interference matrix, see Figure 20. Under free-probability, the training data requirements are shown to be less, owing

to the square value for n in the exponential of the concentration of measure function from Proof (5.15). Figure 26 demonstrates a possible implementation of the fusion center FIFO buffer for the collection of training data.

Figure 27: Concept for Fusion Center Training Data FIFO Buffer

We assume in Figure 27 that there is a total of a nine sample delay required for the FIFO buffer to contain adequate data for the formation of the real-use case measurement noise time-reversal operator; implicit in this assumption is the fact that the training data is homogeneous; though this is not a set requirement, and may require the incorporation of a non-homogeneity detector (NHD) to rectify, see [70] for further details. Each grey block in Figure 27 labeled *Training Data Required* constitutes two homogeneous sample measured time-reversal operators within the fusion center FIFO buffer. Notice the training data is *temporally* adjacent to the *Measured Time-Reversal Operator Under Test*; this is purposefully done to ensure an adequate training data set is chosen to minimize statistical-temporal anomalies in the measurement noise time-reversal operator.

In the initial weak-SNR detection Algorithm 6.1, the threshold value was chosen based upon an estimate of the measurement noise time-reversal operator, and a sufficient number of integration samples to reduce the trace function variance to some pre-determined value, see Figure 21. What is suspiciously absent; however, is a method of controlling the false alarm rate of the weak-SNR detector, the so-called *Neyman-Pearson Criterion*. This lack of false alarm control means a detection is just as likely to be a false alarm as an indicator of a signal present, or a *Type I* statistical error. In an effort to include the Neyman-Pearson criterion, the proceeding section introduces a modified weak-SNR detection algorithm to limit Type I errors based upon an alteration to the threshold value of Equation (6.22).

6.3.3 Weak-SNR Detection Algorithm Corrected for Incorporation of Neyman-Pearson Criterion

The weak-SNR detection algorithm was previously introduced and demonstrated for a *clairvoyant* detection case, for which the noise and measured time reversal operator was known *a priori*. The detection performance was demonstrated based upon Monte Carlo simulations, showing initial promise and efficacy of the proposed

algorithm. However, conspicuously missing from the weak-SNR detection algorithm was a method of false alarm control, or what is typically referred to as the *Neyman-Pearson criterion*. The lack of false-alarm control means that any results did not control for Type I statistical errors, and were idealized and not representative of a practical detection mechanism for weak-SNR regimes. In this section, a method of false-alarm control is introduced, which allows for the formation of a proper *receiver operating characteristics* or *ROC* curves, allowing a false-alarm value to be fixed, and the detection performance analyzed in better context. Again, we make use of Chebyshev's Inequality from [55] to formulate the threshold for the binary detection hypothesis test. From Chebyshev's Inequality, we know that for any distribution in which the standard deviation is defined, the variables that fall within a certain number of standard deviations from the defined mean, $k\sigma$, is at least as much as [55].

Table 13: Empirical Threshold Table

Minimum Population from the Mean	Number of Standard Deviations (k)
$\mathbf{50\%}$	$\sqrt{2}$
$\mathbf{75\%}$	2
$\mathbf{89\%}$	3
$\mathbf{94\%}$	4
$\mathbf{96\%}$	5
$\mathbf{97\%}$	6
$\mathbf{1-\frac{1}{k^2}\%}$	k

From Table 13, we see that for an empirical false alarm rate of 6% we would require the $\gamma_{\text{Threshold}}$, σ, to be equivalent to $\mu + 4\sigma$; likewise, for an empirical false alarm rate of 4% and 3%, we require the $\gamma_{\text{Threshold}}$ to be $\mu + 5\sigma$ and $\mu + 6\sigma$, respectively. For more standard values of false alarm, ranging from 10^{-2}, 10^{-3}, 10^{-4}, 10^{-5}, 10^{-6}, 10^{-7}, and 10^{-8}, we would require the value of k to be 10, 32, 100, 317, 1000, 3155, 9760, respectively.

In order to determine the actual numerical value for the detection threshold based upon the Chebyshev Inequality, initially, refer to Figure 27. In Figure 27, the training data is temporally separated, and the corruptive noise process is assumed homogeneous. Now, in order to make use of the Chebyshev Inequality, there needs to be both a mean value of the threshold and a standard deviation on that same threshold. Let us start by defining the threshold from Equation (6.19)

$$\gamma_{\text{Threshold}} = \frac{\text{Tr}\left(\sum_{n=1}^{N} \widehat{\mathbf{W}}\right)^2}{\text{Tr}\left(\sum_{n=1}^{N} \widehat{\mathbf{W}}\right)} \tag{6.24}$$

Which is the threshold based on an estimate of the corruptive noise time-reversal operator trace functional. In order to solve for the mean of the threshold trace functional, we require a vector of $\gamma_{\text{Threshold}}$ values to be calculated. We do so by rewriting Equation (6.19) as

$$\hat{\gamma}_{\text{Threshold}} = \left[\frac{\text{Tr}\left(\sum_{n=1}^{N} \widehat{\mathbf{W}_1}\right)^2}{\text{Tr}\left(\sum_{n=1}^{N} \widehat{\mathbf{W}}_1\right)}, \frac{\text{Tr}\left(\sum_{n=1}^{N} \widehat{\mathbf{W}}_2\right)^2}{\text{Tr}\left(\sum_{n=1}^{N} \widehat{\mathbf{W}}_2\right)}, \dots, \frac{\text{Tr}\left(\sum_{n=1}^{N} \widehat{\mathbf{W}}_k\right)^2}{\text{Tr}\left(\sum_{n=1}^{N} \widehat{\mathbf{W}}_k\right)}\right] \tag{6.25}$$

The above expression is more simply represented as a vector of threshold values, where the variable k denotes the vector length.

$$\hat{\gamma}_{\text{Threshold}} = \left[\gamma_{\text{Threshold}_1}, \gamma_{\text{Threshold}_2}, \cdots, \gamma_{\text{Threshold}_k}\right] \tag{6.26}$$

Having defined the trace functional vector of threshold values, we are now able to better calculate the mean of $\gamma_{\text{Threshold}_k}$ as follows

$$\bar{\mu}_k = \frac{1}{K} \sum_{k=1}^{K} \gamma_{\text{Threshold}_k} \tag{6.27}$$

The standard deviation is found from the square root of the second central moment, or the square root of the sample variance

$$\bar{\sigma}_\gamma = \sqrt{\frac{1}{K} \sum_{k=1}^{K} \left(\gamma_{\text{Threshold}_k} - \mu_\gamma^2\right)} \tag{6.28}$$

Recall that the left side of Equation (6.27) is the basis for the weak-SNR threshold of (6.20), and the Monte Carlo simulation is attempting to ascertain the threshold value based upon an estimate of the corruptive noise time-reversal operator, based upon presumed homogeneous training data. One important note, as with [79], the threshold value is going to be dependent upon the underlying corruptive noise process. If we knew some fundamental aspect of the measurement noise, then we would have a *knowledge-aided* weak-SNR detector; if the measurement noise is known exactly, then we have a *knowledge-based* weak-SNR detector. In order to have a truly *non-parametric* weak-SNR detector, the threshold values of Table 13 need to be employed to ensure algorithm compatibility with any corruptive noise process in which the mean and standard deviation can be determined. Results of the Monte Carlo simulation are shown for standard Gaussian and non-Gaussian corruptive noise processes in Table 14.

Evident in Table 14 is the variety of threshold values for different standard non-Gaussian distributions. Whilst this may appear to make real-world application challenging, the point of tabulating a variety of common threshold variables is motivational, to demonstrate the inherent power in non-parametric detection algorithms to encompass such a broad-array of corruptive noise processes. In

Table 14 the Gaussian distribution is indicative of a standard thermal background measurement noise processes, whilst the remaining distributions are representative of standard ground clutter models. Rayleigh distributions are typically assumed when a large number of randomly located independent uniform scatterers are illuminated; whilst the Log-Normal distribution is more likely to be used when the resolution cell and the grazing angle are small, potentially resulting in a higher-tailed probability distribution; Weibull distributions are a two-parameter family that can be altered to fit clutter models that lie between Rayleigh and Log-Normal, with the Rayleigh distribution being a special case of the Weibull distribution ($\alpha = 2.0$) [80].

Table 14: Empirical Thresholds

Distribution	$\bar{\mu}$	$\bar{\sigma}$	$\gamma_{\text{Threshold}}$
Gaussian	0.00	1.4141	$\bar{\mu} + k\bar{\sigma}$
Weibull $(\alpha = 0.55)$	28.27	4.49	$\bar{\mu} + k\bar{\sigma}$
Rayleigh $(\alpha = 2.0)$	50.12	1.84	$\bar{\mu} + k\bar{\sigma}$
Log-Normal $(s = 1.5)$	61.58	12.57	$\bar{\mu} + k\bar{\sigma}$

Figure 28 plots the values of Table 14 logarithmically.

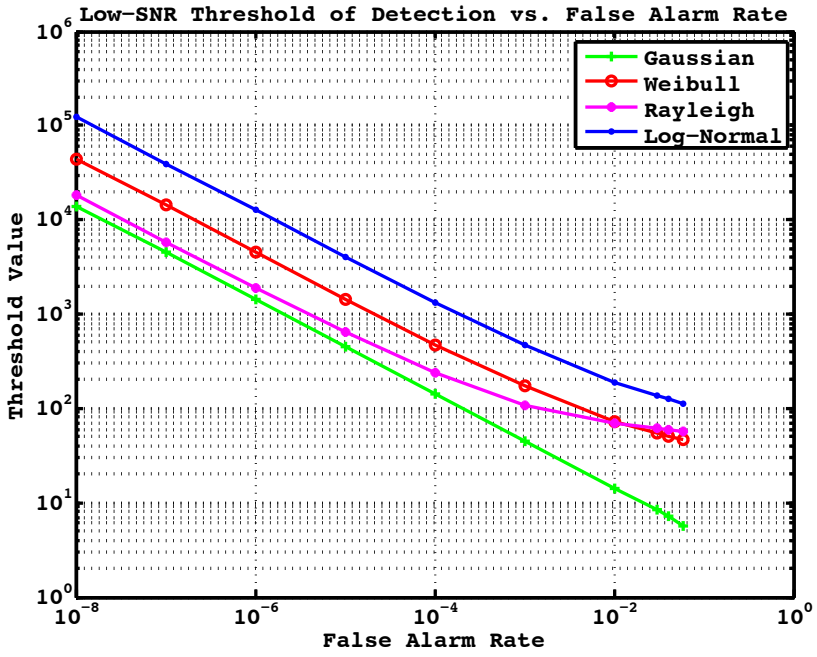

Figure 28: Weak-SNR Threshold vs False Alarm Rate

Again, it is worth mentioning that in [79], the Neyman-Pearson criterion for the *knowledge-aided* detector can be drastically different, resulting in greatly enhanced detection performance. For comparison, when the underlying noise processed is

known to be Gaussian, we can correlate the Chebyshev Inequality P_{FA} to an equivalent Gaussian noise P_{FA}, as shown in the Table 15.

Algorithm 6.2: Weak-SNR Binary Hypothesis Test with False Alarm Control **Fusion Center Weak-SNR Detection Algorithm**
1a: Form the Target Time-Reversal Operator: $\mathrm{A} = \sum_{j=1}^{r} \boldsymbol{\sigma_j \mu}(\mathrm{x}_j)\, \boldsymbol{v}(\boldsymbol{x_j})^*$
1b: Form the Corruptive Noise Time-Reversal Operator: $\mathrm{W} = \frac{\mathbf{1}}{\sqrt{\boldsymbol{N}}} \boldsymbol{C}\mathbb{M}_N \in \boldsymbol{\mathcal{N}}(\mathbf{0}, \boldsymbol{\sigma^2})$
1c: Generate the Measured Time-Reversal Operator: $\mathrm{B} = \sum_{m=1}^{M} (\mathrm{A} + \boldsymbol{c_n}\mathrm{W})$
2: Calculate the OAS Estimate, $\widehat{\boldsymbol{\Sigma}}_{\mathbf{OAS}}$, of **B**
3: Determine $\mathbf{A}_{\mathbf{OAS}}$ and $\mathbf{W}_{\mathbf{OAS}}$
4: Calculate the Corruptive Noise Time-Reversal Operator: $\widehat{\mathrm{W}} = \sum_{m=1}^{M} \left(\frac{\boldsymbol{c_n}}{\sqrt{\boldsymbol{n}}} \boldsymbol{C}\mathbb{M}_N \in \boldsymbol{C\mathcal{N}}(\mathbf{0}, \boldsymbol{\sigma^2}) \right)$
5a: Determine the threshold statistic, $\boldsymbol{\gamma}$, from: $\boldsymbol{\gamma}_{\mathbf{Threshold}_k} = [\boldsymbol{\gamma}_{\mathbf{Threshold}_1}, \boldsymbol{\gamma}_{\mathbf{Threshold}_2}, \cdots, \boldsymbol{\gamma}_{\mathbf{Threshold}_k}]$
5b: Calculate the mean and standard deviation of $\boldsymbol{\gamma}_{\mathrm{Threshold}_k}$: $\bar{\boldsymbol{\mu}}_{\boldsymbol{\gamma}} = \frac{\mathbf{1}}{\boldsymbol{K}} \sum_{k=1}^{K} \boldsymbol{\gamma}_{\mathbf{Threshold}_k}$ $\bar{\boldsymbol{\sigma}}_{\boldsymbol{\gamma}} = \sqrt{\frac{\mathbf{1}}{\boldsymbol{K}} \sum_{k=1}^{K} \left(\boldsymbol{\gamma}_{\mathbf{Threshold}_k} - \bar{\boldsymbol{\mu}}_{\boldsymbol{\gamma}}^2 \right)}$
5c: Calculate Threshold Statistic Based Upon Desired False Alarm Rate, $\boldsymbol{k_{FA}}$: $\boldsymbol{\gamma}_{\mathbf{Threshold}} = \bar{\boldsymbol{\mu}}_{\boldsymbol{\gamma}} + \boldsymbol{k_{FA}} \bar{\boldsymbol{\sigma}}_{\boldsymbol{\gamma}}$, where $\boldsymbol{k} \in [\mathbf{4}, \mathbf{5}, \mathbf{6}, \mathbf{9}, \mathbf{10}, \mathbf{32}]$
6: Determine the Outcome of the Binary Hypothesis Test: $\boldsymbol{\gamma}_{\mathbf{Threshold}} \underset{H_0}{\overset{H_1}{\lessgtr}} \frac{\mathrm{Tr}(\mathbf{A}_{\mathbf{OAS}}^2)}{\mathrm{Tr}(\mathbf{A}_{\mathbf{OAS}})} + \frac{\mathrm{Tr}(\mathbf{W}_{\mathbf{OAS}}^2)}{\mathrm{Tr}(\mathbf{W}_{\mathbf{OAS}})}$

From Table 15 the restrictive nature of the Chebyshev inequality is evident, as is the benefit of having *a priori* knowledge on the underlying corruptive noise process. In either instance, the Type I errors are minimized whilst ensuring the probability of detection values have merit. For the general use case, the nonparametric nature of the Chebyshev Inequality for the Neyman-Pearson criterion.

Table 15: Probability of False Alarm for Chebyshev Inequality vs Knowledge-Aided Detector Under Gaussian Noise Assumption

Chebyshev's Inequality, P_{FA}	$k\sigma$	x	Equivalent P_{FA} for Gaussian Noise
6%	4σ	3.62	$P_{FA} = 10^{-4}$
4%	5σ	4.75	$P_{FA} = 10^{-5}$
3%	6σ	5.61	$P_{FA} = 10^{-6}$
1%	10σ	$x \gg 6.23$	$P_{FA} \gg 10^{-9}$
0.1%	32σ	$x \gg 6.23$	$P_{FA} \gg 10^{-9}$
0.01%	100σ	$x \gg 6.23$	$P_{FA} \gg 10^{-9}$

6.4 Weak-SNR Detection without Oracle Approximation Shrinkage

For the sake of determining the baseline effectiveness of the weak-signal-to-noise ratio (SNR) detection algorithms, we reduce the complexity of the algorithm and assume both the target and noise time-reversal operators, **A** and **W** respectively, are known *a priori*. In the subsequent section, this case is not assumed, and results are derived based on the oracle approximation shrinkage (OAS) estimates of **A** and **W**. Recall that the OAS algorithm determines the asymptotic form of the time-reversal operator, and should result in better weak-SNR performance, at the expense of greater computational complexity. The modified algorithm used in this section is simply Algorithm 6.2, skipping steps $(1c)$, (2) and (3).

Whilst an exhaustive set of simulations were run against sensor network densities of 6, 10, 20, 40, 60, 80 and 100; only those results from simulations involving sensor network densities at 6 and 100 are shown for brevity. Additionally, for each variable sensor density considered, training data lengths were chosen at three distinct values, 4, 14 and 44; which correspond to a decrease in the trace functional variance from 0.1, to 0.01 and 0.001. Since the detection performance desired is in the weak-SNR regime, minimizing the trace functional variance should result in greater detection performance, at the expense of greater training data requirements and computational complexity. A tabulated set of results is shown in Table 17 for all 21 simulation runs. We start by considering a dense sensor network comprised of 100 sensor nodes and a training data length of 4. The object is assumed to consist of 3 point reflectors with the following parameters shown in Table 16.

Table 16: Scattering Center Parametrics

Scattering Center	Dielectric Coefficient (ρ)	Scattering Center Location (x, y)
1	$\rho = 2.0$	$[5,0]$
2	$\rho = 1.75$	$[-2.5, 4.33]$
3	$\rho = 1.5$	$[-2.5, -4.33]$

Each of the scattering centers has a discrete dielectric reflectivity and location within the scene of interest. This should allow for each of the three point reflectors to be uniquely detected. The training length value of 4 is consistent with a trace function variance of 0.10 per Figure 21.

The blue vertical line represents a SNR of $13dB$, consistent with a standard single pulse detector required SNR value. A red line indicates the weak-SNR cross-over point, or the point of matrix congruency between the noise and measured time-reversal operators, see Equation (5.20). Graphically, these weak-SNR cross-over point values versus radar network density were plotted empirically in Figure 25. As Figure 26 shows, the weak-SNR cross-over point is a SNR of $5dB$, and with a probability of detection set at 90%, and probability of false alarm set to 1%, we require a minimum SNR of $-2.2dB$ for the weak-SNR detection algorithm to work.

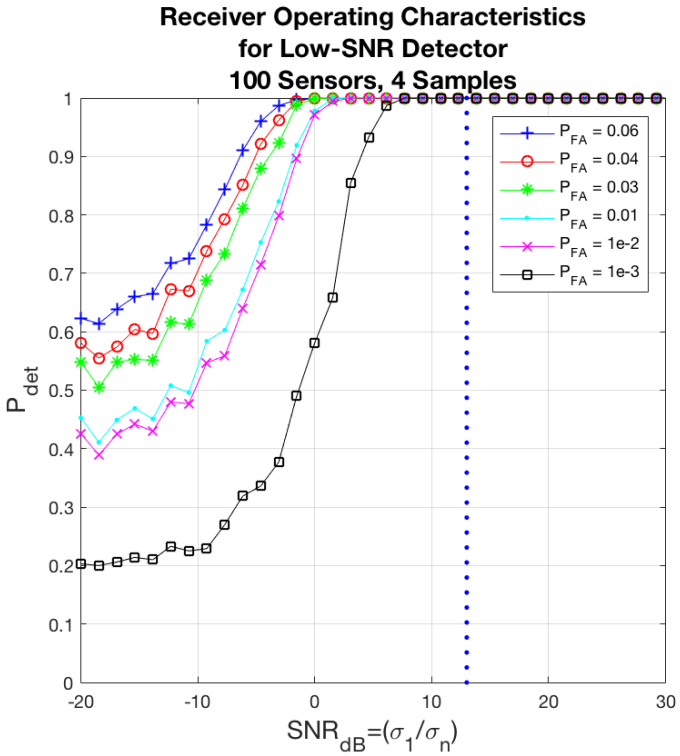

Figure 29: Algorithm 6.2-100 Sensors with Training Data Length of 4 Samples

Now, again, the Neyman-Pearson criterion is set with a rather stringent Chebyshev Inequality parameter that makes lower values of false alarm very difficult to achieve; later, we will relax these conditions with the *knowledge-aided* weak-SNR detection algorithm to show better performance under *knowledge based* scenarios. False alarm rates from 6% to 0.01% are also plotted, showing the sensitivity of this algorithm to the Neyman-Pearson criterion condition imposed on the threshold statistic.

As was discussed previously, the trace functional variance will decrease rapidly as the length of the training data increases. In the next example, the number of training matrices was chosen to be 14, which reduces the trace functional variance to 0.01.

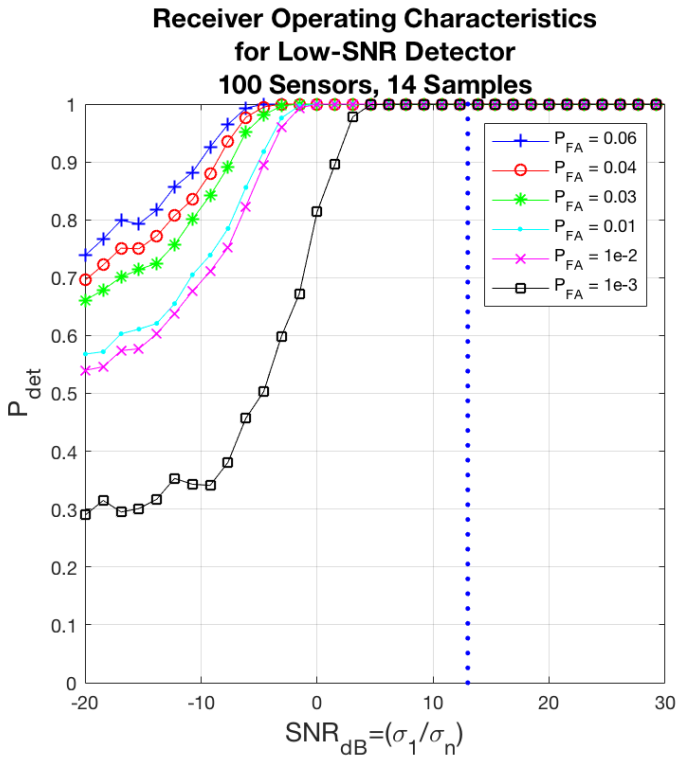

Figure 30: Algorithm 6.2-100 Sensors with Training Data Length of 14 Samples

Again, the blue vertical line represents the single pulse detector SNR requirement of $13dB$, whilst the red vertical line represents the weak-SNR cross-over point of $5dB$. Fixing the probability of detection to 90% with a probability of false alarm of 1%, we find the SNR required for the weak-SNR detection algorithm decreases to $-4.8dB$. Due to the weak-SNR, any variation in the variance of the trace functional has the ability to adversely affect the detection algorithm. For the purposes of these examples, any value lower than the blue vertical line is assumed to be the net gain in performance from utilizing the weak-SNR detection algorithm. Further,

any detection performance to the left of the red vertical line indicates detection performance in the weak SNR regime.

For the next example, the trace functional variance is reduced to 0.001, which requires 44 samples in order to achieve. The sensor network density is kept to 100, and training data length is increased to 44, and the results are shown on Figure 31.

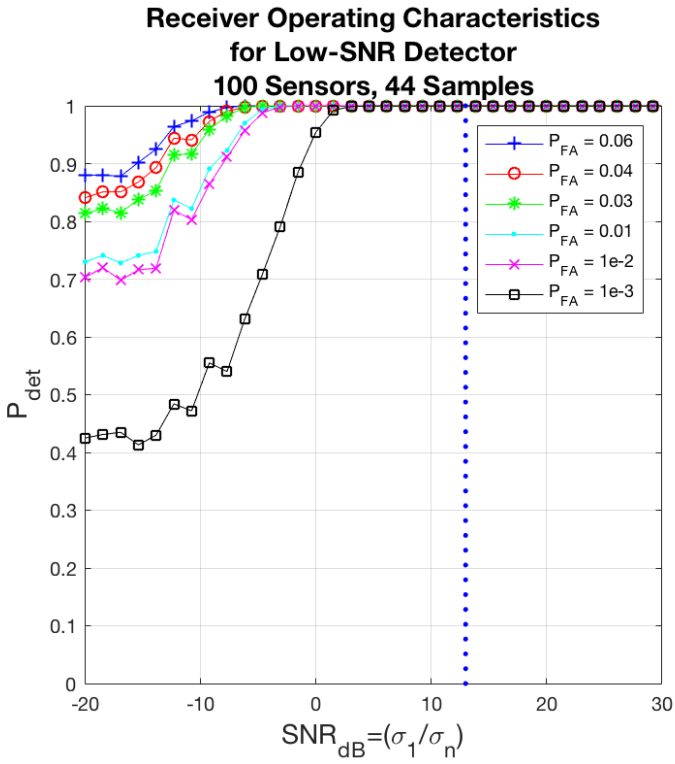

Figure 31: Algorithm 6.2-100 Sensors with Training Data Length of 44 Samples

Immediately evident, is the fact that the receiver operating characteristics (ROC) curves are trending leftward, indicative of an increase in performance at lower-SNR as the training data length increases. Not overall a surprise, as this is true for monostatic radar systems incorporating coherent integration; though technically each time-reversal operator is integrated without concern for coherency, as phase is not a component of the time-reversal operator formulation across operators. Recall from Chapter 5 that our operators under free-probability are now being treated as variables. After the training data is increased to 44, the SNR required for the weak-SNR detector to function for a probability of detection of 90%, with a false alarm fixed at 1% is $-8.5dB$; which is a marked improvement over the traditional single-pulse detector SNR requirement of $13dB$ and $13.5dB$ below the weak-SNR cross-over value of $5dB$. Obviously, as the false alarm rate is decreased, performance tapers off; and that is an accepted trade-off with any detection schema. However, the density of the distributed sensor network is also

a primary factor in the performance of the weak-SNR detection algorithm as will be shown next.

In the following set of examples, the SNR requirement for the weak-SNR cross-over point is empirically found to be $13dB$, which is on par with the traditional monostatic detection algorithm. Again, we demonstrate the value of training data with respect to the detection performance, starting with a training length requirement of 4; in keeping with the variance on the trace functional equaling 0.1.

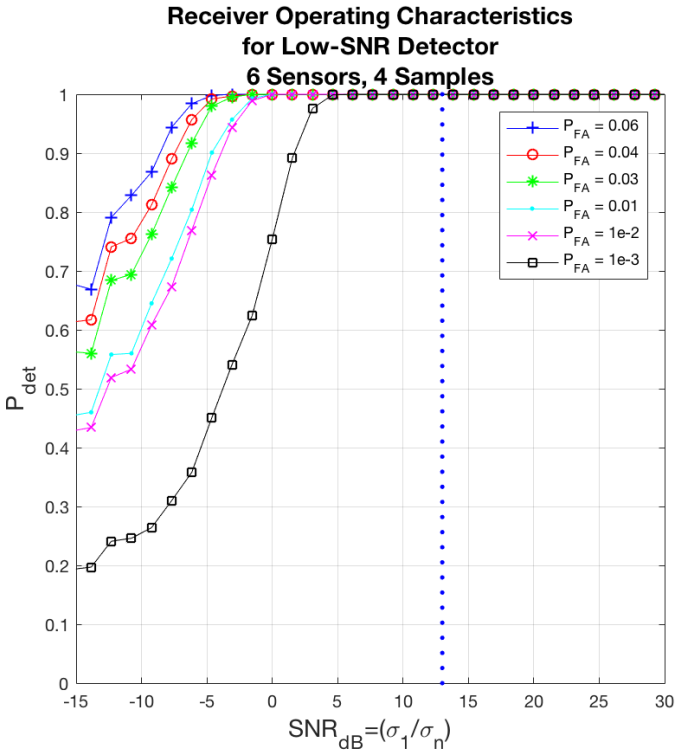

Figure 32: Algorithm 6.2-6 Sensors with Training Data Length of 4 Samples

Focusing on a probability of detection of 90% and a false alarm rate of 1%, we see the SNR required for detection is $-4.6dB$, or $17.6dB$ less than the weak-SNR cross-over point of $13dB$. Obvious from Figure 32 is that the less dense sensor network has a threshold for detection on par with a traditional monostatic radar detector, but achieves similar detection performance under weak-SNR conditions as the denser radio-frequency sensor network of Figure 29. One takeaway from this observation is that the denser a sensor network, the more sensitive it is to detection at weaker SNR values, but detection performance is limited by the higher-rank of the measurement noise time-reversal operator. If this is true, as we progress through the examples, the less dense distributed sensor network should surpass the detection performance of the denser sensor network. Our next example reduces the trace functional variance to 0.01 by utilizing a training data length of 14.

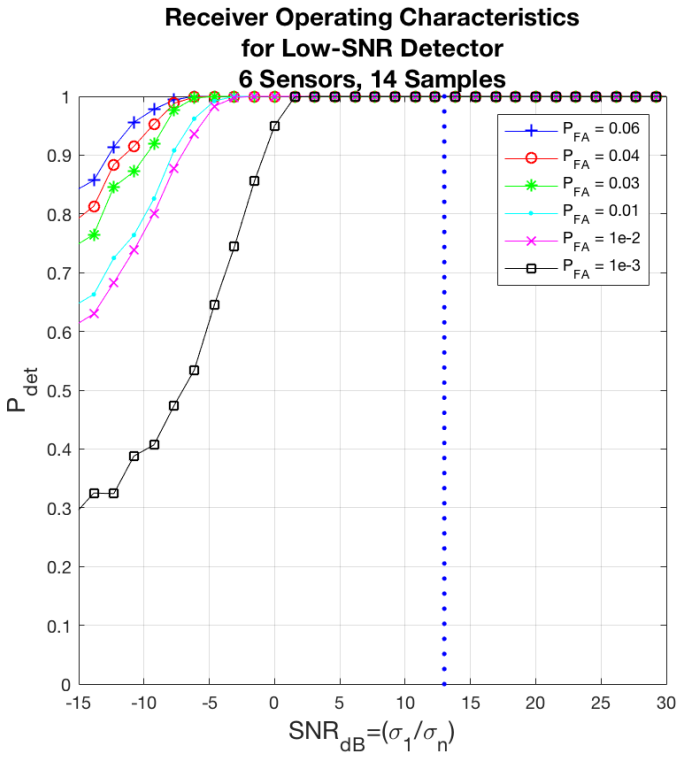

Figure 33: Algorithm 6.2-6 Sensors with Training Data Length of 14 Samples

In keeping with previous examples, $P_D = 90\%$, whilst $P_{FA} = 1\%$, which puts the required SNR for detection at $-7.8dB$, which is a decrease of $20.8dB$ from the weak-SNR cross-over point, and a $-3dB$ difference from the radar network comprised of 100 sensors.

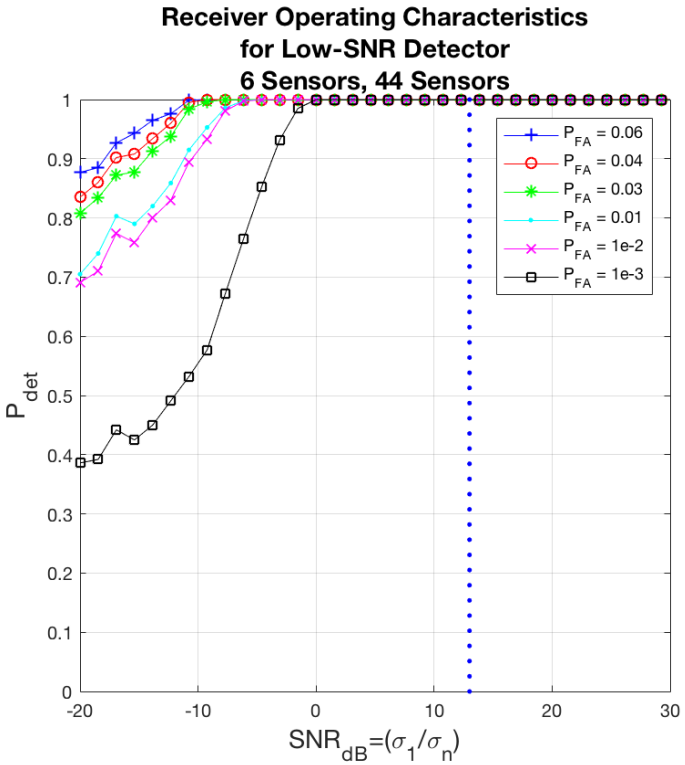

Figure 34: Algorithm 6.2-6 Sensors with Training Data Length of 44 Samples

To determine if this trend continues, the training data length is increased to 44 to keep the trace functional variance at 0.001, and the receiver operating characteristics are plotted for 6 sensors in the figure below.

From Figure 34 the required SNR for detections is approximately $-11.2dB$, which indicates an improvement of nearly $-2.7dB$ from the sensor network comprised of 100 sensors, and an improvement of $-24.2dB$ over the single pulse detector. So, the original hypothesis that the detection performance at weak-SNR is noise-limited is probable, particularly when the rank of the noise time-reversal operator is much greater than the signal rank time-reversal operator, **A** $\ll$ **W**.

To summarize, initial results for the weak-SNR detection algorithm run under ideal, and rather unrealistic, conditions in which the signal and measured time-reversal operator are known, and the threshold statistic is determined from training data, demonstrate the ability of this algorithm to detect the presence of a signal at SNR values that are weak. Specifically, as the training data length is increased, corresponding to a lower variance value on the trace functional, the detection performance increases, allowing detection of signals at lower SNR values-even negative SNR values! In the case where the distributed sensor network density is high-e.g. 100 sensor nodes-detection performance increases by a factor of $6dB$ as the training data length is increased from 4 to 44. For a sparse sensor network of 6 nodes, the detection performance also increases by $\sim 6dB$ as the training data length is increased from 4 to 44. The discrepancy between the dense and sparse radar networks merits further investigation, but for this particular set of simulation results, the difference is assumed to be manifest from the increased number of noise eigenvalues incorporated into the trace functional; however, this is only assumed true if the discrepancy is consistent once the *oracle approximation shrinkage* simulation results are analyzed.

Table 17 lists the results from each simulation run, and shows the weak-SNR cross-over point, see Figure 26, as a point of reference. Recall, that the weak-SNR cross-over value is the point at which the matrix inertia (see definition 1 from Equation (6.15)) of the measured time-reversal operator, **B** is equivalent to the noise time-reversal operator **W**; which is assumed to be the point at which we shift to the weak-SNR regime. A weak signal does not imply negative SNR, but the point at which the singular values of the measured and noise time-reversal operators appear mathematically equivalent. Algorithm 6.2 is an attempt to allow for the detection of signals at weak-SNR regimes; however, this algorithm also

works at higher-ie nominal-SNR values as well. One benefit of using Algorithm 6.2, is that recovery of signals at negative SNR regimes is possible and demonstrated clearly in the results of Table 17; with the proviso that detection performance is very much tightly coupled to the required false-alarm rate; in which case, the values of Table 17 trend rightward in SNR as the false alarm rate is increased. However, since traditional detection algorithms do not typically function at SNR values that are negative, the relaxation of the false alarm rate requirement results in increased detection performance using Algorithm 6.2.

Table 17: Probability of Detection vs Sensor Network Density vs Training Data Length

Sensor Network Density	Weak-Signal Cross-Over Point	Training Data Length $\boldsymbol{N}$	Probability of Detection $\boldsymbol{P_D = 90\%, P_{FA} = 1\%}$
6	$13dB$	$N = [4,14,44]$	$[-4.6dB, -7.8dB, -11.2dB]$
10	$11dB$	$N = [4,14,44]$	$[-4.4dB, -7.5dB, -10.7dB]$
20	$9dB$	$N = [4,14,44]$	$[-2.7dB, -5.8dB, -9.2dB]$
40	$8dB$	$N = [4,14,44]$	$[-2.5dB, -4.8dB, -8.5dB]$
60	$7dB$	$N = [4,14,44]$	$[-2.3dB, -4.8dB, -8.5dB]$
80	$6dB$	$N = [4,14,44]$	$[-2.3dB, -4.8dB, -8.5B]$
100	$5dB$	$N = [4,14,44]$	$[-2.3dB, -4.8dB, -8.5B]$

Evident from Table 17 is the unexpected asymptotic slope of performance increases versus sensor network density. It would seem that sensor network performance peaks at a sparse sensor network density value of 6, and diminishes with any increase in sensor network density of 40-60 nodes. If the results are compared versus the weak-signal cross-over point, performance obviously degrades with increasing number of sensor nodes. In every instance, the empirical weak signal-to-noise ratio value is in excess of the probability of detection metric, demonstrating the efficacy of the proposed low-SNR detection Algorithm 6.1. Future tabulated results will truncate at a sensor network density of 40 nodes, to minimize the number of duplicate entries from node densities of 60-100.

In the next section, the oracle approximation shrinkage (OAS) algorithm is included, which increases the computational complexity of the weak-SNR detection Algorithm in 6.2 with the added benefit that the only required inputs to the algorithm are now the measured time-reversal operator and the estimated corruptive noise time-reversal operator, $\mathbf{B}$ and $\widehat{\mathbf{W}}$ respectively. Since the asymptotic form of the measured time-reversal operator is used, based on the use of the OAS algorithm, detection performance improvements are realized; which

further demonstrates the flexibility and utility of Algorithm 6.2 for the recovery of signals under weak-SNR conditions.

6.5 Weak-SNR Detection with Oracle Approximation Shrinkage

In an effort to better understand whether the underlying mathematics used in Algorithm 6.2 were sound, elements of the algorithm were relaxed to more quickly demonstrate typical results in scenarios where the target and measured time-reversal operators were assumed known *a priori*. From Table 17, detection performance was demonstrated and serves as our baseline for the results presented in this section. Most notable was the omission of the OAS in the previous section; however, for this section the entirety of Algorithm 6.2 is used. The scenario under which the subsequent simulations will be performed, is shown below and each scattering center is assumed to be an isotropic point source with set material properties and location.

Table 18: Scattering Center Parametrics

Scattering Center	Dielectric Coefficient (ρ)	Scattering Center Location (x, y)
1	$\rho = 2.0$	$[5,0]$
2	$\rho = 1.75$	$[-2.5, 4.33]$
3	$\rho = 1.5$	$[-2.5, -4.33]$

Since the only noticeable change in the application of Algorithm 6.2 is the inclusion of the OAS algorithm, any variations in the results from Section 6.4 are solely due to the use of the asymptotic approximation form of the time-reversal operators. No other simulation parameters have been changed; making this section as much a reflection upon Algorithm 6.2, as its intended real-use case within the distributed sensor network fusion center. As before, training data lengths are varied to explore the impact of the trace functional variance on the results. In a reversal from Section 6.4, the results are presented starting with the lower density sensor network configuration; recall this demonstrated improved performance against the dense sensor network, presumably from a reduction in the number of significant noise elements in the trace functional. Another aim of this section is to determine whether the density of the sensor network, when asymptotic forms of the time-reversal operators are utilized, significantly impacts detection performance. Results are presented for the same two scenarios that were described in Section 6.4, with a summary table presenting the exhaustive results from all simulation

trials. In keeping with the general flow from the previous section, each set of receiver operating characteristics (ROC) curves is described and discussed, with a concluding summary section.

Our first set of receiver operating characteristic (ROC) curves is from a sparse sensor network comprised of 6 sensor nodes. The training data length is kept to a value of 4, in keeping with a trace functional variance value of 0.1, see Figure 26.

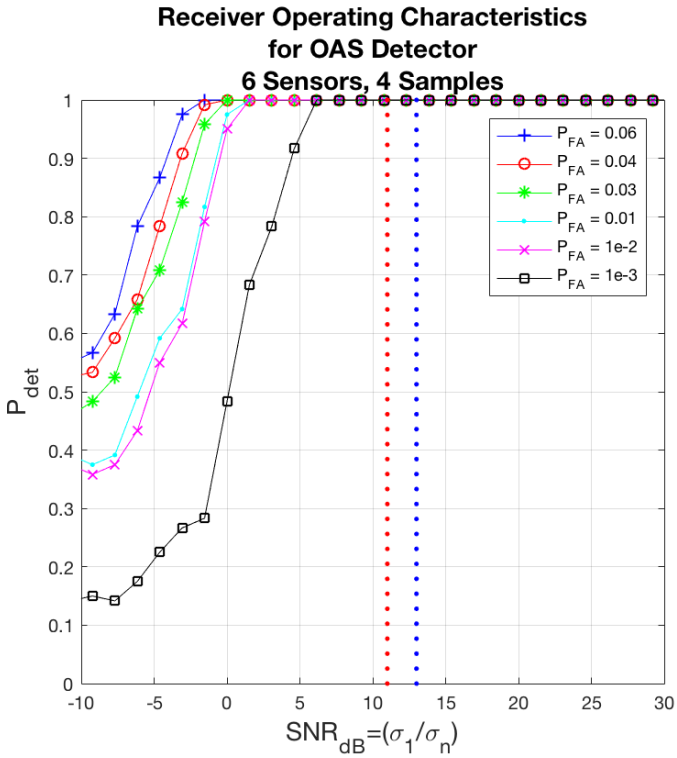

Figure 35: Algorithm 4.2-6 Sensors with Training Data Length of 4 Samples

Again, for the purposes of continuity, a probability of detection value of 90% and a false alarm rate of 1% are assumed. From Figure 35, an immediately obvious change from Figure 32 is the leftward trending of the ROC curves. In fact, this is most noticeable for the lower values of the false alarm rate. However, the point we are most interested in is the value of $-0.8dB$, that is the intersection of the ROC curve for the false alarm rate of 1% at a probability of detection of 90%. This result is an improvement of approximately $14dB$ when compared to the single pulse detector, but arguably represents a $3dB$ decrease in performance in comparison to Section 6.4 for the same example. This comparison is, admittedly unfair, as the target and noise time-reversal operators, **A** and **W**, are now estimated from the measured time-reversal operator, **B** are not known *a priori*.

In the next example, the training data length is increased to 14, which corresponds to a trace functional variance of 0.01. The sparse sensor network is

kept at 6 nodes, and simulation results are shown for the receiver operating characteristic curves below.

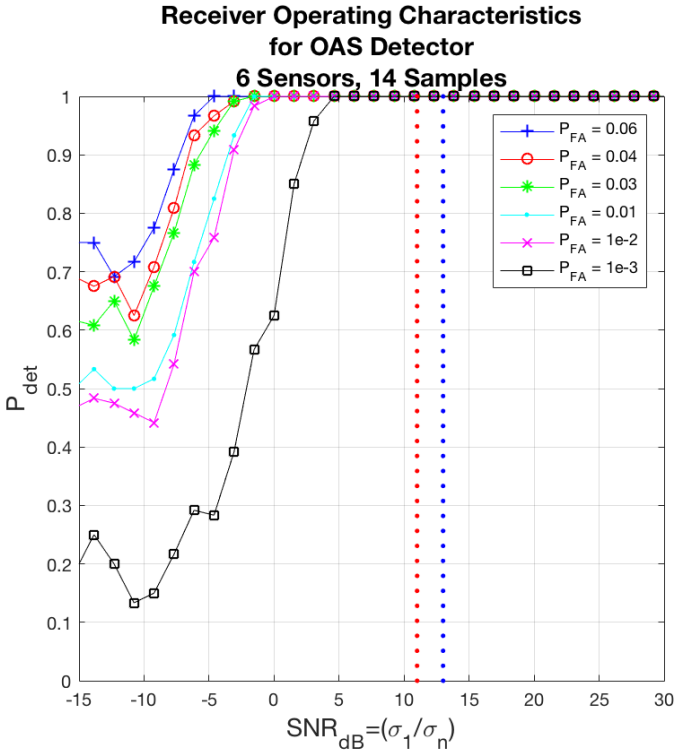

Figure 36: Algorithm 4.2-6 Sensors with Training Data Length of 14 Samples

Assuming a $P_D = 90\%$, and a $P_{FA} = 1\%$, the required signal-to-noise ratio required for detection is $-3.2dB$, which is again $3dB$ less than that of Figure 33. What has changed is the shape of the ROC curve indicates better behavior in the weaker-SNR regimes, but is otherwise represents a consistent performance degradation over the *a priori* use cases of Section 6.4. In this regard, the results show efficacy, and that Algorithm 6.2 is applicable and useful in scenarios under which there is little, or no, *a prior* information.

Our final sparse sensor network set of ROC curves keeps the number of sensor nodes to 6, but increases the training data length to 44, reducing the trace functional variance to 0.001. From Figure 37, the detection performance seems consistent with the previous case in which the target and noise time-reversal operators were known. What is most notable with bespoke Algorithm 6.2, is the fact that the efficacy of the algorithm is consistent whether the target and noise time-reversal operators are known *a priori,* or unknown and estimated from collected data; this demonstrates an incredible flexibility that instills confidence for real-world use cases to accurately reflect simulation trials.

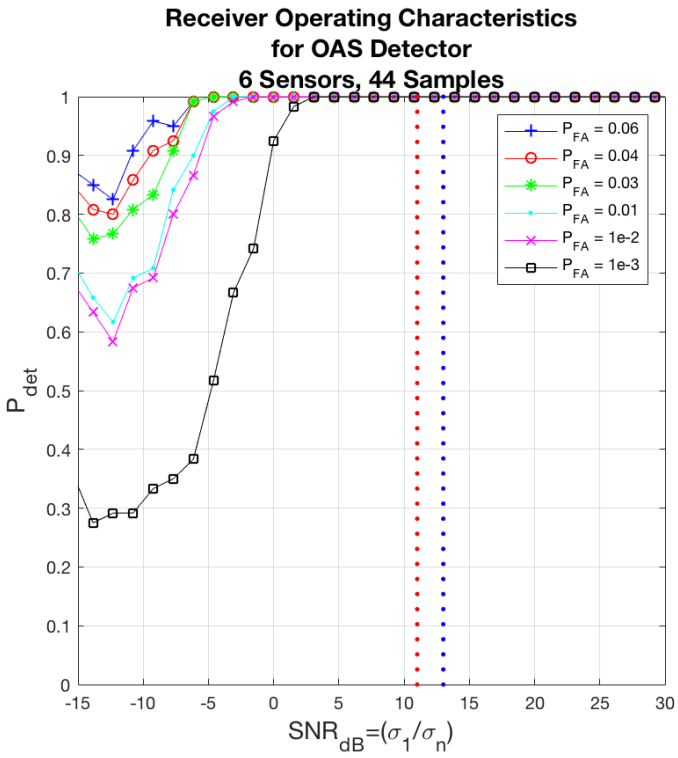

Figure 37: Algorithm 4.2-6 Sensors with Training Data Length of 44 Samples

From Table 19, the trend is indicative of detection performance being closely tied to the length of the training data, as well as the density of the sensor network. Since the time-reversal operators used are approximations of the same operators comprised of an infinite number of samples, there should be minimal outliers present in the trace functional, which would be expected should the sample size of the time-reversal operators be finite. The use of the oracle approximation shrinkage could also be viewed as a smoothing function, which has the same effect as the minimization of outliers, but with the same intended improvement in results.

Table 19: Algorithm 6.2-Probability of Detection vs Sensor Network Density vs Training Data Length

Sensor Network Density	Weak-Signal Cross-Over Point	Training Data Length $\boldsymbol{N}$	Probability of Detection $\boldsymbol{P_D = 90\%, P_{FA} = 1\%}$
6	$13dB$	$N = [4,14,44]$	$[-0.8dB, -3.2dB, -6.2dB]$
10	$11dB$	$N = [4,14,44]$	$[0.0dB, -3.2dB, -6.2dB]$
20	$9dB$	$N = [4,14,44]$	$[0.9dB, -1.6dB, -4.6dB]$
40	$8dB$	$N = [4,14,44]$	$[1.5dB, 1.0dB, -3.1dB]$

6.6 Weak-SNR Subspace Rank Estimation

Following the application of Algorithm 6.2 to determine the presence of a target, the next task is to determine exactly how many scattering centers are present via a process called ranking. Detection and rank estimation are two of the most

germane sensing tasks that the fusion center would accomplish via the distributed sensor network. In Sections 6.4 and 6.5, detection performance results were demonstrated in the form of receiver operating characteristics, or ROC curves.

To determine the rank of **B**, where **B**$\in\mathbb{C}^{mxn}$, and can be decomposed into $\mathbf{A}_{\text{OAS}} + c_n\mathbf{W}_{\text{OAS}}$, with $c_n \in [0,\infty)$ in $\mathbb{R}^n$, and $\mathbf{A}_{\text{OAS}} \in \mathbb{C}^{mxn}$ whose rank is $k \ll M$, and $\mathbf{W}_{\text{OAS}} \in \mathbb{C}^{mxn}$, whose elements are independent identically distributed (IID) and $\mathbf{W}_{\text{OAS}_{ij}} \in \mathcal{CN}(0,\sigma^2)$. We start by rewriting the basic weak-signal-to-noise ratio (SNR) hypothesis test of from Algorithm 6.2

$$\gamma_{\text{Threshold}} \underset{H_0}{\overset{H_1}{\lessgtr}} \frac{\text{Tr}(\mathbf{A}_{\text{OAS}}^2)}{\text{Tr}(\mathbf{A}_{\text{OAS}})} + \frac{\text{Tr}(\mathbf{W}_{\text{OAS}}^2)}{\text{Tr}(\mathbf{W}_{\text{OAS}})} \tag{6.29}$$

We re-label the previous Equation as (6.29), which shows the binary hypothesis detection test for the case in which we are purely interested in the presence of a signal, or reflection from a reflective scattering center on a target body. Multiple scattering centers may be present for a given range-extended target, and in fact there are three for our range-extended target, see Table 16; which is information not reflected in the outcome of Equation (6.29). In order to deduce the presence of multiple scattering centers, we need to incorporate the ability to test for *rank* in the hypothesis test of Equation (6.29). By slightly changing the method in which the binary hypothesis test is performed, the effective rank of the target time-reversal operator is readily found

$$\gamma_{Threshold_{i:M}} \underset{H_0}{\overset{H_1}{\lessgtr}} \frac{\text{Tr}(\mathbf{A}_{\text{OAS}}^2)}{\text{Tr}(\mathbf{A}_{\text{OAS}})} + \frac{\text{Tr}(\mathbf{W}_{\text{OAS}}^2)}{\text{Tr}(\mathbf{W}_{\text{OAS}})}, \forall\, i = 1,2,\dots,g \tag{6.30}$$

Where the values for i indicate the starting singular value passed to the trace function, and M is the maximum rank of the associated measured time-reversal operator. Now, we assume the rank of **B** is $g \ll M$, but in some of our simulations, the rank is more akin to $g < M$; all of which is relative with respect to the sensor network density. In order to determine the threshold statistic, $\gamma_{\text{Threshold}}$, we need to account for the change in the inputs to the trace functional, and resolve for the threshold value thusly

$$\hat{\gamma}_{Threshold_{i:M}} = \left[\frac{\text{Tr}\left(\sum_{n=1}^{N}\widehat{\mathbf{W}}_{1;\,i:M}\right)^2}{\text{Tr}\left(\sum_{n=1}^{N}\widehat{\mathbf{W}}_{1;\,i:M}\right)}, \frac{\text{Tr}\left(\sum_{n=1}^{N}\widehat{\mathbf{W}}_{2;i:M}\right)^2}{\text{Tr}\left(\sum_{n=1}^{N}\widehat{\mathbf{W}}_{2;i:M}\right)}, \dots, \frac{\text{Tr}\left(\sum_{n=1}^{N}\widehat{\mathbf{W}}_{k;i:M}\right)^2}{\text{Tr}\left(\sum_{n=1}^{N}\widehat{\mathbf{W}}_{k;i:M}\right)}\right] \tag{6.31}$$

where n is the length of the training data, and k denotes length of the vector of threshold values, and we have noted the change in the estimated threshold statistic for ranking with the subscript, $\hat{\gamma}_{\text{Threshold}_{i:M}}$.

$$\hat{\gamma}_{\text{Threshold}_{i:M}} = \left[\gamma_{\text{Threshold}_{1;i:M}}, \gamma_{\text{Threshold}_{2;i:M}}, \cdots, \gamma_{\text{Threshold}_{k;i:M}}\right] \tag{6.32}$$

Having defined the ranking trace functional vector of threshold values, we are now able to determine the mean of $\hat{\gamma}_{\text{Threshold}_{i:M}}$ as follows

$$\bar{\mu}_{\gamma;i:M} = \frac{1}{K}\sum_{k=1}^{K}\gamma_{\text{Threshold}_{k;i:M}} \tag{6.33}$$

The standard deviation is found from the square root of the second central moment, or the square root of the sample variance of the ranking trace functional vector of threshold values

$$\bar{\sigma}_{\gamma;i:M} = \sqrt{\frac{1}{K}\sum_{k=1}^{K}\left(\gamma_{\text{Threshold}_{k;i:M}} - \bar{\mu}_{\gamma;i:M}^{2}\right)} \tag{6.34}$$

Now that the final ranking threshold statistic is found from the desired false-alarm rate, k_{FA}, as follows

$$\hat{\gamma}_{\text{Threshold}_{i:M}} = \bar{\mu}_{\gamma;i:M} + k_{FA}\bar{\sigma}_{\gamma;i:M} \tag{6.35}$$

Algorithm 6.3 is the designation for the weak-SNR ranking binary hypothesis test, with false-alarm control. This algorithm is processed by the fusion center, and can be run in serial or parallel depending on the processing resources available to the fusion center platform.

Algorithm 6.3: Weak-SNR Ranking Binary Hypothesis Test with False Alarm Control

Fusion Center Weak-SNR Ranking Algorithm

1a: Form the Target Time-Reversal Operator:

$$\mathbf{A} = \sum_{j=1}^{r}\boldsymbol{\sigma}_j\boldsymbol{\mu}(\boldsymbol{x}_j)\boldsymbol{\nu}(\boldsymbol{x}_j)^{*}$$

1b: Form the Corruptive Noise Time-Reversal Operator:

$$\boldsymbol{W} = \frac{\mathbf{1}}{\sqrt{\boldsymbol{N}}}\boldsymbol{C}\mathbb{M}_{\boldsymbol{N}} \in \boldsymbol{C\mathcal{N}}(\mathbf{0},\boldsymbol{\sigma}^{2})$$

1c: Generate the Measured Time-Reversal Operator:

$$\mathbf{B} = \sum_{m=1}^{M}(\mathbf{A} + \boldsymbol{c}_{\boldsymbol{n}}\mathbf{W}_{\text{OAS}})$$

2: Calculate the OAS estimate, $\widehat{\boldsymbol{\Sigma}}_{\text{OAS}}$, of **B**

3: Determine $\mathbf{A}_{\text{OAS}}$ and $\mathbf{W}_{\text{OAS}}$

4: Calculate the Corruptive Noise Time-Reversal Operator:

$$\widehat{\mathbf{W}} = \sum_{m=1}^{M}\left(\frac{\boldsymbol{c}_{\boldsymbol{n}}}{\sqrt{\boldsymbol{n}}}\mathbb{C}^{mxn} \in \boldsymbol{C\mathcal{N}}(\mathbf{0},\boldsymbol{\sigma}^{2})\right)$$

5a: Determine the Vector of Threshold Statistics, from

$$\hat{\boldsymbol{\gamma}}_{\text{Threshold}_{i:M}} = \left[\boldsymbol{\gamma}_{\text{Threshold}_{1;i:M}}, \boldsymbol{\gamma}_{\text{Threshold}_{2;i:M}}, \cdots, \boldsymbol{\gamma}_{\text{Threshold}_{k;i:M}}\right]$$

5b: Calculate the Mean and Standard Deviation of $\boldsymbol{\gamma}_{\text{Threshold}_{k;i:M}}$

$$\bar{\boldsymbol{\mu}}_{\boldsymbol{\gamma};i:M} = \frac{\mathbf{1}}{\boldsymbol{K}}\sum_{k=1}^{K}\boldsymbol{\gamma}_{\text{Threshold}_{k;i:M}}$$

$$\bar{\boldsymbol{\sigma}}_{\boldsymbol{\gamma};i:M} = \sqrt{\frac{\mathbf{1}}{\boldsymbol{K}}\sum_{k=1}^{K}\left(\boldsymbol{\gamma}_{\text{Threshold}_{k;i:M}} - \bar{\boldsymbol{\mu}}_{\boldsymbol{\gamma};i:M}^{2}\right)}$$

5c: Calculate Threshold Statistics Based Upon Desired False Alarm Rate, $\boldsymbol{k_{FA}}$

$\widehat{\boldsymbol{\gamma}}_{\textbf{Threshold}_{i:M}} = \overline{\boldsymbol{\mu}}_{\gamma;i:M} + \boldsymbol{k_{FA}}\overline{\boldsymbol{\sigma}}_{\gamma;i:M}$, where $\boldsymbol{k} \in [\mathbf{4,5,6,9,10,32}]$

6: Determine the Outcome of the Binary Hypothesis Test:

$\boldsymbol{j}_{\text{Rank}} = \mathbf{0}$

for $\boldsymbol{g} = \mathbf{1}{:}\,\boldsymbol{k}$

if $\boldsymbol{\gamma}_{\boldsymbol{Threshold};i:M} < \dfrac{\text{Tr}\left(\mathbf{A}^2_{\text{OAS};i:M}\right)}{\text{Tr}\left(\mathbf{A}_{\text{OAS};i:M}\right)} + \dfrac{\text{Tr}\left(\mathbf{W}^2_{\text{OAS};i:M}\right)}{\text{Tr}\left(\mathbf{W}_{\text{OAS};i:M}\right)}$

$\boldsymbol{j}_{\text{Rank}} = \boldsymbol{j}_{\boldsymbol{Rank}} + \mathbf{1}$

else

Rank=$\boldsymbol{j}_{\text{Rank}}$

end

end

6.7 Weak-SNR Rank Estimation without Oracle Approximation Shrinkage

With both the ranking Algorithm 6.3, and the definition of the revised ranking threshold statistic, Equation (6.35), we are at liberty to begin exercising through simulation. As in Section 6.4 we assume for the initial demonstration of Algorithm 6.3 we know both the target and the measured time-reversal operators. Per the results of Section 6.5, we also know the results for the oracle approximation shrinkage (OAS) estimate closely track those of the known signal and noise time-reversal operator, see Table 17 and Table 19. Following a now familiar format, we assume the scenario consists of 3 point reflectors situated on a 2-D plane, with these defined parameters

Table 20: Scattering Center Parameters

Scattering Center	Dielectric Coefficient (ρ)	Scattering Center Location (x, y)
1	$\rho = 2.0$	$[5,0]$
2	$\rho = 1.75$	$[-2.5, 4.33]$
3	$\rho = 1.5$	$[-2.5, -4.33]$

Simulations are run with network densities varying from 6 to 40 sensor nodes, and with training data lengths from 4 to 44; which is required to reduce the trace functional variance, see Figure 21. In a departure from previous results sections, there is a new variable that is changed across simulations, which involves modifying the effective rank variable, j. Receiver operating characteristic (ROC) curves are the outcome of each simulation run, with the required SNR for detection

of a rank i reflector discussed, and ultimately tabulated at the conclusion of this section. Previously, results were shown for an assumed $j = 1$, with no regard given to the number of target scattering centers present; having already tabulated results with and without the use of the oracle approximation shrinkage algorithm, there is little need to repeat results for $j = 1$ within this ranking section.

Starting with a sparse sensor network, comprised of 6 nodes, and a training data length of 4, we run Algorithm 6.3; however, we neglect to include steps 2 and 3 for this initial use case. Recalling we previously ran this simulation assuming a rank 1 signal, see Figure 32, we push the value of $j = 2$; corresponding to a rank 2 signal.

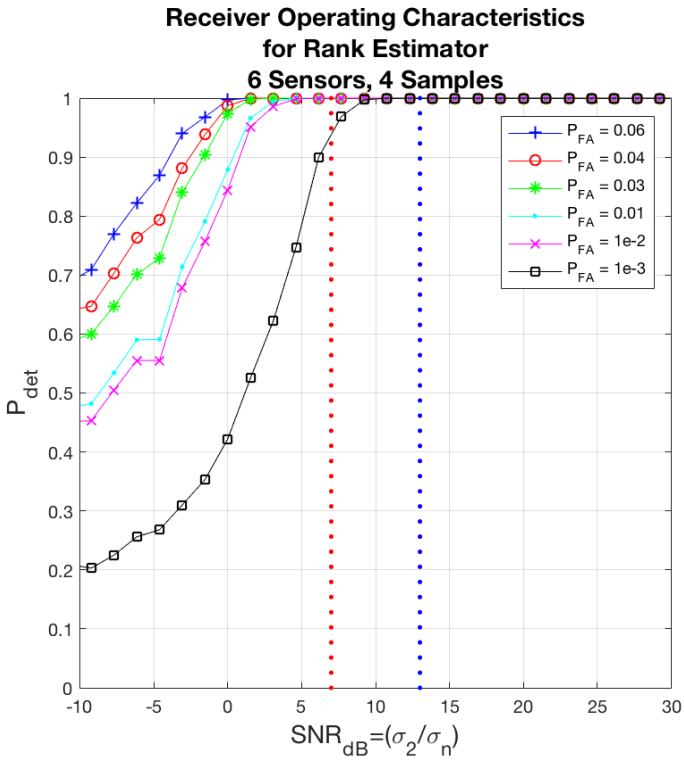

Figure 38: Algorithm 4.3-6 Sensors with Training Data Length of 4 Samples

The results for this section are receiver operating characteristic (ROC) curves, indicating the required signal-to-noise ratio (SNR) for detection of the rank 2 signal. So, from Figure 38, the required SNR for detection, assuming a $P_D = 90\%$ and $P_{FA} = 1\%$, is $-4dB$. Reducing the trace functional variance to a value of 0.01, the training data length is increased to 14, we find the required SNR for detection is $-11dB$.

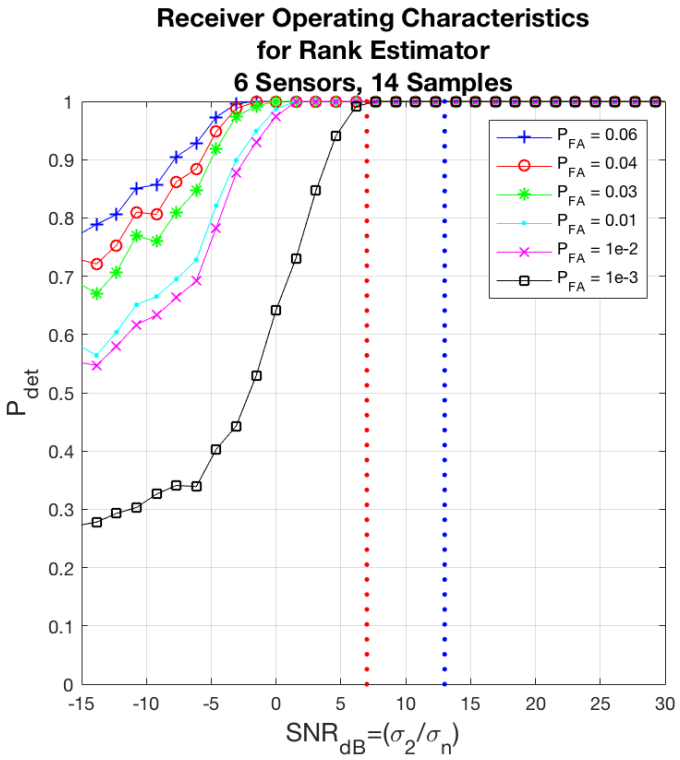

Figure 39: Algorithm 4.3-6 Radar Sensors with Training Data Length of 14 Samples

Continuing on to a training data length of 44, the required SNR for detection with a trace functional variance of 0.001 is $-19dB$. Thus far, the results are tracking closely with Table 17.

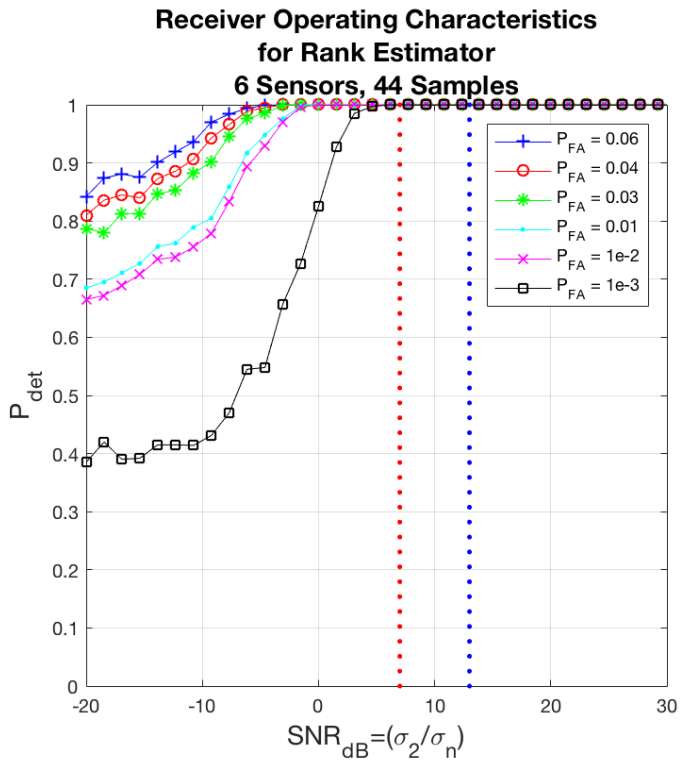

Figure 40: Algorithm 4.3-6 Sensors with Training Data Length of 44 Samples

In summary, the determination of rank is not an insurmountable problem, and actually requires only a slight modification of the low-SNR Algorithm 6.2 to achieve

acceptable receiver operating characteristic curves for a multitude of scenarios. More importantly, from Table 17, the tabulated results for this section-for both rank 2 and 3 signals-closely follows the required SNR for an assumed rank 1 signal, see Table 21. As was the case with Section 6.4 however, we have made the rather conscious decision to assume that both the target and noise time-reversal operators were known *a priori*, and that only the noise time-reversal operator, $\widehat{\mathbf{W}}$, needed to be estimated. In the proceeding section, this assumption is not made; instead, the entirety of Algorithm 6.3 is exercised with the oracle approximation shrinkage (OAS) algorithm, to show the efficacy of the ranking approach under low-SNR conditions.

Table 21: Algorithm 4.3-Probability of Detection vs Radar Network Density vs Training Data Length

Sensor Network Density	Weak-SNR Cross-Over Point	Training Data Length $\boldsymbol{N}$	Probability of Detection for Rank = 2 $\boldsymbol{P_D = 90\%}$ and $\boldsymbol{P_{FA} = 1\%}$
6	$13dB$	$[4,14,44]$	$[1dB, -3.1dB, -6.5dB]$
10	$11dB$	$[4,14,44]$	$[1.5dB, -2.9dB, -6.2dB]$
20	$9dB$	$[4,14,44]$	$[2.5dB, 1.2dB, -4.5dB]$
40	$8dB$	$[4,14,44]$	$[2.8dB, -1dB, -3dB]$

Table 22: Algorithm 4.3-Probability of Detection vs Sensor Network Density vs Training Data Length

Sensor Network Density	Weak-SNR Cross-Over Point	Training Data Length $\boldsymbol{N}$	Probability of Detection for Rank = 3 $\boldsymbol{P_D = 90\%}$ and $\boldsymbol{P_{FA} = 1\%}$
6	$13dB$	$[4,14,44]$	$[-3dB, -10dB, -6.2dB]$
10	$11dB$	$[4,14,44]$	$[-3dB, -11dB, -6.2dB]$
20	$9dB$	$[4,14,44]$	$[-2dB, -8dB, -3.5dB]$
40	$8dB$	$[4,14,44]$	$[-2dB, -8dB, -15dB]$

6.8 Weak-SNR Rank Estimation Using the Oracle Approximation Estimation

Previously in Section 6.5, the target and corruptive noise time-reversal operators were recovered with the assistance of the oracle approximation shrinkage (OAS) estimator from the measured time-reversal operator, $\mathbf{B}$, and detection results making use of this approach were detailed algorithmically, and demonstrated using modeling and simulation. Using Algorithm 6.3 in its entirety, this section demonstrates the efficacy of ranking at low-signal-to-noise ratios (SNR). Owing to the increase in complexity of making use of the OAS estimator, we will not

exhaustively discuss results unless those results differ drastically between Section 6.5 and the present section, however, Table 24 and Table 25 include the comprehensive set of results for both rank 2 and 3 detection SNR requirements.

From Section 6.5 we discussed the purpose of the OAS estimator was to determine an asymptotic form of the measured time-reversal operator, **B**. Since under Algorithm 6.2, we do not presume to know the form of the target time-reversal operator, **A**, this must be determined or estimated from available data; the process for doing so comprise steps 2 and 3 of Algorithm 6.3. Previous results showed good agreement between the OAS estimator approach and the *a priori* approach in which both the target and noise measurement time-reversal operators were known, **A** and **W** respectively.

Now, let us begin by starting with a sparse sensor network comprised of 6 nodes. The test scenario is the now familiar table, see below

Table 23: Scattering-Center Parameters

Scattering Center	Dielectric Coefficient (ρ)	Scattering Center Location (x, y)
1	$\rho = 2.0$	$[5,0]$
2	$\rho = 1.75$	$[-2.5, 4.33]$
3	$\rho = 1.5$	$[-2.5, -4.33]$

Simulation results utilizing the oracle approximation shrinkage estimator algorithm rely on only two inputs: the estimated noise time-reversal operator, $\widehat{\mathbf{W}}$; and the measured time-reversal operator, **B**. Steps 2 and 3 of Algorithm 6.3 provide the necessary estimated target and noise time-reversal operators, $\mathbf{A}_{\text{OAS}}$ and $\mathbf{W}_{\text{OAS}}$ respectively, providing the necessary inputs for the trace functionals that comprise the binary hypothesis test. Initially, the focus is on a sparse sensor network comprised of 6 nodes, with a training data length of 44 samples. This should provide the highest required SNR for detection as previously seen in Tables 24 and 25. Setting the required probability of detection, $P_D = 90\%$, and the required probability of false alarm, $P_{FA} = 1\%$, the required SNR for detection of a rank 2 signal is $-6.2dB$, which is $-19.2dB$ lower than the low-SNR cross-over point of $13dB$.

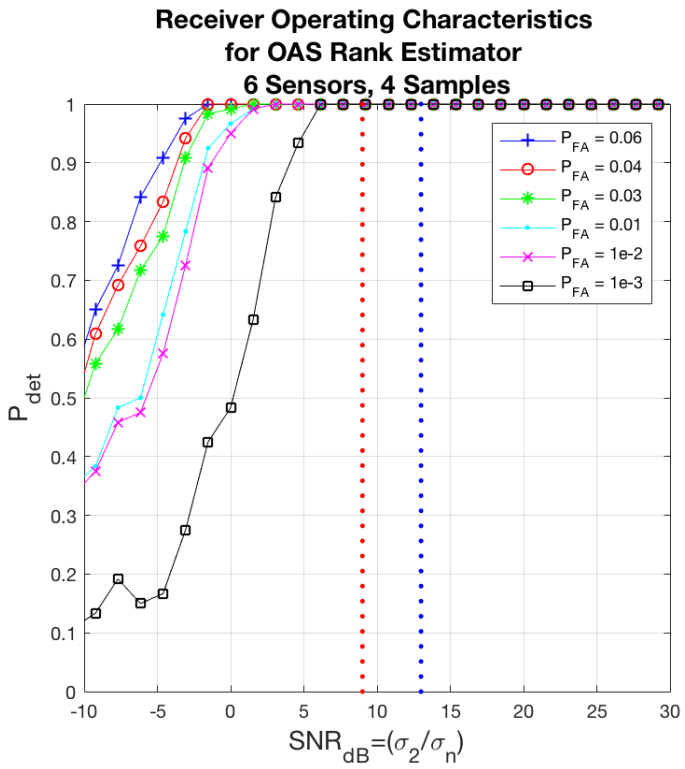

Figure 41: Algorithm 4.3-6 Sensors with Training Data Length of 4 Samples

Figure 41 shows the detection performance using the OAS estimator is nearly identical to that of Section 6.4 in which the signal and noise measurement operators, **A** and **W** were known *a priori*.

Table 24: Algorithm 4.3-Probability of Detection vs Sensor Network Density vs Training Data Length

Sensor Network Density	Weak-SNR Cross-Over Point	Training Data Length $\boldsymbol{N}$	Probability of Detection for Rank = 2 $\boldsymbol{P_D = 90\%}$ and $\boldsymbol{P_{FA} = 1\%}$
6	$13dB$	$[4,14,44]$	$[-1.5dB, -4.5B, -6.2B]$
10	$11dB$	$[4,14,44]$	$[0.5dB, -3.1dB, -4.6dB]$
20	$9dB$	$[4,14,44]$	$[1.2dB, -1.5B, -3.2dB]$
40	$8dB$	$[4,14,44]$	$[1.3dB, -1.2dB, -3.2dB]$

Table 25: Algorithm 4.3-Probability of Detection vs Sensor Network Density vs Training Data Length

Sensor Network Density	Weak-SNR Cross-Over Point	Training Data Length $\boldsymbol{N}$	Probability of Detection for Rank = 3 $\boldsymbol{P_D = 90\%}$ and $\boldsymbol{P_{FA} = 1\%}$
6	$13dB$	$[4,14,44]$	$[0.5dB, -3.2dB, -4.6dB]$
10	$11dB$	$[4,14,44]$	$[1.0B, -3.2dB, -4.6dB]$
20	$9dB$	$[4,14,44]$	$[1.4dB, -3.2dB, -4.6B]$
40	$8dB$	$[4,14,44]$	$[2.7ddB, -0.5\ dB, -3.1dB]$

6.9 Summary

Whether a signal is strong or weak, there is always a push by the sensor designer to extend the useful bounds of detection performance; thereby increasing the seeming utility of the product, and potentially carving out new potential markets for their system. Whilst the detection of objects against a background of noise is fairly well explored for positive signal-to-noise ratio regimes; the motivation for studying detection and ranking in low signal-to-noise ratio regimes stems from this desire to advance the boundaries of current sensing modalities into regimes that have traditionally remained off-limits to modern radar systems. In this chapter, a mathematical foundation was presented that introduced the concept of *concentration of measure*; this theory was extended to encompass the *concentration of measure for eigenvalues*, and presented the *trace functional* as a potentially mathematical useful quantity for use in detection algorithms. Boundaries for the low-signal-to-noise ratio were presented and mathematically defined as being the point at which the measured response matrix had a matrix *inertia* equivalent to the noise time-reversal operator; this quantity was dubbed the *weak-signal-to-noise ratio cross-over point*. Detection and ranking algorithms were introduced that allowed for the recovery of isotropic scattering centers with signal-to-noise ratio values less than those of the weak-signal-to-noise cross-over point.

6.10 Conclusion

In this chapter, the concept of the weak signal-to-noise ratio regime was introduced, along with definitions for determining the weak signal-to-noise ratio cross-over point for a distributed sensor network. Further, algorithms were introduced for the case in which the underlying corruptive noise process was assumed known *a prior*, and those cases in which the underlying corruptive noise process was unknown. Detection performance versus a variety of sensor network configurations was discussed, along with the relative performance differences between the known and unknown noise cases. Finally, a ranking algorithm permitted a confidence bound determination of the effective perturbation of the measured time-reversal operators for both the known and unknown corruptive noise scenarios. Follow-on efforts are underway to investigate whether further performance may be gained from the use of adaptive and/or cognitive intelligent thresholding formulations of the low-SNR detection and ranking algorithms of this section.

7 Summary

Motivated to develop an algorithm that allows for heterogeneous sensor heterogeneous data fusion, this work sought to develop the algorithmic framework for pre-detection fusion of a distributed RF sensor network such that the requirement for any a-priori target information is eliminated. This pre-detection fusion process is unique, in that it makes use of an outer product formulation in order to preserve the data in a higher-dimensional space; which runs counter to traditional matched filter approaches used by fielded radar sensor systems, that make use of more conventional inner product space for their formulations. Through the application of various non-parametric statistical mathematics, a bespoke depth-based detector was introduced for a distributed radio-frequency sensor network. This particular detector required no prior knowledge of the target to be known, and is applicable across a range of background corruptive noise processes-owning to its non-parametrical underpinnings. Performance was deemed acceptable in instances where the target signal-to-noise ratio (SNR) was favorable and above unity, but performance was lacking when the SNR strayed lower. In Chapter 6, a bespoke algorithm was introduced based upon the mathematics of concentration of measure. Whilst decidedly less non-parametric in nature than Chapter 4, the threshold statistic was kept non-parametric, to allow application of this algorithm across a broad spectrum of corruptive noise process-both known and unknown. The bespoke algorithm of Chapter 6 required no knowledge of the target *a priori*, and performance was acceptable across a range of SNR values-including negative! Chapter 6 explored the boundaries of performance for a network that exploits target reflectivity coherence in the *angular-domain* versus a traditional monostatic radar that seeks to enhance detection performance through *coherent integration* in the *time-domain*.

Throughout this thesis, the *range-extended/over-resolved target*-or a target that is comprised of multiple-scattering centers in close proximity to one another-is repeatedly referenced. In order to detect each scattering center of the over-resolved target, a ranking algorithm is introduced for each respective detector introduced in Chapters 4 and 6. The concept of statistical ranking allows us to determine the effective number of targets in a background of additive corruptive noise (to include parametric and non-parametrically derived additive corruptive noise processes-including heavy-tailed distributions like the *k*-distribution). The

incorporation of bespoke statistical ranking algorithm allows us to determine the exact number of scattering centers comprising each *range-extended target*.

Previous efforts to assess the lower-bound of detection performance were discussed by Sadowsky and Bucklew [83] in the context of the low-energy coherence receiver; however still required explicit knowledge of the target covariance function in order to be applicable. The author investigated detection performance in the context of the generalized inner product (GIP) in [35-37], where the GIP still required knowledge of the target structure in order for the proposed detection algorithm to have any merit; though for small variations in the target template, a limited amount of information could be gained from investigation of the template mis-match errors. Further investigations into low-SNR detection were investigated by the author in [48-49] and [61-62]. In each instance, the detection algorithm formulations were more explicit in their requirement, and were specifically developed to address a particular problem space. Whilst these previous efforts may have limitations, in terms of applicability, they reinforce the results presented in Chapter 6, and corroborate the ability of sensing systems to detection targets-and, if applicable, associated target structures-in the low-SNR domains.

In summary, this thesis focuses on the development of mathematical paradigms for distributed radio-frequency sensor network to enable:

1. Development of a pre-detection fusion algorithm that coalesces the received signals from each RF sensor in the network into a unified time-reversal operator, thereby simplify subsequent processing algorithms
2. Detection of range-extended target without requirements for knowing the target operator function *a priori*
3. Ranking of a range-extended target to determine effective number of scattering centers comprising the target body, without knowing the nature of the extended target *a priori*
4. Development of detection threshold criterion that is non-parametric and does not require *a priori* knowledge of the background interference environment; to include noise and/or clutter
5. Detection and ranking in signal-to-noise ratio regimes that are weaker than typically required for monostatic radar system detection algorithms.
6. Detection and ranking that is independent of sensor network density, and is able to operate under both sparse and dense sensor density regimes

8 Open Problems

8.1 Introduction

This chapter is focused on identifying research problems that have arisen as part of this thesis, and are potential areas of future exploration. For each potential follow-on research topic, an effort has been made to identify the research topic and provide a synopsis of work to be completed, followed by important sub-tasks within each topic to be addressed.

8.1.1 Threshold that Accounts for Target Partial Coherence

We want to analyze the impact of adjusting the detection threshold based upon the presumed partial coherence of the target. By accounting for the fact, the detection performance is lower for a partially coherent target (PCT), we can augment the detection performance based upon the optimization of the detection threshold.

We may also want to link this method with the method suggested in Section 8.1.2.

1. Fully-Coherence: no change in threshold value
2. Fully-Incoherent: threshold will be low, but increases the corresponding False Alarm rate
3. High-Partial Coherence: minor medication of the threshold
4. Moderate-Partial Coherence:
5. Low-Partial Coherence: similar to Fully-Incoherent case, results in a lower threshold with higher corresponding false-alarm rate

The question becomes: can exploiting the degree of coherence that a particular over-resolved target exhibits, allow us to modify our detection and ranking algorithm thresholds, in such a manner, as to increase our results over those introduced in Chapter 6?

8.1.2 Optimal Integration of Sensors Comprising the Distributed Network

We seek to integrate the angular ambits in an optimal manner that results in a higher gain than just randomly integrating over all the available angular ambits. The ability to pick the proper angular sectors to integrate could be based upon

1. Integration over similar complex domain distributions in the angular-domain
2. Peak amplitude values (real-valued)

3. Peak amplitude values that coincide with similar complex domain distributions in the angular-domain
4. Removing the low peak amplitude values (real-valued)
5. Removing complex domain values that exceed a defined variance from the population mean

The question to be answered is: are there more optimal methods and/or processes that enhance the detection and ranking performance of those algorithms introduced in Chapter 6?

8.1.3 Random Failure of Sensor Nodes

In this case, we want to examine the case in which there is a failure of sensor(s) under the following assumptions

1. Random radio-frequency sensor locations within the distributed sensing network
2. A complete angular ambit fails to report to the central fusion center across multiple adjacent sensors within the distributed network

The question to be answered is simply: does the failure of one or more sensor nodes compromise the declaration performance of the distributed sensing network?

8.1.4 Faulty Radar Sensor Information

We seek to understand the impact of a sensor(s) that capture faulty information, such as noise or random information that would be deleterious if integrated in the response matrix. More importantly, we seek to answer the germane question of whether the algorithms are robust to sensor nodes passing along corrupt data? To what degree are our algorithms from Chapters 4 and 6 sensitive to corrupted sensor node data, and should there be a supervisory algorithmic function for parsing and excising this potential corrupted data-ie a pre-detection fusion input data culling function?

8.1.5 Sensor Network Trust

What is the impact of a compromised sensor(s)? We could assume that information is flowing in to the network that is compromised in some manner, such that the overall impact the sensor network is negative. We seek to determine the

optimal method to establish trust among the sensors comprising the network, such that we can adaptively remove those sensors that fail to establish trust in the network. This couples with Sections 8.1.3 and 8.1.4.

This question is rather important from a practical implementation concern: does spoofed, jammed, falsified, hacked, or altered data corrupt our results from utilizing the algorithms introduced in Chapters 4 and 6? To what degree are our algorithms sensitive to non-trustworthy data? Does the inclusion of a fusion center trust algorithm warrant the additional complexity and time-delays necessary to ensure our declaration results are valid-ie how do we ensure "trusted data" is being received for any given sensor node?

8.1.6 Experimental Data

We need to collect a great deal of data on a variety of target models to determine the existence of target partial coherence for a wide variety of target types: bi-spheres, tri-spheres, aggregates of spheres, cubes, boxes, complex models of vehicles and commercial airliners. The challenge is really determining the optimal subset of tests that will prove the basic concept. More importantly, can the existence of target partial coherence be exploited to develop better, more optimal/robust detection and target identification algorithms? To what extent is target partial coherence unique to a given target, class of targets, or any targets in general?

8.1.7 Bounds of Performance

Bounds on the number of sensors required for our bespoke detection and ranking algorithms to be applicable under real-world scenarios should be an area of further investigation. These bounds are, at present, established based upon the assumed rank of the time-reversal operator. Whilst there is a benefit to incorporating an infinite number of sensors, what concerns us most is keeping the effective dimensionality of the problem low-enough to ensure optimal processing of the received data. This problem will be compounded when clutter is considered. The question to ponder is simply: what is the lowest sensor node density to ensure adequate receiver-operating characteristics, based upon the environmental corruptive processes, and for the particular sensing mission set? Is there an algorithm that would allow us to modify the sensor node locations to more optimally

"sense" and "learn" about a given declared target? What is the role of target partial coherence in determining performance bounds or sensor node placement and density?

8.1.8 Recovery of Reflectivity Estimates for Point-Type Isotropic Scattering Centers

Thus far no algorithm is discussed for the recovery of point-type reflector reflectivity recovery. This is not an oversight, but a method to ensure a cogent document that focuses primarily on detection and ranking algorithms, rather than muddle the conversation with post-detection algorithmic considerations. Methods for the automated recovery of reflectivity parameters for point-type reflectors exist and are a relatively straightforward way in which to expand the utility of this document beyond detection and ranking considerations. Does our declaration algorithm benefit from recovering reflectivity estimates on the detected and ranked target scattering centers? More importantly, does this information lead to better discrimination of false targets, allowing for an adjunct algorithm to be developed that will increase the receiver operating characteristics, based upon an analysis of detected and ranking target scattering centers reflectivity properties?

8.1.9 Recovery of Permittivity and Permeability for Finite-Sized Target Scattering Centers

Methods for the establishment of algorithms for the recovery of permittivity and permeability estimates for finite-sized inclusions, to include-but not limited-to: isotropic medium permittivity and permeability estimates; anisotropic material permittivity and permeability estimation; permittivity and permeability associated for a given inclusion; method and procedure for automated recovery of permittivity and permeability under low-SNR and partially-coherent conditions.

Does our declaration algorithm benefit from recovering permittivity and permeability estimates on the detected and ranked target scattering centers? More importantly, does this information lead to better discrimination of false targets, allowing for an adjunct algorithm to be developed that will increase the receiver operating characteristics, based upon an analysis of detected and ranking target scattering centers dielectric material properties?

8.1.10 Optimal Methods for Determining the Material Composition of a Finite-Sized Target Scattering Center

Put simply: for a fully coherent target, the material properties can easily be determined from a single tone. Now, if the target is not fully coherent, then we have a problem: the permeability and permittivity are based upon the determination of the target singular value. So, if the singular value is perturbed based upon target partial coherence, the material properties are not so easily estimated; no matter, we can still accomplish this goal, albeit with a bit more work and some inevitable ambiguity. How will we accomplish the material property estimation? We start by considering the response of a material over a band of frequencies. The material will exhibit a variety of changes that are easily mapped from the response domain to a function domain. The function domain will take the multidimensional data and reduce the dimensionality to two-dimensions. We need to go out on a bit of a limb now, and assume the dispersive properties of the target are stable over a range of frequencies (we are not transitioning from dielectric to conductor for example), such that the reflectivity of the target is only a function of frequency and the response allows for the easy parameterization of the reflectivity over a number of probing tones.

We now will assume the reflectivity is simply scaled by some variable $\mathbf{A}(f_j)$, such that we can normalize the response of the object over a continuum of frequencies and compare with the normalized response from a set of frequency tones. We assume we have a family of normalized responses from a variety of materials, we then compare which response most closely matches that captured by the sensor network. This should permit the effective estimation of the permeability and permittivity.

One issue not discussed, but is always assumed is the nature of the material comprising the reflector. In this case, we have assumed an isotropic material, thereby negating the necessity of determining the polarization tensor matrix for the reflector. If we have to incorporate the polarization tensor matrix, then the problem becomes a bit easier, in that the initial family of normalized responses can be parsed by polarization iso- versus anisotropy.

Ultimately, the question becomes: is the added computational and system complexity worth the additional information to be gleaned from knowing what material comprises each detected and ranked target scattering center? I would argue, simply, yes!

8.2 Follow-On PhD Topics

The following is a list of proposed PhD topics that expand upon the concepts introduced within this thesis. Each topic presented embodies an entire work unto itself and would suffice as a self-contained PhD thesis. No attempt has been made to exhaustively explore each particular research thrust area, but a cursory explanation is included as a first-attempt at quantifying the general question that would be addressed in the associated thesis document.

8.2.1 Incorporation of Bandwidth into Detection Algorithms

Here we need to be concerned with the time-reversal operator from a target over a number of angular sectors, and for a number of frequencies in which the bandwidth may lead to a frequency-dependent dispersive response. What changes are required to the bespoke algorithms introduced in Chapters 4 and 6?

8.2.2 Computationally Efficient Methods for Data Depth Functional Processing

Data Depth is an extremely versatile and useful field of statistical mathematics and computational geometry that holds the power to fundamentally transform the field of sensor processing for multivariate data in d>2. However, the challenge in determining the data depth functional is not mathematical-its computational. The problem is compounded as the

Whilst this is an active area for computer scientists studying data depth, there is little published work in the area of computationally efficient methods for data depth processing, and remains an open area of investigation.

8.2.3 Contextual Classifier

Contextual data processing permits high dimensional data to be processed into actionable bits of data that are appropriate for a subset of end users. Taking this one step further, if we know we are only interested in a few bits of data-ie location and the direction of a moving object, or the materials that comprise that object-we can begin to make a contextual data processor that takes high dimensional data, and returns a low-dimensionality subset of data that meets the end-users requirements. The information of interest is easy to state (Order n) and the data processing requirements are modest to implement (order np). An order n problem

has a definite answer-our analyst needs a few well-defined values from the sensing network; whereas the data processing requirement for our contextual data processor is order np-there could be an answer, but not always. Contextual data processing can handle ambiguities, as can our analyst, but our analyst has a requirement that can be better met by removing ambiguities prior to turning raw data into information.

9 Bibliography

[1] H.L. Van Trees, Detection, Estimation, and Modulation Theory, Part III, Wiley & Sons, New York, NY, 2001.

[2] C.W. Therrien, Discrete Random Signals and Statistical Signal Processing, Prentice Hall, Englewood Cliffs, NJ, 1992.

[3] M.A. Richards, *Fundamentals of Radar Signal Processing*, McGraw-Hill, New York, NY, 2005.

[4] J. Garnier, "Use of Random Matrix Theory for Target Detection, Localization, and Reconstruction," *Contemporary Mathematics*, vol. 548, pp. 151-163, 2011.

[5] P.M. Woodward, *Probability and Information Theory, with Applications to Radar*, New York, NY: Pergamon Press, 1955.

[6] H. Borrin, H.D. Griffiths, P. Tait, D. Money, and C.J. Baker, "Scattering Centre Extraction for Extended Targets," *IEEE International Radar Conference*, pp. 173- 178, 9-12 May 2005.

[7] G.A. Showman, W.L. Melvin, and M. Greenspan, "Radar Detection and Angle Estimation of Over-Resolved Ground Vehicles," *IEEE Radar Conference, 2008 ,* pp.1-6, 26-30 May 2008.

[8] E. Conte, A. De Maio, and G. Ricci, "GLRT-based Adaptive Detection Algorithms for Range-Spread Targets," *Signal Processing, IEEE Transactions on* , vol.49, no.7, pp.1336-1348, Jul 2001.

[9] M. Vespe, C.J. Baker, and H.D. Griffiths, "Automatic Target Recognition Using Multi-Diversity Radar," *IET Radar, Sonar & Navigation*, vol.1, no.6, pp.470-478, Dec. 2007.

[10] M.I Skolnik, *Radar Handbook, 3rd Ed.*, SciTech Publishing, Raleigh, NC, 2008.

[11] N.J. Willis, *Bistatic Radar*, SciTech Publishing, Raleigh, NC, 2005.

[12] N.J. Willis, and H.D. Griffiths, *Advances in Bistatic Radar*, SciTech Publishing, Raleigh, NC, 2007.

[13] H.D. Griffiths, "Bistatic Radar: Principals and Practice," *SBMO International Microwave Conference/Brazil*, vol. 2, pp. 519-526, 2-5 August 1993.

[14] T. Tsao, D. Weiner, P. Varshney, H. Schwarzlander, and M. Slamani, "Ambiguity Function for a Bistatic Radar," *IEEE Transactions on*

Aerospace and Electronic Systems, vol.33, no.3, pp.1041-1051, July 1997.

[15] T. Tsao, D. Weiner, P. Varshney, H. Schwarzlander, and M. Slamani, "Ambiguity Function for a Bistatic Radar," *Proceedings of the IEEE-SP International Symposium* on *Time-Frequency and Time-Scale Analysis*, pp.497-500, 4-6 Oct 1992.

[16] M. Greco, F. Gini, and A. Farina, "Cramer-Rao Bounds for Bistatic Radars," *IEEE Transactions on Geoscience and Remote Sensing*, vol.46, no.10, pp.3252-3264, Oct. 2008.

[17] W.L. Melvin, M.C. Callahan, and M.C. Wicks, "Bistatic STAP: Application to Airborne Radar," *Proceedings of the IEEE Radar Conference*, pp. 1-7, 2002.

[18] J. Ward. "Space-Time Adaptive Processing for Airborne Radar," MIT Lincoln Laboratory, Tec. Rep. F19628-95-C-0002, December 1994.

[19] R.S. Adve, L. Applebaum, M.C. Wicks, R.A. Schneible, "Space-Time-Waveform Adaptive Processing for Frequency Diverse Distributed Radar Apertures," *40th Annual Conference on Information Sciences and Systems*, pp.1413-1417, 22-24 March 2006.

[20] W.L. Melvin, G.A. Showman, and R.K. Hersey, "Adaptive Radar: Beyond the RMB Rule," *IEEE Radar Conference*, pp.1-8, 26-30 May 2008.

[21] L.E. Brennan, J.D. Mallet, and I.S. Reed, "Adaptive Arrays in Airborne MTI Radar," *IEEE Transactions on Antennas and Propagation*, vol.24, no.5, pp. 607- 615, Sep 1976.

[22] L.E. Brennan and L.S. Reed, "Theory of Adaptive Radar," *IEEE Transactions on Aerospace and Electronic Systems*, vol.AES-9, no.2, pp.237-252, March 1973.

[23] F. Bandiera, A. De Maio, and G. Ricci, "Adaptive Radar Detection with Conic Rejection," *International Radar Symposium,* pp.1-4, 24-26 May 2006.

[24] A. De Maio, A. Farina, "Adaptive Radar Detection: A Bayesian Approach," *International Radar Symposium,* pp. 1-4, 24-26 May 2006.

[25] G.T. Capraro, A. Farin, H.D. Griffiths, and M.C. Wicks, "Knowledge-Based Radar Signal and Data Processing," *IEEE Signal Processing Magazine,* vol.23, no.1, pp. 18- 29, Jan. 2006.

[26] W.L. Melvin and J.R. Guerci, “Knowledge-Aided Signal Processing: A New Paradigm for radar and other Advanced Sensors,” *IEEE Transactions on Aerospace and Electronic Systems*, vol.42, no.3, pp.983-996, July 2006.

[27] E. Conte., A. De Maio, A. Farina, and G. Foglia, “Design and Analysis for a Knowledge-Aided Radar Detector for Doppler Processing,” *IEEE Transaction on Aerospace and Electronic Systems,* vol.42, no.3, pp.1058-1079, July 2006.

[28] D. Kazakos , V. Vannicola, and M.C. Wicks, “Advances in Signal Detection or Distributed Multisensor Data,” *IEEE International Conference on Systems, Man and Cybernetics,* pp.1283-1288 vol.3, 14-17 Nov 1989.

[29] S.R. Doughty, K. Woodbridge, and C.J. Baker, “Improving Resolution Using Multistatic Radar,” *IET International Conference on Radar Systems*, pp.1-5, 15-18 Oct. 2007.

[30] Y. Teng, H.D. Griffiths, C.J. Baker, and K. Woodbridge, “Netted Radar Sensitivity and Ambiguity,” *IET Radar, Sonar & Navigation,* vol.1, no.6, pp.479-486, Dec. 2007.

[31] I. Bradaric, G.T. Capraro, M.C. Wicks, and P. Zulch, “Signal Processing and Waveform Selection Strategies in Multistatic Radar Systems,” *International Waveform Diversity and Design Conference*, pp. 307-311, 4-8 June 2007.

[32] G.T. Capraro, I. Bradaric, and M.C. Wicks, “Waveform Diversity in Distributed Radar,” *International Conference on Electromagnetics in Advanced Applications,* pp.954-957, 14-18 Sept. 2009.

[33] W. Elmenreich and R. Leidenfrost, “Fusion of Heterogeneous Sensors Data,” *International Workshop on Intelligent Solutions in Embedded Systems*, pp.1-10, 10-11 July 2008.

[34] H. Hotelling, “The Generalization of Students Ratio,” *Annals of Mathematical Statistics*, vol. 2, no. 3, pp. 360-378, 1931.

[35] M. Wicks, Y. Zhang, R. Schneible, and J.P. Browning, ”A Hotelling T-Squared GIP Test for Detection of Over Resolved Targets,” *European Wireless Conference*, pp. 766-773, Lucca, Italy, April 2010.

[36] M. Wicks and Y. Zhang, ”Optimized Detection of Spatially Extended Fixed Objects in Clutter,” *Proceedings of the IEEE Radar Conference, Pasadena*, CA, 4-8 May 2009.

[37] M. Wicks, Y. Zhang, and R. Schneible,” Detection of Spatially Extended Objects in Clutter,” *International Conference on Electromagnetics in Advanced Applications*, vol., no., pp.970-973, 14-18 Sept. 2009.

[38] H.L. Van Trees, Detection, Estimation, and Modulation Theory, Part I, Wiley & Sons, New York, NY, 2001.

[39] S. Kingsley, S. Quegan, *Understanding Radar Systems*, SciTech Publishing, Raleigh, N.C., 2005.

[40] M.A. Richards, J.A. Scheer, W.A. Holm, Editors, *Principles of Modern Radar: Basic Principles*, SciTech Publishing, Rayleigh, NC, 2010.

[41] G. W. Stimson, Introduction to Airborne Radar, 2nd Ed., SciTech Publishing, Raleigh, NC, 2000.

[42] P.J. Bickel and E.L. Lehmann, “Descriptive Statistics for Nonparametric Models III. Dispersion,” *The Annals of Statistics*, vol. 4, no. 6, pp. 1139-1158, 1976.

[43] D. Middleton, “On the Detection of Stochastic Signals in Additive Normal Noise,” *IRE Transactions*, PGIT-3, pp. 86-121, 1957.

[44] D. Middleton, An Introduction to Statistical Communication Theory, McGraw-Hill, New York, NY, 1960.

[45] D. Middleton, *“*On Singular and Nonsingular Optimum (Bayes) Tests for the Detection of Normal Stochastic Signals in Normal Noise*,” IRE Transactions,* IT-7, no. 2, pp. 105-113, April 1961.

[46] R. Price and P.E. Green, Jr., Signal Processing in Radar Astronomy: Communication via Fluctuating Multipath Media, Massachusetts Institute of Technology, Lincoln Laboratory, Technical Report 234, October 1960.

[47] R. Price, “Detectors for Radar Astronomy,” *Radar Astronomy*, Edited by J.V. Evans and T. Hagfors, McGraw-Hill, New York, NY, 1968.

[48] Shujie Hou; Qiu, R.; Browning, J.P.; Wicks, M.; , ”Target detection with linear and kernel subspaces matching in the presence of strong clutter,” 2012 IEEE Radar Conference (RADAR), pp.0372-0376, 7-11 May 2012.

[49] Lin, F.; Qiu, R.C.; Hu, Z.; Hou, S.; Browning, J.P.; Wicks, M.C., "Generalized FMD Detection for Spectrum Sensing under Low Signal-to-

Noise Ratio," *IEEE Communications Letters*, vol. 16, no. 5, pp. 604-607, May 2012.

[50] H. Ammari, J. Garnier, and V. Jugnon, ”Detection, Reconstruction, and Characterization Algorithms for Noisy Data in Multistatic Wave Imaging,” *Discrete and Continuous Dynamical Systems,* American Institute of Mathematical Science, vol. 8, no. 3, pp. 389-417, 2015.

[51] R.Y. Liu, J.M. Parelius, and K. Singh, “Multivariate Analysis by Data Depth: Descriptive Statistics, Graphic and Inference,” *The Annals of Statistics*, vol. 27, no. 3, pp. 783-840, 1999.

[52] J.L Hodges, “A Bivariate Test,” *Annals of Mathematical Statistics*, vol. 26, pp. 523-527, 1955.

[53] J.W. Tukey, “Mathematics and the Picturing of Data,” in (R.D. James, ed.), *Proceedings of the International Congress of Mathematicians, Vancourver 1974*, vol. 2, pp. 523-531, 1974.

[54] Y. Zou, and R. Serfling, “General Notions of Statistical Depth Functions,” *The Annals of Statistics*, vol. 28, no. 2, pp. 461-482, 2000.

[55] S. Ghahramani, Fundamentals of Probability, 2nd Ed., Prentice Hall, Upper Saddle River, NJ, 2000.

[56] T. Tao, *An Introduction to Measure Theory*, American Mathematical Society, Providence, RI, 2011.

[57] D. Huang and S. Tseng, “A Decision Procedure for Determining the Number of Components in Principal Components Analysis,” *Journal of Statistical Planning and Inference*, vol. 30, pp. 63-71, 1992.

[58] P. Chen, G.J. Genello, M.C. Wicks, “Estimating the Number of Signals in Presence of Colored Noise,” *Proceedings of the IEEE Radar Conference*, pp. 432-437, April 2004.

[59] P. Chen, “An Interval Estimate for the Number of Signals,” *Proceedings of the IEEE ICSP*, 2004.

[60] P. Chen, “An Interval Estimate for the Number of Signals,” *5th IEEE International Symposium on Multi-Dimensional Mobile Communications*, 2004.

[61] Lin, F.; Qiu, R.C.; Browning, J.P.; Wicks, M.C., ”Target Detection with Function of Covariance Matrices Under Clutter Environment,” *2012 IET Radar Conference*, Glasgow, UK, 22-25 October, 2012.

[62] Feng Lin; Qiu, R.C.; Zhen Hu; Shujie Hou; Browning, J.P.; Wicks, M.C.; , "Generalized FMD Detection for Spectrum Sensing under Low Signal-to-Noise Ratio," *IEEE Communications Letters*, vol.16, no.5, pp.604-607, May 2012.

[63] Robert C. Qiu; Wicks, M.C., Cognitive Networked Sensing and Big Data, Springer, New York, NY, USA, *Preprint*, 2013.

[64] M. Ledoux, The Concentration of Measure Phenomenon, American Mathematical Society, Providence, RI, 2000.

[65] U. Haagerup, and S. Thorbjrnsen, "Random Matrices with Complex Gaussian Entries," *Expositiones Mathematicae*, vol. 21, no. 4, pp. 293-337, 2003.

[66] T.M Cover, J.A. Thomas, *Elements of Information Theory*, John Wiley, New York, NY, 2006.

[67] A. Guionnet, and O. Zeitouni, "Concentration of the Spectral Measure for Large Matrices," *Electronic Communications in Probability*, vol. 5, pp. 119-136, 2000.

[68] L.L. Scharf, Statistical Signal Processing: Detection, Estimation, and Time-Series Analysis, Addison-Wesley, New York, NY, 1991.

[69] T.K. Moon, and W.C. Stirling, Mathematical Methods and Algorithms for Signal Processing, Prentice Hall, Upper Saddle River, NJ, 2000.

[70] M.C. Wicks, W.L. Melvin, and P. Chen, "An Efficient Architecture for Non-Homogeneity Detection in Space-Time Adaptive Processing Airborne Early Warning Radar," *Radar 97 (Conference Publication No. 449),* pp. 295-299, Edinburgh, U.K., 14-16 October 1997.

[71] N. Berestycki and R. Nickl, "Concentration of Measure," *Technical Report*, University of Cambridge, 2009.

[72] R.A. Horn and C.R. Johnson, Matrix Analysis, Cambridge University Press, Cambridge, U.K., 1994.

[73] R.C. Qiu; Hu, Z.; Li, H.; Wicks, M.C., Cognitive Radio Communications and Networking: Principles and Practice, John Wiley & Sons, West Sussex, United Kingdom, 2012.

[74] Y. Chen, A. Wiesel, Y.C. Eldar, and A.O. Hero, "Shrinkage Algorithms for MMSE Covariance Estimation," *IEEE Transactions on Signal Processing*, vol. 58, no. 10, pp. 5016-5029, October 2010.

[75] Y. Chen, A. Wiesel, Y.C. Eldar, and A.O. Hero, ”Robust Shrinkage Estimation of High-Dimensional Covariance Matrices,” *IEEE Transactions on Signal Processing*, vol. 59, no. 9, pp. 4097-4107, September 2011.

[76] P.E. Pace, *Detecting and Classifying Low Probability of Intercept Radar*, Artech House, Boston, MA, 2003.

[77] P. Chen, and M.C. Wicks, “A Lower Confidence Limit for the Number of Signals,” *Proceedings of the IEEE Radar Conference*, pp. 356-361, 2002.

[78] P. Chen, “A Confidence Interval for the Number of Principal Components,” *Journal of Statistical Planning and Inference*, vol. 136, pp. 2630-2639, 2006.

[79] Browning, J.P.; Griffiths, H.D.; Entner, J.; Chen, P., ”Depth-Based Method for Target Detection in Noisy Environments,” *IEEE Radar Conference*, Ottawa, Canada, May 2013.

[80] E.P. Blasch, and M. Hensel, “Fusion of Distributions for Radar Clutter Modeling,” *Proceedings of the International Conference on Information Fusion*, June 28-July 1, 2004.

[81] Patzold, Martin, et. al., “Rosetta Radio Science Investigations (RSI),” *Space and Science Review*, vol. 128, pp. 599-627, 2007.

[82] Williams, Lance, *Low Cost Radar and Sonar Using Open Source Hardware and Software*, MSc Dissertation, University of Cape Town, Cape Town, South Africa, 2008.

[83] Sadowsky, J., and Bucklew, J., “On the Detectability of Weak Signals,” *IEEE Transactions on Information Theory*, vo. 31, pp. 433-436, 1985.